

Copyright Warning & Restrictions

The copyright law of the United States (Title 17, United States Code) governs the making of photocopies or other reproductions of copyrighted material.

Under certain conditions specified in the law, libraries and archives are authorized to furnish a photocopy or other reproduction. One of these specified conditions is that the photocopy or reproduction is not to be “used for any purpose other than private study, scholarship, or research.” If a user makes a request for, or later uses, a photocopy or reproduction for purposes in excess of “fair use” that user may be liable for copyright infringement,

This institution reserves the right to refuse to accept a copying order if, in its judgment, fulfillment of the order would involve violation of copyright law.

Please Note: The author retains the copyright while the New Jersey Institute of Technology reserves the right to distribute this thesis or dissertation

Printing note: If you do not wish to print this page, then select “Pages from: first page # to: last page #” on the print dialog screen

The Van Houten library has removed some of the personal information and all signatures from the approval page and biographical sketches of theses and dissertations in order to protect the identity of NJIT graduates and faculty.

ABSTRACT

MOLECULAR MODELING STUDIES OF ACETYLCHOLINESTERASE

by

Charilaos E. Linaras

The controversial role of electrostatic interactions in the process of steering of acetylcholine into the active site of acetylcholinesterases was investigated in this study. A novel methodology was implemented to simulate the process of recognition of acetylcholine by *Torpedo Californica* and both wild type and charge neutralized mutated *Human* AChE. The obtained results suggest the important role of coulombic interactions in the steering process. The steering process of selected irreversible AChE inhibitors was also simulated supporting the role of electrostatic interactions in the recognition process.

A novel methodology was also employed to model the covalent adducts of *Torpedo Californica* and *Human* AChE's with various organophosphate inhibitors and the interactions of the organophosphate moieties with the surrounding amino acid residues of the active sites of the modeled complexes were analyzed.

Finally, an automated docking environment and methodology were designed and implemented in the prediction of the binding sites in *Human* AChE of three reversible acetylcholinesterase inhibitors, clinically investigated for the treatment of Alzheimer's type senile dementia. The results of the docking analysis reproduce the potency rank of the studied inhibitor molecules providing with a wealth of structural information consistent with similar studies on *Torpedo Californica* AChE. The developed tools and methodology can be directly applied in database screening for the discovery of new lead compounds.

MOLECULAR MODELING STUDIES OF ACETYLCHOLINESTERASE

by
Charilaos E. Linaras

**A Dissertation
Submitted to the Faculty of
New Jersey Institute of Technology
in Partial Fulfillment of the Requirements for the Degree of
Doctor of Philosophy**

Department of Chemical Engineering, Chemistry and Environmental Science

May 1998

Copyright © 1998 by Charilaos E. Linaras

ALL RIGHTS RESERVED

APPROVAL PAGE

MOLECULAR MODELING STUDIES OF ACETYLCHOLINESTERASE

Charilaos E. Linaras

1/26/98

Dr. David Kristol, Dissertation Advisor
Professor of Chemistry, New Jersey Institute of Technology

Date

1/26/98

Dr. Arthur B. Ritter, Committee Member
Adjunct Professor of Chemical Engineering, New Jersey Institute of Technology
Associate Professor of Physiology, UMDNJ, New Jersey Medical School

Date

1/27/98

Dr. Lou Barash, Committee Member
Adjunct Professor of Chemistry, New Jersey Institute of Technology

Date

1/26/98

Dr. Tamara Gund, Committee Member
Professor of Chemistry, New Jersey Institute of Technology

Date

1/27/98

Dr. Prem Yadav, Committee Member
Adjunct Assistant Professor of Biochemistry and Molecular Biology
Coordinator of Molecular Modeling and Genetic Engineering
Academic Computing Center, UMDNJ, New Jersey Medical School

Date

BIOGRAPHICAL SKETCH

Author: Charilaos E. Linaras

Degree: Doctor of Philosophy

Date: May 1998

Date of Birth:

Place of Birth:

Undergraduate and Graduate Education:

- Doctor of Philosophy in Chemical Engineering, New Jersey Institute of Technology, Newark, NJ, 1998
- Diploma in Chemical Engineering, University of Patras, Patras, Greece, 1993

Major: Chemical Engineering

Presentations and Publications:

C. E. Linaras, K. Singh, D. Kristol and A. B. Ritter, "Effect of Electrostatic Interactions in Recognition of Acetylcholine by Acetylcholinesterase", *Journal of Molecular Structure (THEOCHEM)*, in Press.

C. E. Linaras, K. Singh, D. Kristol and A. B. Ritter, "Redifining the Ion Pairs in Proteins", *Proteins: Structure, Function and Genetics*, Submitted.

J. Vaidyanathan, P. Yadav, C. E. Linaras and T. K. Vaidyanathan, "Computer Simulation of Potential Adhesive Nature of Dentin Bonding Molecules", International Association for Dental Research, Nice, France, 1998.

C. E. Linaras, K. Singh, D. Kristol and A. B. Ritter, "Effect of Electrostatic Interactions in Recognition of Acetylcholine by Acetylcholinesterase", 5th Conference on Current Trends in Computational Chemistry, Vicksburgh, MS, 1996.

C. E. Linaras, D. Kristol and A. B. Ritter, "Molecular Modeling Studies of Inhibition of Acetylcholinesterase by Sarin", IEEE 22nd Annual Northeast Bioengineering Conference, New Brunswick, NJ, 1996.

*To my parents Eleftherios and Stamatina, my sister Efrosini, my grandmother Efrosini
and the memory of my beloved grandfather Christos*

ACKNOWLEDGMENT

I would like to express my sincere appreciation and gratitude to my advisors Dr. David Kristol and Dr. Arthur B. Ritter for the unlimited support, encouragement and confidence they provided me with throughout the course of my doctoral experience.

Special thanks to Dr. Tamara Gund and Dr. Lou Barash for serving in my doctoral dissertation committee and to Dr. Prem Yadav for not only serving as a committee member but also for his friendly assistance and sharing of his enormous experience and deep knowledge of the field of molecular modeling.

This work wouldn't be possible without the resources and technical support generously provided by Mrs. Tina Brezenoff and Mr. Constantine Tsatsos of the Academic Computing Center at the New Jersey Medical School to whom I am indebted.

I also acknowledge the continuous financial support by the Department of Chemical Engineering, Chemistry and Environmental Science of the New Jersey Institute of Technology and especially the excellent cooperation of Dr. Gordon Lewandoski and Mrs. Cindy Wos.

Finally, I would like to thank from the bottom of my heart Mrs. Peggy Schel and Ms. Nina Sedorenko at the Department of Chemical Engineering, Chemistry and Environmental Science for their unique assistance and support.

TABLE OF CONTENTS

Chapter	Page
1 INTRODUCTION.....	1
2 ELECTROSTATIC INTERACTIONS IN THE PROCESS OF RECOGNITION OF ACETYLCHOLINE BY ACETYLCHOLINESTERASE	4
2.1 Structure and Function of Acetylcholinesterases	4
2.2 Literature Review	8
2.3 Methodology	18
2.4 Results and Discussion.....	21
3 IRREVERSIBLE ORGANOPHOSPHATE INHIBITION OF ACETYLCHOLINESTERASES: STRUCTURAL AND ELECTROSTATIC ASPECTS.....	29
3.1 Introduction	29
3.2 Methodology	31
3.3 Results and Discussion.....	33
4 AN AUTOMATED DOCKING ANALYSIS OF SELECTED REVERSIBLE INHIBITORS IN HUMAN ACETYLCHOLINESTERASE	44
4.1 Literature Review	44
4.2 Methodology	57
4.3 Results	60
5 CONCLUSIONS AND RECOMMENDATIONS FOR FUTURE WORK.....	64
APPENDIX A TABLES.....	68
APPENDIX B FIGURES	89
REFERENCES	123

LIST OF TABLES

Table	Page
1 Energy variation with distance of ACh from <i>Torpedo</i> AChE	69
2 Energy variation with distance of ACh from <i>Human</i> AChE	70
3 Energy variation with distance of ACh from charge neutralized <i>Human</i> AChE..	71
4 Structural features of modeled AChE-organophosphate adducts	72
5 Energy variation with distance of Sarin PR from <i>Torpedo</i> AChE.....	73
6 Energy variation with distance of Sarin PS from <i>Torpedo</i> AChE	74
7 Energy variation with distance of DFP from <i>Torpedo</i> AChE.....	75
8 Energy variation with distance of Sarin PR from <i>Human</i> AChE	76
9 Energy variation with distance of Sarin PS from <i>Human</i> AChE.....	77
10 Energy variation with distance of DFP from <i>Human</i> AChE	78
11 Summary of steering process simulation results.....	79
12 Pattern percentages and energies of docked Analog 1	80
13 Pattern percentages and energies of docked Analog 2.....	81
14 Pattern percentages and energies of docked Analog 3.....	82
15 Interactions of carbonyl oxygen of docked analogs with active site residues	83
16 Interactions of piperidine nitrogen of docked analogs with active site residues...	84
17 Interactions of indanone ring of docked analogs with active site residues	85
18 Interactions of piperidine ring of docked analogs with active site residues	86
19 Interactions of methyl substituent of piperidine ring of docked analogs with active site residues	87
20 Selected homologous amino acid residues of <i>Torpedo</i> and <i>Human</i> AChE's	88

LIST OF FIGURES

Figure	Page
1 Schematic of neuromuscular junction.....	90
2 Mechanism of hydrolysis of acetylcholine by acetylcholinesterase	91
3 Space-fill model of crystal structure of <i>Torpedo</i> Acetylcholinesterase	92
4 Sequence alignment of <i>Torpedo</i> and <i>Human</i> Acetylcholinesterases	93
5 Superposition of structures of <i>Torpedo</i> and <i>Human</i> Acetylcholinesterases	94
6 Sequence alignment of <i>Torpedo</i> and charge neutralized <i>Human</i> AChE's.....	95
7 Superposition of structures of <i>Torpedo</i> and charge neutralized <i>Human</i> AChE's..	96
8 Superposition of structures of <i>Human</i> and charge neutralized <i>Human</i> AChE's...	97
9 Electrostatic potential map around acetylcholine	98
10 Three dimensional model of <i>Torpedo Californica</i> Acetylcholinesterase	99
11 Homology-based model of charge neutralized <i>Human</i> Acetylcholinesterase	100
12 Total energy plot with distance of ACh from <i>Torpedo</i> AChE.....	101
13 Total energy plot with distance of ACh from <i>Human</i> AChE	102
14 Total energy plot with distance of ACh from charge neutralized <i>Human</i> AChE..	103
15 Selected reversible and irreversible acetylcholinesterase inhibitors	104
16 Hydrogen bonding and hydrophobic interactions of OP moiety with active site residues in <i>Torpedo</i> AChE-Sarin PR adduct	105
17 Hydrogen bonding and hydrophobic interactions of OP moiety with active site residues in <i>Torpedo</i> AChE-Sarin PS adduct.....	106
18 Hydrogen bonding and hydrophobic interactions of OP moiety with active site residues in <i>Human</i> AChE-Sarin PR adduct	107

LIST OF FIGURES
(Continued)

Figure	Page
19 Hydrogen bonding and hydrophobic interactions of OP moiety with active site residues in <i>Human</i> AChE-Sarin PS adduct.....	108
20 Hydrogen bonding and hydrophobic interactions of OP moiety with active site residues in <i>Torpedo</i> AChE-DFP adduct	109
21 Hydrogen bonding and hydrophobic interactions of OP moiety with active site residues in <i>Human</i> AChE-DFP adduct	110
22 Total energy plot with distance of Sarin PR from <i>Torpedo</i> AChE.....	111
23 Total energy plot with distance of Sarin PS from <i>Torpedo</i> AChE	112
24 Total energy plot with distance of DFP from <i>Torpedo</i> AChE.....	113
25 Total energy plot with distance of Sarin PR from <i>Human</i> AChE.....	114
26 Total energy plot with distance of Sarin PS from <i>Human</i> AChE	115
27 Total energy plot with distance of DFP from <i>Human</i> AChE.....	116
28 Minimum energy docking conformations of Analog 1.....	117
29 Minimum energy docking conformations of Analog 2.....	118
30 Minimum energy docking conformations of Analog 3.....	119
31 Predicted lowest energy binding conformations of Analog 1.....	120
32 Predicted lowest energy binding conformations of Analog 2.....	121
33 Predicted lowest energy binding conformations of Analog 3.....	122

CHAPTER 1

INTRODUCTION

Acetylcholinesterase is an enzyme of remarkable physiological significance since it serves to terminate impulse transmissions at cholinergic synapses by rapidly hydrolyzing the neurotransmitter acetylcholine. It is an extremely effective catalyst, acting on its natural substrate acetylcholine at rates usually associated with diffusion-controlled reactions, in accordance with the enzyme's physiological role, a role whose consequences are of interest to a wide range of backgrounds, the following list being by no means exhaustive. In pharmacotherapy, the treatment of diseases such as Alzheimer's, glaucoma and myasthenia gravis which have their etiology to malfunctionings in the impulse termination process, passes through acetylcholinesterase. In the military, the study of chemical warfare agents is almost exclusively associated with the irreversible reaction of organophosphate compounds with acetylcholinesterase that causes paralysis and death. In agriculture, organophosphate insecticides are widely used.

This study is an attempt to shed more light into the functioning of this biologically important enzyme taking advantage of the enormous advances in the field of molecular modeling that closely follows those in the computer hardware and software. Of particular emphasis in this study was the controversial role of the electrostatic interactions in the process of recognition of cationic ligands by acetylcholinesterases, the irreversible poisoning of the enzyme by compounds that are used as chemical warfare agents and the binding of reversible inhibitors/promising drugs in the treatment of Alzheimer's type senile dementia to *Human* acetylcholinesterase.

This thesis is organized into five chapters. In Chapter 2, the focus is on the controversial role of electrostatic interactions in the process of recognition of the physiological substrate acetylcholine by the acetylcholinesterases. The history, biological function and some key structural features of acetylcholinesterases are covered in 2.1. The literature on the influence of the enzyme's electrostatic field on the rate of diffusional encounter between the enzyme and the substrate with all the surrounding controversy is critically reviewed in 2.2. In 2.3, details of the approach used in this part of the study that involved *Torpedo Californica*, *Human* and charge neutralized mutated *Human* acetylcholinesterases are provided and the results with an accompanied discussion follow in 2.4.

Chapter 3 is devoted to two aspects of the phenomenon of irreversible organophosphate inhibition of acetylcholinesterases, the simulation of the steering process of selected irreversible acetylcholinesterase poisons into the enzymes' binding cavity to evaluate the influence of the enzymes' surrounding electrostatic field and the modeling of the covalent adducts of the studied organophosphate compounds with *Torpedo* and *Human* acetylcholinesterases to correlate important structural features of the modeled complexes with the potency of inhibition and the efficiency of the steering process. An introduction to the military significant phenomenon of irreversible poisoning of acetylcholinesterases is given in 3.1. The methodology involved in this part of the study with the obtained results and their discussion are presented in 3.2 and 3.3 respectively.

The final point of interest of this thesis concerned a systematic docking analysis of the binding of three reversible acetylcholinesterase inhibitors in *Human* acetylcholinesterase and is treated in Chapter 4. The progress in the process of developing new efficient and selective therapeutic agents in the fight against the Alzheimer's disease is reviewed in 4.1. The automated docking-based methodology of this part of the study is given in 4.2 while 4.3 contains the results and their analysis in the identification of the plausible binding sites and the implications in the area of drug discovery.

Finally, general conclusions from this work are derived and summarized in Chapter 5 along with some recommendations for future work.

CHAPTER 2

ELECTROSTATIC INTERACTIONS IN THE PROCESS OF RECOGNITION OF ACETYLCHOLINE BY ACETYLCHOLINESTERASES

2.1 Structure and Function of Acetylcholinesterases

Cholinesterases constitute a family of enzymes which differ in their substrate specificity and susceptibility to inhibitors among different species. Depending on their substrate preference, cholinesterases fall broadly into two types although this division is not absolute and it holds true more in mammalian than in non-mammalian species. Acetylcholinesterases (AChE) are the enzymes that preferentially hydrolyze acetyl esters like acetylcholine (ACh) while butyrylcholinesterases (BChE) are non-specific cholinesterases that prefer other types of esters such as butyrylcholine.

Acetylcholinesterase (AChE, Acetylcholine Hydrolase, E.C. 3.1.1.7) was discovered in 1938 by David Nachmansohn. It is a 260-kd enzyme located in the synaptic cleft and can be readily separated from the acetylcholine receptor (Figure 1). Its physiological role is the termination of impulse transmission at cholinergic synapses by rapid hydrolysis of the neurotransmitter acetylcholine. A striking feature of this enzyme is its very high turnover number of $25,000\text{ s}^{-1}$ which means that it cleaves an acetylcholine molecule in $40\mu\text{s}$ (Stryer, 1988).

Neurotransmitters are extracellular signaling molecules released by the presynaptic neuron at a chemical synapse that relay the signal to the postsynaptic cell. A neurotransmitter can elicit either an excitatory or inhibitory response with the kind of response being determined by the receptor activated by the neurotransmitter and not by the chemical nature of the neurotransmitter.

Acetylcholine, the physiological substrate of acetylcholinesterase, is a small positively charged molecule utilized as a neurotransmitter in the process of nerve impulse transmission. Synapses in which acetylcholine is the neurotransmitter are defined as cholinergic synapses.

Acetylcholine has short life span. Once it has been exocytosed into the synaptic cleft and has transferred its chemical signal to its target receptor, the synapse must be restored to its original resting state through the destruction of the neurotransmitter. In spite of the fact that most neurotransmitters are taken up by the presynaptic neuron, acetylcholine is being enzymatically degraded to acetate and choline by acetylcholinesterase.

AChE's catalytic mechanism resembles that of a diverse group of proteolytic enzymes known as the serine proteases. Serine proteases, like trypsin and chymotrypsin, are the most thoroughly understood family of enzymes and they are characterized by the possession of a peculiarly active serine residue that is essential for their enzymatic activity.

This serine residue, identified as Ser200 in *Torpedo Californica* AChE, is ideally positioned (proximity and orientation effects) to carry out the nucleophilic attack of the carbonyl carbon of the physiological substrate ACh to form a tetrahedral intermediate (Figure 2). In this acetylation step, the imidazole ring of a neighboring histidine residue (His440 in *Torpedo* AChE) takes up the liberated proton forming an imidazolium ion (general base catalysis). This general basis catalysis is aided by a glutamic acid residue (Glu327 in *Torpedo*) that is hydrogen bonded to the histidine residue. The tetrahedral intermediate has a transient existence, decomposing to the acetyl-enzyme intermediate

under the driving force of proton donation (general acid catalysis) from His440 with the leaving amine group being replaced by water from the surrounding solvent. Finally, a reversal of the previous steps, with the water serving as the attacking nucleophile and Ser200 being the leaving group, known as the deacylation step, leads to the regeneration of the enzyme.

One of the landmarks in the study of acetylcholinesterases was the elucidation of the x-ray crystal structure (Figure 3) to 2.8 Å of *Torpedo Californica* acetylcholinesterase in 1991 by Joel Sussman's group (Sussman et al., 1991).

Acetylcholinesterase molecule is a homodimer, has an ellipsoidal shape with dimensions ~45Å by 60 Å by 65 Å and belongs to the class of α/β proteins ($\alpha_2\beta_2$ structure) consisting of a 12-stranded central mixed β sheet surrounded by 14 α helices.

The traditional view of the active site of AChE consisted of two subsites; a negatively charged 'anionic' site to which the positively charged quaternary nitrogen moiety of ACh binds and an esteratic subsite containing the actual catalytic residues. A second 'anionic' site, the 'peripheral anionic' site, around 14 Å from the active site, was proposed on the basis of the binding of long bisquaternary ligands.

The esteratic site was identified as being consisted of Ser200, His440 and a glutamate residue, Glu327, instead of the usual aspartate residue in serine proteases. These three residues form a planar array, constitute the enzyme's catalytic triad and they are positioned with respect to the rest of the protein as a mirror image of that seen in the serine proteases.

The most remarkable feature of this enzyme though is the existence of a deep and narrow gorge, the 'active site gorge', ~ 20 Å long, that penetrates halfway into the enzyme and widens out close to its base. The catalytic triad is located towards the bottom of that gorge. The O γ atom of Ser200, which can be seen from the surface of the enzyme, is located ~ 4 Å above the base of the gorge. Fourteen aromatic residues line a substantial portion of the surface of the gorge. These residues and their flanking sequences are highly conserved among acetylcholinesterases and they may be important in guiding the substrate into the active site.

No discernible 'anionic' or 'peripheral anionic' binding sites were identified. Instead, it is now well established that the quaternary nitrogen of the choline moiety binds through interactions with the π electrons of the aromatic ring of the residue Trp84 (constituting what was believed to be an 'anionic' site) while bisquaternary ammonium ligands in addition interact with the π electrons of Trp279, the previously called 'peripheral anionic' binding site.

2.2 Literature Review

Electrostatic fields around the surface of proteins are known to play an important role in molecular recognition and binding due to the long-range nature of the Coulombic interactions.

The effect of electrostatic steering was shown to enhance catalytic rates of superoxide dismutase with superoxide ion (Davis et al., 1991) and of triose phosphate isomerase with glyceraldehyde-3-phosphate (Luty et al., 1993). On the other hand, global charge-charge interactions do not appear to contribute to the association of dihydrofolate reductase with folate or NADPH since although the net charge of enzymes from different sources varies from +3 to -10 they display equivalent catalytic activity (Bajorath et al., 1991). Therefore the contribution of the electrostatic properties of an enzyme to its catalytic activity has to be evaluated for each particular enzyme.

Acetylcholinesterase is an extremely efficient enzyme believed to operate at or near the diffusion control limit (Quinn, 1987). Amino acid sequences of acetylcholinesterases from different species indicate that these enzymes carry a net negative charge ranging from -11e up to -14e (Doctor et al., 1990). Early estimates from studies of the dependence of the association rates of AChE with various substrates, led to the conclusion that electrostatic attraction is a driving force for the rapid binding of ACh to AChE (Quinn, 1987).

The first theoretical study of the role of electrostatic interactions in the process of recognition of cationic ligands by acetylcholinesterase was in 1993 from J. McCammon's group (Tan et al., 1993). In their study, Tan et al. computed the electrostatic field around the enzyme by solving the Poisson equation

$$\nabla \Phi = \frac{4\pi}{\epsilon} \rho \quad (1)$$

via a finite difference scheme. The equation relates the electrostatic potential Φ to the charge density ρ in the enzyme and the dielectric coefficient ϵ . They modeled the enzyme-solvent system as a heterogeneous dielectric continuum in which point charges are embedded. The solvent was modeled as a continuum with a high dielectric coefficient ($\epsilon=80$) and each atom of AChE as a point charge embedded in a low dielectric ($\epsilon=2$) sphere. The effect of added salt was not included. The net charge used for the AChE was -16.

Their results indicated that the electrostatic potential has the general characteristics of a monopole plus a quadrupole field. Near the enzyme active site the potential becomes negative while on the side opposite to the active site it becomes positive. They therefore postulated a mechanism for steering the a positively charged substrate or inhibitor towards the active site. According to their results, if the substrate is far from the enzyme, it only sees the net negative charge and is attracted to the enzyme from all directions. Near the enzyme, the substrate begins to feel the quadrupole field. If the substrate approaches the active site directly, it is attracted and reacts, if it approaches the side opposite the active site, it is repelled and then steered toward the active site.

Tan et al. also used Brownian dynamics simulations to calculate the diffusion-controlled rate constants for the binding of a positively charged ligand to AChE. Brownian dynamics simulations are used to compute and analyze a large number of trajectories of one reactant diffusing toward its partner under the influence of any intermolecular forces. They performed calculations under three different conditions:

diffusion subject to full electrostatic forces, diffusion subject only to the monopole moments of the monomers and diffusion without electrostatic forces. For the monopole calculations a charge of -8 was placed at the center of each monomer. Their results suggested that electrostatic interactions play a major role in enzyme-substrate encounter. The diffusion-controlled rate constant increased by an order of magnitude when the charge on the enzyme was increased by 16 units upon including the monopole interactions. The rate constant increased by another 65% when the higher moments (quadrupole) were considered. The rate constant calculated in that study with the full charge distribution was though 10 times higher than the one calculated by Quinn (Quinn, 1987). The oversimplified model used in that study with the ligand represented by a sphere and the negligence of orientational criteria were reasoned for the discrepancies.

In 1995, J. McCammon's group, in an attempt to bridge the gap between their computed rate constants and the experimentally measured ones and improve their prediction of the dependence of the rate constants on the ionic strength, modified the model used in the previously performed Brownian dynamics simulations and the criteria for the encounter of the ligand with the enzyme. The modifications involved improved representations of the ligands and the electrostatic field of the enzyme. Orientational in addition to the translational steering effects were considered this time along with dumbbell-shaped ligand models, consisting of two spheres the diffusion properties and charge distribution of which approximate those of ACh instead of the bead models they previously employed. In their published work (Antosiewicz et al., 1995a), they compare the results on the rate constants calculated for different models of the ligands under the new electrostatic field model and for different reaction criteria. They concluded that their

results support the contribution of the electrostatic field to the significant increase of the encounter rate. It is important to note that the electrostatic field favored one particular orientation of the dumbbell ligands but it accelerated encounter with the substrate in either orientation relative to the case of a neutral dumbbell. The steering effect of the electrostatic field was greater on the dumbbell than on the single-bead ligands. Once again though the computed rate constants exceeded the experimental values even though they were lower than the rate constants obtained for the single-bead models. Moreover, the strong dependence observed experimentally of the encounter rates on the ionic strength disagrees markedly with the experimental data. Therefore this work didn't challenge the role of the electrostatic interaction in the recognition process of acetylcholine by acetylcholinesterase. A combination of Brownian dynamics with Molecular dynamics simulations was proposed though as a way to overcome the conformational rigidity imposed on the enzyme.

In 1993, Joel Sussman's group, proposed an 'electrostatic mechanism for substrate guidance down the aromatic gorge of acetylcholinesterase' (Ripoll et al., 1993). They evaluated the electrostatic potential and field of AChE assuming a net charge of $-8e$ for the x-ray resolved structure of the enzyme. A strong electrostatic dipole was revealed with a negative potential extending roughly over half of the protein surface and a positive potential covering the other half. The electrostatic dipole was aligned directly along the axis defining the center of the active site gorge. This indicated that positively charged molecules, such as the physiological substrate ACh could be drawn toward and down the aromatic gorge to the active site. Their results basically supported the results of Tan et. al. mentioned previously (Tan et al., 1993). The number of charges in the active site gorge is

very small, just four acidic residues are present, one of which is a member of the catalytic triad, but there is a marked preponderance of acidic amino acids in the 'northern' hemisphere lying above the active site triad and a somewhat smaller preponderance of basic amino acids in the 'southern' hemisphere.

The contribution of the four acidic residues of the active site gorge to the overall dipole moment was assessed by neutralizing the charges on their side chains. They realized then that the dipole is generated by the overall charge distribution throughout the enzyme and is not merely due to the acidic residues in the active site gorge. Since most of the acidic residues in the 'northern' hemisphere lie behind the residues that line up the gorge, they proposed that the electrostatic dipole drives the cationic ACh down the gorge and the aromatic groups provide a series of low-affinity binding sites for the quaternary choline group, much like what takes place in an affinity electrophoresis column. The aromatic groups at the same time play a shielding role since a gorge lined with acidic residues would bind ACh too avidly to the active site triad.

The up to 1993 undisputed role of the electrostatic interactions in the steering of charged ligands and inhibitors to the active site of the enzyme was shattered in 1994 by another milestone publication in the field of cholinesterases of experimental data that suggested that the surface electrostatic properties of AChE do not contribute to the catalytic rate, that this rate is probably not diffusion-controlled and that long-range electrostatic interactions play no role in stabilization of the transition states of the catalytic process (Shafferman et al., 1994). The authors claim that the assumption of the catalytic bimolecular rate being diffusion-limited contradicts the fact that the actually

measured rate constants for various acetylcholinesterases are about an order of magnitude lower than the expected rates of diffusion-controlled reactions.

To investigate the contribution of the electrostatic interactions to the catalytic rate of AChE they generated mutant forms of *Human* AChE in which up to seven of the surface negative charges located near the rim of the active-site gorge were neutralized. A gradual shrinking of the electrostatic potential over the 'northern' hemisphere corresponding to the progressive reduction of the surface negative charge was observed. Both single and multiple replacements of acidic residues were studied to ensure no indirect effects such as conformational changes affecting enzyme stability or allosteric modulation of the active site could mask the specific contribution of the electrostatic attraction and complicate the interpretation of the kinetic data. Indeed, none of the single-site replacements had a major effect on the catalytic properties of the resulting enzymes. The effect though on the enzyme stability of the enzymic forms carrying multiple amino acid replacements was not assessed in that study.

The catalytic activity of the single- and multiple-site mutants was examined using the charged substrate acetylthiocholine (ATC) and its isosteric uncharged analog 3,3-dimethyl butylacetate (TB) to allow examination of the net effect of charge on the catalytic properties of the mutated enzymes. These two molecules differ in that the trimethylammonium moiety is replaced by a t-butyl group and the carbonyl oxygen is replaced by a sulfur. The kinetics of inhibition of the various mutants were studied also using edrophonium, a charged, reversible, active-center AChE ligand that is known (Harel et al., 1993) to interact with regions of the active center similar to those responsible for the binding of the charged substrate ATC.

The kinetic constants for reactivity of the mutants towards both the charged and the uncharged substrates and inhibitor were practically invariant indicating that the electrostatic attraction doesn't contribute to the reaction rates. Some minor variations in the values of the Michaelis-Menten constant K_m were attributed to two specific residues one of which is known to affect moderately the binding of active-center ligands (Barak et al., 1994) while the other is located very near the active center.

The conclusion of the work of Shafferman et. al. (Shafferman et al., 1994) that the rate of the enzyme-substrate reaction is not diffusion-controlled is consistent with the lack of correlation of the catalytic rate with the charge of the substrate that was previously reported (Quinn, 1987). They also suggest (Shafferman et al., 1994) that it is possible that the electrostatic attraction in aqueous solutions is cryptic while in the viscous milieu of the synaptic cleft it becomes operational. This statement along with the lack of thorough and careful assessment of the effect of the mutations vicinal to the active-site gorge studied on the enzymatic stability could be used to challenge the findings reported in this study.

A yet another Brownian dynamics study inspired by the exciting experimental findings of the work of Shafferman et. al. (Shafferman et al., 1994) appeared in 1995 by J. Andrew McCammon and Michael K. Gilson's groups (Antosiewicz et al., 1995b). The purpose of their work was to investigate whether their previously reported results from Brownian dynamics simulations, which suggested that the electrostatic steering increases the hydrolysis rate by increasing the rate of encounter of cationic substrates with the active site, could be reconciled with the experimental study of Shafferman et al. (Shafferman et al., 1994) which suggested exactly the opposite. Although their study was

based on the *Torpedo Californica* AChE existing crystal structure, the high degree of sequence homology between *Torpedo Californica* and *Human* AChE can provide the justification for their results. This theoretical study considered the 20 single- and multiple-site *Torpedo Californica* AChE homologous mutants of the study of Shafferman et al. (Shafferman et al., 1994).

They reported that although the induced mutations progressively increase the net negative charge of the enzyme to zero with a concomitant shrinking of the electrostatic potential of the enzyme, the magnitude of the dipole moment does not go to zero but falls off only about 40% while the orientation with the respect to the gorge axis does not change significantly. They did not, however, observe a clear correlation between the computed dipole moments of the various mutants and their corresponding measured apparent bimolecular rate constants. The previous observation of the authors (Antosiewicz et al., 1995a) that the encounter rate constants for cationic substrates largely exceed those for neutral ones when the reaction criteria are a short distance inside the active site gorge suggested that the degree to which the field increases the encounter rate is likely to correlate best with the fields in the immediate vicinity of the gorge. The examination of the electrostatic potentials along the gorge axis for both the wild type and the mutated enzymes showed that the potentials indeed become progressively less negative as more acidic residues are neutralized but even when all the acidic residues are neutralized, the potentials along the axis are strongly negative. This fact was reasoned to explain the agreement of the simulations results with the previous experimental findings (Shafferman et al., 1994).

Although the computations in the study of Antosiewicz et al. (Antosiewicz et al., 1995b) assumed diffusion limitation and predicted electrostatic steering, they reproduced the experimental results of Shafferman et al. (Shafferman et al., 1994) although the encounter rate constants for a cationic substrate were found to be significantly larger than those for a neutral substrate suggesting a significant electrostatic steering effect. The inherent limitation of this study of course was that the results concerned *Torpedo* AChE.

Recently, another Brownian dynamics study was published again by J. Andrew McCammon's group (Antosiewicz et al., 1996) whose objective was to correlate the calculated rate constants of the charge neutralized mutated *Torpedo* enzymes considered in their previous work (Antosiewicz et al., 1995b) with the direction of the dipole moments of those enzymes.

Their simulations indicated that the modest effects of mutations of surface acidic residues of *Human* AChE observed previously experimentally were consistent with the changes introduced by these mutations in the electrostatic field of the enzyme. The results obtained revealed that there are no simple correlations between rate constants and such global quantities as the net charge and the dipole moment. However, for all mutants characterized by the same direction of dipole moment, the calculated rate constants were nearly linearly correlated with the number of mutations. Deviations from this correlation were accompanied by larger changes in the direction of the dipole moment within the subset of mutants. They claim that their results remain in agreement with the concept of electrostatic steering by the enzyme. Moreover, they observed that this steering is limited to relatively short distances from the surface of the protein which could be attributed to any possible perturbations of the electrostatic field of the enzyme by surrounding (macro)

molecules. They suggested that the electrostatic steering is accomplished in part by directing substrate molecules that diffusively approach the enzyme at the distance of a few angstroms to the entrance of the gorge and in part by increasing the commitment to reaction for substrates as they move deeper into the gorge. They warned though that *Human* and *Torpedo* AChE are somewhat different and therefore it couldn't be expected that mutations of homologous acidic residues have the same effect in both enzymes but qualitative correspondence might be expected.

This chapter attempts a different approach targeted at the elucidation of the influence of the electrostatic field surrounding acetylcholinesterases on the process of steering positively charged substrates or inhibitors into the binding cavity of the enzyme.

Three acetylcholinesterase representatives were studied; *Torpedo Californica* acetylcholinesterase, whose x-ray crystal structure has been already elucidated and is available; *Human* acetylcholinesterase, whose structure was generated in this study based on the available structure of the homologous *Torpedo Californica* AChE; and a charge neutralized mutated *Human* acetylcholinesterase, whose structure was also generated through mutant modeling of the *Human* AChE. This charge neutralized enzyme which has seven surface acidic residues mutated has been employed in the experimental study of Shafferman et al. (Shafferman et al., 1994) which was reviewed above.

The next section describes the methodology used to carry out the investigation of the role of electrostatic interactions in the substrate steering. This includes the calculation of the electrostatic potential around acetylcholine, the modeling of *Human* and mutated *Human* AChE and the simulation of the process of steering of acetylcholine into the active site of the studied enzymes.

Section 2.4 contains the results obtained from the calculation of the electrostatic potential of ACh and the simulations of its steering process into the active site gorge along with the conclusions from this study. A further discussion of the role of electrostatics in the steering process in view of the results of this investigation.

2.3 Methodology

The x-ray crystallographic coordinates for *Torpedo Californica* acetylcholinesterase (Sussman et al., 1991) were obtained from the Brookhaven Protein Databank (PDB Entry # 1ace) and the ligand acetylcholine was extracted from the AChE-ACh complex.

The structure of the extracted ligand ACh was minimized to the local minimum energy state closest to the starting set of atomic coordinates with MAXIMIN2 using SYBYL 6.2 molecular modeling software (Tripos Inc., 1995) running on a Silicon Graphics Indigo II workstation. The Powell minimization method of MAXIMIN2 was utilized which is well suited for a wide variety of problems and is the default minimization procedure in SYBYL. The Tripos force field (Clark et al., 1989) was used throughout this study.

The partial charges of the atoms of ACh were calculated using the MNDO semiempirical molecular orbital method in MOPAC 6.0 (Stewart and Seiler). Subsequently, the electrostatic potential map around ACh was calculated and displayed using SYBYL.

The missing atoms from the side chains of 27 amino acid residues (19, 26, 42, 46, 74, 88, 89, 107, 162, 163, 253, 257, 260, 261, 268, 270, 284, 286, 299, 310, 325, 344, 350, 353, 365, 382, 413, 434, 455, 461, 478, 484, 498, 499, 508, 511, 515, 526, 533) in

the obtained structure of *Torpedo Californica* AChE were then added with SYBYL. These are polar surface residues not seen in the electron density map. The orientation of the added side chains was adjusted to eliminate steric hindrances. The Loop Search algorithm of SYBYL was then used to construct the missing 486-489 four-amino-acid segment. The Loop Search facility of SYBYL enables the use of fragments of proteins of known three-dimensional structure for building of models of unknown protein structures. The polar hydrogens were added to the structure thus obtained which was then minimized to achieve good covalent geometry, energetically acceptable hydrogen bonds and total or near total absence of steric overlaps, until the energy gradient reached a cut-off value of $0.5 \text{ kcal mol}^{-1} \text{ \AA}^{-1}$.

The modeled structure of *Torpedo Californica* AChE was used as a template to generate the three dimensional structure for *Human* AChE through the Homology Modeling module of LOOK 2.0 (Molecular Applications Group, 1995). The amino acid sequences of *Torpedo Californica* and *Human* AChE's were aligned using the Needleman-Wunsch algorithm (Needleman and Wunsch, 1970).

This homology modeling methodology of LOOK is based on the work M. Levitt (Levitt, 1992 and Levitt, 1983). The polar hydrogens were then added to the structure which was then minimized with MAXIMIN2 of SYBYL 6.2 until again the energy gradient reached a cut-off value of $0.5 \text{ kcal mol}^{-1} \text{ \AA}^{-1}$.

The three dimensional structure of a charge neutralized mutant *Human* AChE enzyme was modeled using again the Homology Modeling module of LOOK. This enzyme contained mutations of seven acidic surface amino acid residues located in the rim of the active site gorge as was utilized in the study of Shafferman et al. (Shafferman

et al., 1994) which was thoroughly discussed previously. The mutations involved were E84Q, E285A, E292A, D349N, E358Q, E389Q and D390N. This time, the amino acid sequences of *Torpedo Californica* AChE and *Human* AChE bearing these mutations were aligned and the three dimensional structure of *Torpedo Californica* was used as a template again for the modeling of the mutant *Human* enzyme.

Polar hydrogens were added to the structure of the mutated *Human* enzyme obtained through the process described above for the wild type *Human* AChE and its geometry was then optimized with MAXIMIN2 of SYBYL 6.2 until the energy gradient reached a cut-off value of $0.5 \text{ kcal mol}^{-1} \text{ \AA}^{-1}$.

The dipole axes of each one of the three AChE's modeled as previously described and ACh were aligned with SYBYL 6.2 to create the direction of the most favorable orientation for the interaction between AChE and ACh.

To study the effect of electrostatic interactions in the steering of ACh towards the active site of each one of these AChE's a code was developed using the SYBYL Programming Language to drive ACh from a distance of about 35\AA towards the $C\alpha$ of the serine residue of the enzymes' catalytic triad in the direction of the most favorable orientation, i.e. the direction of the aligned dipole axes, in 1\AA steps. The code calculated the total, electrostatic, 1-4 electrostatic and van der Waals energies of the AChE-ACh complex at each distance while ACh was rotated around the common dipole axis. The energy minimum for the most favorable rotation angle at each distance of the center of mass of the ligand from the $C\alpha$ of the serine of the catalytic triad was then recorded and the structure of the enzyme-ligand complex for the most favorable rotation angle at each

step was energy minimized with MAXIMIN2 to an energy gradient value of $0.5 \text{ kcal mol}^{-1} \text{ \AA}^{-1}$.

2.4 Results and Discussion

The amino acid sequences of *Torpedo Californica* AChE (SwissProt Accession ID: P04058) and of *Human* AChE (SwissProt Accession ID: P22303) were aligned using the Needleman-Wunsch algorithm (Needleman and Wunsch, 1970) as it is implemented in the Gap function of GCG 8.0 (Genetics Computer Group, 1994) and the generated alignment is shown in Figure 4. The percent similarity calculated is 62.628 while the percent identity is 54.096.

The root-mean-square deviation of the $C\alpha$ of the superimposed structures of *Torpedo Californica* and *Human* AChE's is 0.827 \AA (Figure 5).

The alignment of the amino acid sequences of *Torpedo Californica* (SwissProt Accession ID: P04058) and the charged neutralized mutant *Human* AChE's was also performed with GCG and is shown in Figure 6. Their percent similarity calculated is 62.116 and the percent identity is 53.754.

The root-mean-square deviation of the $C\alpha$ of the superimposed structures of *Torpedo Californica* and charge neutralized mutant *Human* AChE's is 0.865 \AA (Figure 7).

The three dimensional modeled structures of the *Human* and mutated *Human* AChE's were also superimposed (Figure 8). The calculated root-mean-square deviation of the $C\alpha$ is 0.672 \AA .

The dipole moments calculated for the wild type *Human* AChE and the charge neutralized mutant *Human* AChE based on the models constructed during the course of this study were 1018 D and 331 D respectively. This means that the charge neutral enzyme retains only 32.5% of the dipole moment of the wild type enzyme. In the case of *Torpedo Californica* AChE studied by Antosiewicz et al. (Antosiewicz et al., 1995b), the charge neutralized enzyme that contained mutations of amino acid residues homologous to the ones of the mutated *Human* AChE retained 64.5% of the dipole moment of the corresponding wild type enzyme. Consequently, in the case of the *Human* enzyme, the effect of the studied mutations on the dipole moment and therefore on the electrostatic field surrounding the enzyme is more pronounced than in the case of the *Torpedo* AChE. The significant amino acid sequence homology between the *Torpedo* and *Human* AChE's therefore should be used with particular caution in any attempt to explain experimental results concerning the *Human* enzyme by performing theoretical calculations on the *Torpedo* AChE. This is very significant since, by far, in the absence of a crystal structure for the *Human* AChE, the results from theoretical calculations on *Torpedo* AChE were extrapolated on the basis of sequence homology.

In the all-trans structure of the extracted ligand ACh, generated as described above, the calculated MNDO partial charges of its atoms suggest that the +1 total charge of this molecule is not localized on the quaternary ammonium atom as long regarded; however, it is the result of the contribution of the partial charges of all the atoms. The calculated electrostatic potential map around ACh is displayed in Figure 9 with the red contour representing positive electrostatic potential region.

The complete three dimensional structure of *Torpedo Californica* AChE is displayed in Figure 10. Figure 11 is a depiction of the three dimensional structure of the charge neutralized mutated *Human* AChE modeled during the course of this study as described above. The mutated residues near the rim of the active site gorge of the enzyme are colored purple.

The values of the total, electrostatic, 1-4 electrostatic and van der Waals energies of the minimized structures for the most favorable rotation angle at each step of the three complexes studied, *Torpedo Californica* AChE-ACh, *Human* AChE-ACh and mutated *Human* AChE-ACh, relative to the corresponding energy values of the global energy minimum, at various distances of the center of mass of the ligand from the C α of the serine residue of the enzymes' catalytic triad (whose O γ is located $\sim 4\text{\AA}$ above the bottom of the gorge in *Torpedo Californica* AChE) are presented in Table 1, Table 2 and Table 3 respectively. A perusal of these tables indicates that the electrostatic energy is the predominant form of energy. The only exception found were the *Human* AChE - ACh and mutated *Human* AChE - ACh complexes at 7, 9 and 10 \AA and at 7, 9 and 11 \AA , respectively. This is due to the existence of significant steric overlaps between atoms of the substrate and the enzymes, in close proximity to the surface of the enzymes, that give rise to high van der Waals energy values. The presence of the steric hindrances can be attributed to the relative enzyme-substrate orientation imposed by the alignment of their dipole axes. In close proximity of the substrate to the enzyme, there may be a slight deviation from the direction of the most favorable orientation caused by the particular

features that characterize the behavior of the electrostatic fields of the enzymes very close to their surfaces.

The total energy values of the *Torpedo Californica* AChE-ACh complex relative to the global energy minimum at various distances of the center of mass of ACh from the C α of the Ser200 residue are presented in Figure 12. No change in the energy of the complex was observed beyond $\approx 34\text{\AA}$ of the center of mass of ACh from the C α of the Ser200 residue of the enzyme's catalytic triad. This indicates that the electrostatic field of AChE doesn't affect ACh until they are $\approx 34\text{\AA}$ apart. As the ligand moves closer, the energy of the complex slightly changes denoting interaction between enzyme and ligand. A drastic change in energy was observed between 20 and 24\AA , suggesting that the electrostatic interactions affect the steering of the ligand once it reaches $\approx 20\text{-}24\text{\AA}$ from the active site, that is only when the ligand is in close proximity to the entrance of the active site gorge. Since the energy of the complex doesn't change significantly from $\approx 34\text{\AA}$ to $\approx 24\text{\AA}$, the steering of the ligand beyond 24\AA appears to be diffusion-controlled. Four other steep changes in energy were observed at $\approx 5\text{\AA}$, $\approx 11\text{\AA}$, $\approx 13\text{\AA}$ and at $\approx 15\text{\AA}$ preceding the local minimum energy states at $\approx 10\text{\AA}$, $\approx 12\text{\AA}$, and $\approx 14\text{\AA}$ and the global energy minimum at $\approx 16\text{\AA}$ respectively. This indicates the presence of at least four transition states, at $\approx 5\text{\AA}$, $\approx 11\text{\AA}$, $\approx 13\text{\AA}$ and at $\approx 15\text{\AA}$, and the existence of multiple steps in the catalytic reaction. Only the transition state at $\approx 5\text{\AA}$ is associated with the catalytic reaction since it meets orientation and availability requirements for the nucleophilic attack to take place.

Figure 13 presents a plot of the total energy values of the wild type *Human* AChE-ACh complex relative again to the global energy minimum at various distances of the center of mass of the ligand ACh from the C α of the Ser234 of the catalytic triad of *Human* AChE. Similarly to the case of *Torpedo Californica* AChE discussed above, the energy of the complex remained invariable beyond $\approx 35\text{\AA}$ while a steep energy change was again observed between $\approx 21\text{\AA}$ and $\approx 24\text{\AA}$. These results support again the significance of the role of the electrostatic interactions in close proximity of the ligand to the active site gorge of the enzyme.

A number of local energy minima were identified in the case of the *Human* enzyme, at $\approx 6\text{\AA}$, $\approx 8\text{\AA}$, $\approx 11\text{\AA}$, $\approx 15\text{\AA}$, $\approx 17\text{\AA}$ and at $\approx 20\text{\AA}$ with the global minimum at 17\AA (16\AA in *Torpedo* AChE). Six steep energy changes, suggesting the existence of at least six transition states, were also located at $\approx 5\text{\AA}$, $\approx 7\text{\AA}$, $\approx 9\text{\AA}$, $\approx 12\text{\AA}$, $\approx 16\text{\AA}$ and at $\approx 18\text{\AA}$ ($\approx 5\text{\AA}$, $\approx 11\text{\AA}$, $\approx 13\text{\AA}$ and $\approx 15\text{\AA}$ in *Torpedo*) preceding the local energy minima at $\approx 6\text{\AA}$, $\approx 8\text{\AA}$, $\approx 11\text{\AA}$, and $\approx 15\text{\AA}$, the global minimum at $\approx 17\text{\AA}$ and the local minimum at $\approx 20\text{\AA}$, respectively. The *Human* enzyme seems therefore to retain three out of the four transition states identified in *Torpedo Californica*, at $\approx 5\text{\AA}$ at $\approx 12\text{\AA}$ ($\approx 11\text{\AA}$ in *Torpedo*) and at $\approx 16\text{\AA}$ ($\approx 15\text{\AA}$ in *Torpedo*). The transition state at $\approx 5\text{\AA}$ is believed to be again associated with the catalytic reaction, for meeting the proximity and orientation criteria for a nucleophilic attack.

Finally, the total energy values relative to the global energy minimum for the large neutralized mutated *Human* AChE-ACh complex studied as a function of the distance of the center of mass of ACh from the C α of the active site serine residue is

plotted in Figure 14. Once more, the energy of the complex remains unchanged beyond $\approx 36\text{\AA}$, while no significant change in the energy is observed between $\approx 20\text{\AA}$ and $\approx 36\text{\AA}$. A steep energy change takes place at $\approx 19\text{\AA}$. This phenomenon is in contrast to the behavior seen in *Torpedo* and wild type *Human* AChE's where the corresponding steep energy change takes place between 20 and 24\AA and between $\approx 21\text{\AA}$ and $\approx 24\text{\AA}$ respectively. This behavior suggests that the impact of the role of the electrostatic interactions appears when the ligand is even closer to the active site gorge. This may be attributed to the weakened electrostatic field as a result of the mutations of the acidic amino acid residues near the rim of the active site gorge.

The local energy minima identified in the case of the mutant *Human* AChE were at $\approx 6\text{\AA}$, $\approx 8\text{\AA}$, $\approx 10\text{\AA}$, $\approx 12\text{\AA}$ and $\approx 16\text{\AA}$ ($\approx 10\text{\AA}$, $\approx 12\text{\AA}$, $\approx 14\text{\AA}$ and $\approx 16\text{\AA}$ in *Torpedo*, $\approx 6\text{\AA}$, $\approx 8\text{\AA}$, $\approx 11\text{\AA}$, $\approx 15\text{\AA}$, $\approx 17\text{\AA}$ and $\approx 20\text{\AA}$ in wild type *Human*). The global energy minimum is located at $\approx 10\text{\AA}$ ($\approx 16\text{\AA}$ in *Torpedo*, $\approx 17\text{\AA}$ in wild type *Human*). Therefore a shift in the global energy minimum of the complex is observed relative to the consistently located global energy minimum in *Torpedo* and wild type *Human* AChE which could be a consequence of a 'delayed' role of electrostatic interactions due to the presence of the mutations and the altered electrostatic field.

A number of transition states were also identified at $\approx 5\text{\AA}$, $\approx 7\text{\AA}$, $\approx 9\text{\AA}$, $\approx 11\text{\AA}$ and $\approx 13\text{\AA}$ preceding the local energy minima mentioned previously. It is suggested that the transition state at $\approx 5\text{\AA}$ be associated with the catalytic reaction in this case in accordance with the proximity and orientation requirements for the occurrence of a nucleophilic attack.

The results from the simulation of the process of steering of acetylcholine to the entrance of the active site gorge and into the binding cavity of the three acetylcholinesterases studied, indicate the significance of the influence of the charge interactions on the phenomenon. The consistency that both *Torpedo* and wild type *Human* AChE's have to offer in a number of aspects evaluated, the global minimum energy location, the location of local minima and transition states and the location of the diffusion-electrostatics border, the point where electrostatic interactions become effective, is very significant for a number of reasons.

It first serves the validity of the homology-based model generated in the course of this study. The modeling of the three dimensional structures of enzymes in the absence of their x-ray image, using a variety of methods developed for the purpose, is a dream come true for the field of protein structure prediction, yet undoubtedly a remedy which should be treated with caution. Second, the observed agreement in the behavior of both the *Torpedo* and the wild type *Human* enzymes is not only important for the phenomenon studied here, suggesting the similarity in the functioning of the two enzymes, but it also adds credibility to the geometry of the predicted structure on which the entire study is based.

The observed consistency also serves to identify the different behavior exhibited by the mutated *Human* enzyme as a consequence of the weakened electrostatic field of the enzyme caused by eliminating the negatively charged amino acid residues near the rim of the active site gorge.

A summary and a more complete discussion of the influence of the Coulombic interaction is attempted in 3.3 where the results from the simulation of the steering process of some irreversible inhibitors become available.

CHAPTER 3

IRREVERSIBLE ORGANOPHOSPHATE INHIBITION OF ACETYLCHOLINESTERASES: STRUCTURAL AND ELECTROSTATIC ASPECTS

3.1 Introduction

Acetylcholinesterases are the main targets of organophosphorous pesticides, insecticides and cholinergic nerve agents. Inhibition of acetylcholinesterases by organophosphates occurs through phosphorylation of the active site serine and often leads to paralysis and death (Aldridge and Reiner, 1972). The acetylcholinesterase-organophosphate conjugates can then undergo postinhibitory processes, the nature and extent of which depend upon the structure of the inhibitor and the particular enzyme. Spontaneous reactivation through displacement of the phosphoryl moiety from the active site is usually very slow (Main, 1976). However, reactivation of phosphorylated cholinesterases is possible using nucleophilic agents such as atropine and oximes that are used in the therapy of organophosphate poisoning (Aldridge and Reiner, 1972). However, after phosphorylation by certain organophosphate compounds, acetylcholinesterases progressively lose their ability to be reactivated according to first-order kinetics. This process called 'aging' is due to acetylcholinesterase-mediated dealkylation, through alkyl-oxygen bond scission, of an alkyl/alkoxy group on the organophosphate moiety, resulting in a formal negative charge in the acetylcholinesterase-organophosphate conjugate (Berman and Decker, 1986). The phenomenon of aging is particularly pronounced for acetylcholinesterase-organophosphate conjugates in which the organophosphate moiety contains a secondary alkyl group such as isopropyl or pinacolyl group (Aldridge and Reiner, 1972).

The cleavage of the C-O bond may be promoted by the negative charge on the glutamate adjacent to the phosphorylated serine (Qian and Kovach, 1993) although it appears that other residues involved in the stabilization of the functional architecture of the active center play a role in this reaction. A salt bridge formed between the P-O⁻ of the dealkylated organophosphoryl moiety and histidine of the catalytic triad could be responsible for resistance of “aged” acetylcholinesterases to reactivators (Harel et al., 1991).

Although the aging process is understood on the basis of a carbonium ion mechanism and depends on the phosphorous stereochemistry in the conjugates, the role of the enzyme environment in facilitating the process is not well understood.

The objective of this chapter is two-fold; to investigate the role of the electrostatic interactions in the steering process of selected organophosphate compounds into the active site gorge of *Torpedo Californica* and *Human* Acetylcholinesterases as well as the interactions of the organophosphate moiety in the acetylcholinesterase-organophosphate conjugates with the surrounding amino acid residues of the poisoned enzymes. The results of the structural investigations performed are also correlated with published experimental data of the phosphorylation and aging rate constants of the studied nerve agents.

3.2 Methodology

The three dimensional structures of the two organophosphate inhibitors under investigation in the present study, Sarin (isopropyl methylphosphonate) and DFP (diisopropylphosphorofluoridate) (Figure 15) were built by using the Build module of Insight (Insight 95.0, Biosym 1995). The phosphorous atom in Sarin constitutes a stereocenter and the two corresponding enantiomers are designated as Sarin PR and Sarin PS according to the Cahn-Ingold-Prelog system. The geometries for all these three small molecules, Sarin PR, Sarin PS and DFP, were then energy minimized to their nearest local energy minimum states, with MAXIMIN2 using SYBYL 6.2 molecular modeling software (Tripos Inc., 1995).

To identify low energy conformers for the three molecules under study overcoming energy barriers, a protocol constituted by molecular dynamics and energy minimization was devised. In that protocol, the local energy minimum conformations primarily obtained for the three molecules were subjected to 100 runs of a simulated annealing schedule implemented through the Dynamics module of SYBYL 6.2. The schedule involved heating of the molecules to 2000 K for 5000 ps and subsequent exponential cooling to 300 K for 2000 ps. The results of the simulated annealing calculations were then analyzed through a SYBYL Programming Language code that subjected all the generated geometries to energy minimization using MAXIMIN2. The lowest energy conformation for each molecule was then selected and the MNDO partial charges of its atoms were subsequently calculated with MOPAC 6.0 (Stewart and Seiler) implemented through SYBYL. The electrostatic field generated as a result of those

charges was also calculated and displayed in the form of isopotential contours for each one of the inhibitors employing SYBYL (Figure 15).

For the elucidation of the role of the electrostatic interactions in the process of recognition of these three irreversible inhibitors by acetylcholinesterase, the methodology followed in the study of the steering process of acetylcholine into the active site of acetylcholinesterase and described in the section 2.3 was undertaken. In the case of the organophosphate inhibitors only the *Torpedo Californica* and the wild type *Human* enzymes were employed. The low energy conformations obtained as described above were employed in this part of the study.

To obtain the geometries of the covalent adducts of these irreversible acetylcholinesterase inhibitors with *Torpedo Californica* and *Human AChE*'s, 50 runs of the simulated annealing schedule described above were performed to each one of the small molecules. A SYBYL Programming Language code was then developed that generated the covalent adduct of each one of the enzymes with each one of the conformations generated for each inhibitor by the simulated annealing calculations. The adduct formation involved simply the creation of a covalent bond between the O_γ of the serine residue of the active site and the phosphorous atom of inhibitor with the removal of the halogen substituent of the organophosphate and of the polar hydrogen of the hydroxyl of the side chain of the active site serine.

For each adduct, the torsional angle associated with the O_γ - P bond was then varied and the energy of the adduct was recorded for each value of this torsional angle. The conformation corresponding to the torsional angle of the lowest energy adduct was

subsequently selected for each enzyme and each inhibitor. Six structures were thus obtained, Torpedo - Sarin PR, Torpedo - Sarin PS, Torpedo - DFP, Human - Sarin PR, Human - Sarin PS, Human - DFP which were subjected to energy minimization to a gradient of $0.05 \text{ kcal mol}^{-1} \text{ \AA}^{-1}$. This methodology constitutes a very fast, less resource-demanding yet reliable alternative to the use of molecular dynamics for the generation of the three dimensional models of the covalent adducts of acetylcholinesterases with irreversible organophosphate inhibitors. Furthermore, the use of the simulated annealing calculations and the covalent bond's torsional angle variation conserves the exploration of space for the covalent modification - modified side chain of the active site serine while holding the rest of the enzyme rigid.

3.3 Results and Discussion

The structures of the three organophosphate inhibitors considered in the study of the effect of the electrostatic interactions in the process of irreversible poisoning of acetylcholinesterase are shown in Figure 15. These are the geometries for Sarin PR, Sarin PS and DFP, obtained through the combination of the use of simulated annealing and energy minimization calculations described in the previous section. The calculated electrostatic maps for these molecules are also depicted in Figure 15. All three inhibitors are polar molecules and the red and blue contours represent negative and positive electrostatic potential regions respectively.

Acetylcholinesterase-organophosphate Conjugates

In the modeled three dimensional structure of the *Torpedo Californica* AChE - Sarin PR adduct (Figure 16), the phosphoryl oxygen forms a hydrogen bond (1.58 Å) with the amide hydrogen of Gly119 maintaining close contacts to the amide hydrogens of the rest two members of the enzyme's 'oxyanion hole', Gly118 (2.75 Å) and Ala201 (2.97 Å). The O_γ of the phosphorylated Ser200 residue also hydrogen-bonds with the amide hydrogen of Ala201 (1.69 Å). Glu199, whose negative charge has been proposed to stabilize the resulting carbonium ion, is located very distantly from the leaving isopropyl group and the two oxygens of its sidechain hydrogen-bond with the amide hydrogen of Gly118 (1.67 and 2.80 Å). The methyl and isopropyl substituent groups of the organophosphate moiety are engaged in hydrophobic interactions with the aromatic sidechains of Trp84 and Phe331, Phe288, Phe290 and Trp233 respectively. The distance of the N_ε2 atom of the His440 residue of the enzyme's catalytic triad from the alkylated oxygen is 2.70 Å.

In the *Torpedo Californica* AChE-Sarin PS adduct (Figure 17), which is higher energetically than the *Torpedo Californica* AChE-Sarin PR conjugate analyzed above, the phosphoryl oxygen forms again a hydrogen bond (1.61 Å) with the amide hydrogen of Gly119 and is located close to Gly118 (3.53 Å from the amide hydrogen) and Ala201 (2.92 Å from the amide hydrogen). The O_γ of the phosphorylated Ser200 residue forms a hydrogen bond (1.70 Å) with the amide hydrogen of Ala201 and is 3.18 Å away from the N_ε2 atom of His440. Glu199 is in this adduct closer to leaving isopropyl group while the N_ε2 atom of the His440 is 2.93 Å away from the alkylated oxygen atom of the

phosphonyl moiety. The methyl and isopropyl groups of the phosphonyl moiety interact with the aromatic sidechains of Trp233, Phe290, Phe288 and Phe331 and Trp84 respectively.

The phosphonyl oxygen in the *Human* AChE-Sarin PR conjugate (Figure 18), forms a hydrogen bond (1.64 Å) with the amide hydrogen of Gly153 (homologous to Gly119 in *Torpedo Californica* AChE) and interacts with the amide hydrogens of Gly152 (3.08 Å) and Ala235 (3.15 Å). Gly152 and Ala235 are homologous to the Gly118 and Ala201 residues of the oxyanion hole of *Torpedo Californica* AChE. The O γ of the phosphorylated active site Ser234 forms a hydrogen bond (1.66Å) with the amide hydrogen of Ala235 and is located 3.35 Å away from the N ϵ 2 atom of active site His478. The distance between the alkylated oxygen and the N ϵ 2 atom of active site His478 is 2.69 Å in this adduct. Glu233, which is homologous to Glu199 in *Torpedo Californica* AChE, is located distantly to the leaving isopropyl group but it forms a hydrogen bond (1.59 Å) with the amide hydrogen of Gly152. The isopropyl moiety of the organophosphate engages in hydrophobic interactions with the aromatic sidechains of Trp267, Phe328, Phe326 and Phe369 (which are homologous to Trp233, Phe290, Phe288 and Phe331 amino acid residues respectively of *Torpedo Californica* AChE).

The *Human* AChE-Sarin PS conjugate is characterized by a lower energy than the corresponding conjugate with Sarin PR (Figure 19). The phosphonyl oxygen forms a hydrogen bond (1.59 Å) with the amide hydrogen of Gly153 interacting with the amide hydrogens of Gly152 (3.88 Å) and Ala235 (3.13 Å). The O γ of the phosphorylated active site Ser234 forms a hydrogen bond (1.72 Å) with the amide hydrogen of Ala235. The

distance of the alkylated oxygen atom from the N ϵ 2 atom of the active site His478 residue is 3.41 Å while the Glu233 residue is ~ 4 Å away from the leaving isopropyl group. The methyl group of the phosphonyl moiety interacts with the aromatic sidechains of Trp267, Phe328, Phe326, Phe369 and His478.

The phosphonyl oxygen in the *Torpedo Californica* AChE-DFP adduct (Figure 20), forms a hydrogen bond (1.60 Å) with the amide hydrogen of Gly119 and is 2.64 Å and 3.16 Å away from the amide hydrogens of Gly118 and Ala201 respectively. The O_y of the phosphorylated active site Ser200 residue forms a hydrogen bond (1.66 Å) with the amide hydrogen of Ala201 and is 3.54 Å away from the N ϵ 2 atom of His440. The distances of the N ϵ 2 atom of His440 from the alkylated oxygen atoms are 3.01 and 4.11 Å. Glu199 is located close to the isopropyl group (3.53 Å) whose corresponding alkylated oxygen is further away from the N ϵ 2 atom of His440 and it is involved in a hydrogen bond network with Gly118 (1.64 Å and 2.71 Å) and Gly117 and Tyr130. Only the isopropyl group whose corresponding alkylated oxygen is closer to the N ϵ 2 atom of His440 engages in hydrophobic interactions with the aromatic sidechains of Phe288, Phe331, Trp233, Phe290 and His440.

Finally, in the *Human* AChE-DFP conjugate (Figure 21), which is energetically higher than the *Torpedo* AChE-DFP adduct, the phosphonyl oxygen forms a hydrogen bond (1.59 Å) with the amide hydrogen of Gly153 and is located 3.02 and 3.07 Å away from the amide hydrogens of Gly152 and Ala235 respectively. The O_y of the phosphorylated Ser234 residue of the active site forms a hydrogen bond (1.70 Å) with the amide hydrogen of Ala235 and is 3.28 Å away from the N ϵ 2 atom of the His478 residue

of the catalytic triad. Both alkylated oxygens are located within 2.88 Å away from the Nε2 of the His478 residue. Glu233 is 3.95 Å away from the closest isopropyl moiety and it forms a hydrogen bond with the amide hydrogens of Gly152 (1.59 Å) and Gly151 (1.6 Å). The isopropyl group more distantly located from the Glu233 residue interacts with the aromatic groups of Phe369, Phe326, Trp267, Phe328 and His478.

The interactions identified above of the various organophosphate moieties studied with the neighboring amino acid residues of the poisoned enzymes are summarized in Table 4 and are in excellent agreement with previously published results (Qian et al., 1993, Ordentlich et al., 1993, Barak et al., 1992).

For the adducts of Sarin PR and Sarin PS with the *Human* AChE, the previously observed (Barak et al., 1992) more unfavourable energy of the Sarin PR adduct is successfully reproduced. Since the distance of the Nε2 atom of the His amino acid residue of the catalytic triad from the alkylated oxygen atom of the phosphonyl moiety is indicative of the facilitation of aging, our results indicate that the proton transfer and therefore the aging process most readily occur in the *Human*-Sarin PR adduct than in *Human*-Sarin PS. This conflicts with the results of Barak et al. (Barak et al., 1992). The distance of the Nε2 atom of the active site His from the alkylated oxygen of the acetylcholinesterase-organophosphate adducts can be used to compare the aging tendency of the conjugates.

Simulation of the Steering Process

The values of the total, electrostatic, 1-4 electrostatic and van der Waals energies of the minimized structures for the most favorable rotation angle at each step, obtained with the

methodology described in detail in Section 2.3, of the six complexes considered, *Torpedo Californica* AChE - Sarin PR, *Torpedo Californica* AChE - Sarin PS, *Torpedo Californica* AChE - DFP, *Human* AChE - Sarin PR, *Human* AChE - Sarin PS, *Human* AChE - DFP, are presented in Tables 5-10. These values, which are relative to the corresponding energy values of the global energy minimum, are given at various distances of the center of mass of the inhibitors from the C α of the serine residue (Ser200 for *Torpedo* and Ser234 for *Human* AChE) of the enzymes' catalytic triad.

As mentioned in Section 2.4, in the case of acetylcholine, a positively charged molecule, the electrostatic energy is the predominant form of energy in the steering process of acetylcholine into the active site of *Torpedo Californica* AChE while in the cases of the wild type and charge neutralized mutant *Human* AChE's the presence of significant steric overlaps in close proximity to the surface of the enzyme results in high van der Waals energy values near the surface of the enzyme and in the predominance of this form of energy. Although the surface morphology of the enzyme can be the cause of those steric overlaps, the expected difference in the direction of the aligned dipole moment axes of the enzyme - ligand system can also function as a major contributor.

A perusal of the Tables 5-10 indicates that the electrostatic energy is by large the predominant form of energy in all six cases studied. There are three notable though very isolated exceptions to the above statement, in the *Torpedo* AChE - Sarin PR, *Torpedo* AChE - DFP and the *Human* AChE - DFP complexes with the steric overlaps appearing at 16, 15 and 10 Å respectively. As mentioned previously, these phenomena are probably the result of the modified direction of the aligned dipole moment axes of the complexes.

Also the values reported reflect the energy minimization to which the complexes were subjected, which leads to the local energy minimum closest to the initial conditions. These phenomena occur however at distances very close to the active site gorge and cannot affect any conclusions concerning the behavior at the diffusion-electrostatics border region.

The total energy values of the *Torpedo Californica* AChE - Sarin PR complex relative to the global energy minimum at various distances of the center of mass of Sarin PR from the C α of the Ser200 residue are presented in Figure 22. The total energy of this complex is constant beyond 35 Å and as the inhibitor moves closer to the enzyme, the energy of the complex changes only slightly until enzyme and inhibitor are 24 Å apart. This indicates that the steering of Sarin PR appears to be diffusion - controlled beyond 24 Å. This is in agreement with the observed behavior of the *Torpedo* AChE - ACh complex reported in Section 2.4. A steep energy change occurs at 24 Å suggesting that the electrostatic interactions affect the steering of the inhibitor when it is in close proximity to the entrance of the active site gorge of the enzyme. The global energy minimum of the complex is present at 18 Å versus at 16 Å in the case of acetylcholine, the natural substrate of the enzyme. A number of energy minimum states preceding steep energy changes is indicative of the existence of multiple transition states and therefore of multiple steps in the catalytic reaction with Sarin PR preserving the pre-global minimum point transition state behavior exhibited by acetylcholine. The trend observed for the electrostatic energy values of the complex resembles that of the total energy values since,

as aforementioned, the electrostatic energy is the predominant form of energy. The only difference exists at 16 Å and its etiology was covered also above.

Figure 23 presents the graphical representation of the relative total energy values of the *Torpedo* AChE - Sarin PS complex, versus the distance of the center of mass of Sarin PS from the C α of the Ser200 residue of *Torpedo* AChE. The global energy minimum of the complex is present at 17 Å (versus at 18 Å in Sarin PR and at 16 Å in acetylcholine). The phenomenon of the multiple transition states - multiple transition steps in the catalytic reaction is also present here with two out of the three pre-global minimum transition states of the acetylcholine being conserved. Again in the case of Sarin PS, the total energy of the complex remains constant beyond 35 Å, while it is effectively invariant between 22 Å and 35 Å and the steep change in energy, previously experienced at 24 Å now appears at 22 Å. The significant identity in the trends of the total and the electrostatic energy values of the complex supports the predominance of the electrostatic energy in the steering process.

The results from the simulation of the steering process of DFP into the active site of *Torpedo* AChE are presented in Figure 24. The first notable difference with the behavior seen so far for Sarin and ACh is the location of the global minimum at 11 Å (16 Å in acetylcholine, 18 Å in Sarin PR and 17 Å in Sarin PS). The energy of the complex is even in the case of this inhibitor constant beyond 34 Å and effectively invariant between 23 Å and 34 Å. The total and electrostatic energy values exhibit the previously observed similarity in their trends as a result of the predominant role of the electrostatic energy.

We start analyzing the steering processes of the three inhibitors into the active site of the *Human* AChE considering Sarin PR. The plot of the relative total energy values with the distance of the center of mass of Sarin PR from the C α of the Ser234 of the *Human* AChE is given in Figure 25. The global energy minimum of the complex is located in this case at 15 Å (18 Å in the complex with *Torpedo*, 17 Å in the complex *Torpedo* AChE - ACh). The relative total energy of the complex is consistently constant beyond 34 Å exhibiting only slightly changes between 22 Å and 34 Å, behavior which has been invariantly experienced for all three inhibitors and the natural substrate with both the *Torpedo* and the *Human* AChE. The pattern of the local energy minimum states is very similar with the one in the *Human* AChE - ACh case with the trends of the total and electrostatic energy values being identical in the case of *Human* AChE - Sarin PR due to the predominant role of the electrostatic energy in the steering process.

Figure 26 contains the plot of the relative total energy values of the *Human* AChE - Sarin PS complex as a function of the distance of the center of mass of Sarin PS from the C α atom of the Ser234 residue of the active site of *Human* AChE. A shift in the location of the global energy minimum, this time found at 11 Å is surprising since so far it consistently resided within 1 - 2 Å from 16 Å. No surprises though in the location of the diffusion - electrostatic energy border region, with constant energy beyond 33 Å and the steep energy change happening at 22 Å signaling the commencement of the electrostatic energy affecting the energetics of the steering process. The pattern of the locations of the local energy minimum states is within 1 - 2 Å preserved when the pattern of the *Torpedo* AChE - Sarin PS is considered.

Finally, the graphical representation of the relative total energy values for the *Human* AChE - DFP complex with the distance of the inhibitor from the active site gorge of the enzyme is given in Figure 27. Two significant deviations from an overall similar picture in the behavior of the inhibitors and the natural substrate during their steering process are observed, the location of the global energy minimum of the complex at 5 Å and the absence of the steep character in the energy change signaling the “take-over” of the electrostatic interactions from the diffusion-controlled regime, at 21 Å. This is also the only difference in the trends of the total and electrostatic values.

The results of the simulation of the steering process of acetylcholine and the three irreversible organophosphate acetylcholinesterase inhibitors into the active site gorge of *Torpedo Californica* and *Human* acetylcholinesterases have been summarized in Table 11 to further facilitate their proceeding evaluation. The results have been categorized according to the global energy minimum location, the location of the various transition states and the diffusion-electrostatics border which signifies the ‘take-over’ of the coulombic interactions from the pure diffusional movement of the small molecules.

The location of the diffusion-electrostatics border is consistently present within 1-2 Å from 23 Å. The only notable exception existing the charge neutralized mutated *Human* AChE and has been attributed (section 2.3) to the weakened electrostatic field of the enzyme.

The location of the global energy minimum of the complexes follows a more complicated behavior. The global energy minimum for DFP is consistently present at very close distances of the inhibitor from the enzyme, closer than in the case of Sarin and ACh. This could be attributed to the very low affinity of DFP for acetylcholinesterases

relative to the affinity of Sarin and the natural substrate. The exception in this trend though is in the case of Sarin PS in the *Human* AChE when it is known that acetylcholinesterases exhibit a stereoselectivity towards the S isomers.

With the exception of the cases just described above, the small molecules investigated exhibit a similar behavior during the simulation of the steering process. More significantly, our results support the crucial role of the coulombic interactions in the recognition process. A further and more critical consideration of the effect of the induced mutations in the human enzyme on the electrostatic field and the architecture of the active site of the enzyme is necessary to ensure the preservance of the structural integrity and the credibility of the published experimental data that deny the influential role of electrostatic interactions in the steering process. A preliminary investigation in the course of this study based on the solvation energy calculations of the wild type and the charge neutralized mutant human enzymes indicates a possible 'refolding' of the mutant enzyme which could be held responsible for the surprising experimental results of Shafferman et al. (Shafferman et al., 1994).

CHAPTER 4

AN AUTOMATED DOCKING ANALYSIS OF SELECTED REVERSIBLE INHIBITORS IN HUMAN ACETYLCHOLINESTERASE

4.1 Literature Review

The principal biological role of acetylcholinesterase is to terminate impulse transmission at cholinergic synapses by rapid hydrolysis of the neurotransmitter acetylcholine. One strategy to enhance cholinergic neurotransmission is to inhibit acetylcholinesterase. Anticholinesterase agents are therefore of therapeutic importance and they are currently under active consideration for managing Alzheimer's disease. Reversible acetylcholinesterase inhibitors have been tested as alternative drugs for Alzheimer's disease and produced some mixed results but suggest that these agents may be able to enhance memory in patients with Alzheimer's type senile dementia.

Different chemical classes of reversible acetylcholinesterase inhibitors have been synthesized and evaluated as possible therapeutic agents in the treatment of Alzheimer's type of dementia. Treatment with 1,2,3,4-tetrahydro-9-aminoacridine (THA) has demonstrated moderate but significant efficacy in Alzheimer's type senile dementia. THA was recently approved by the FDA becoming the first available treatment for Alzheimer's disease in the United States. However the aminoacridines suffer from dose-limiting hepatotoxic effects which are believed to be structure related. 1-benzyl-4-[(5,6-dimethoxy-1-indanon-2-yl)methyl]piperidine (E-2020) has attracted much attention as a possible therapeutic agent in the treatment of mild or moderate forms of Alzheimer's disease. E-2020 is readily synthesized and has higher potency in inhibiting acetylcholinesterase, higher selectivity for acetylcholinesterase versus

butyrylcholinesterase and longer duration of action in comparison with tacrine (THA) and appears also to be devoid of the unfavorable side-effect profile of THA because of its novel benzylpiperidine structure. E-2020 has successfully completed phase III clinical studies in the United States for treatment of senile dementia disease.

A primary goal behind the synthesis of new series of acetylcholinesterase inhibitors has been to overcome the serious, potentially lethal side effects of short duration of action and a narrow therapeutic window of existing anticholinesterase agents towards the development of more effective and selective compounds. Ligand - receptor docking analysis along with structure - activity relationship data can aid significantly the rational drug design process providing further insight into the relationship between the biological activity and the structure of various anticholinesterase agents through an understanding of the key modes of interactions of the ligand with the receptor.

The availability of the crystal structure of the receptor *Torpedo Californica* acetylcholinesterase (Sussman et al., 1991) provided a wealth of information regarding the existence of multiple ligand binding sites and the functionality of a number of amino acid residues in those sites. A good fit of the extended all - trans conformation of acetylcholine was obtained by manual docking (Sussman et al., 1991). The acyl group was positioned to make a tetrahedral bond with the O γ of the Ser200 residue of the catalytic site of the enzyme, while the quaternary group of the choline moiety was placed within van der Waals distance (~ 3.5 Å) of Trp84. The model suggested that the ester oxygen may interact with the imidazole of His440. Glu199, which was suspected of serving as an anionic component of the substrate - binding site, appeared to make close

contacts ($\sim 3 \text{ \AA}$) both to one of the quaternary methyl groups and to the α -carbon of the choline moiety.

It has been proposed that the active site of acetylcholinesterase comprises an esteratic subsite, containing the catalytic machinery of the enzyme and an 'anionic' subsite which binds the quaternary group of acetylcholine while the presence of a second, 'peripheral' anionic subsite, distal to the active site was also postulated. The crystal structures of the complexes of *Torpedo Californica* acetylcholinesterase with three reversible inhibitors, EDR [ethyl(3-hydroxyphenyl)dimethylammonium], THA and decamethonium (DECA) showed the presence of Trp84 and Phe330 in the 'anionic' subsite and suggested that a distal residue, Trp279, near the top of the gorge is also involved in ligand binding and may be part of the 'peripheral' anionic site (Harel et al., 1993 and Silman et al., 1993). In the case of DECA (Figure 15), both quaternary groups are in van der Waals contact with tryptophan indole rings. One is apposed to that of Trp84 at the base of the gorge and the distal quaternary group is similarly apposed to the indole ring of Trp279, $\approx 12 \text{ \AA}$ distant, at the top of the gorge. In edrophonium (EDR) (Figure 15), the quaternary group nestles adjacent to the indole of Trp84, a position virtually equivalent to that of the proximal quaternary group of DECA. The m-hydroxyl group is positioned between Ne2 of His440 and Oy of Ser200, making hydrogen bonds of 3.0 and 3.5 \AA respectively, to two of the three members of the catalytic triad. There is also a 3.5 \AA hydrogen bond to N of Gly119 which is part of the oxyanion hole of acetylcholinesterase. THA (Figure 15) was found to be stacked against Trp84, its ring nitrogen hydrogen-bonding to the main - chain carbonyl oxygen of His440. Its amino

nitrogen forms a hydrogen bond to a water molecule. In all three complexes, the only residue undergoing a conspicuous conformational change is Phe330. THA is 'sandwiched' between the rings of Phe330 and Trp84.

Pang et al. performed automated docking studies to predict the binding sites of Huperzine A (Figure 15), one of the most potent and selective reversible inhibitors of acetylcholinesterase (Pang et al., 1994a). Their docking strategy, accomplished through their in-house developed code SYSDOC, allowed for flexibility of both the ligand and the receptor to permit conformational changes upon binding and accounted for steric, electrostatic, hydrogen bonding and cation - π interactions, which are very important in the binding of acetylcholinesterase. Molecular flexibility was accomplished by generating complexes with different conformers of the guest and the host. A systematic search procedure was used to obtain the different guest conformers while for the host, a series of molecular dynamics calculations was performed, in the presence of water molecules in the binding cavity to prevent shrinkage or collapse of the binding site during the dynamics simulations. In each of the derived complexes, the guest was systematically translated and rotated in the putative binding pocket of the host, within a box encompassing the space confined by the 14 aromatic amino acid residues on the surface of the gorge of acetylcholinesterase, to evaluate energetically favorable binding sites for each available conformation of the host - guest pair. The affinity of binding in the docking study is estimated from the potential energy of the complex relative to the potential energies of the guest and host in their free state, assuming that the differences in entropy and solvation energies between two binding sites can be neglected. The effect of

the solvent was not included in the calculations. A single low-potential-energy conformer of Huperzine A (HA) was generated with systematic search and 69 different conformers of *Torpedo Californica* AChE with the molecular dynamics simulations. SYSDOC revealed that HA binds to the bottom of the gorge in of *Torpedo Californica* AChE above Trp84 (catalytic domain) and to the opening of the gorge near Trp279 (peripheral domain). Three partially overlapping subsites were identified in the catalytic domain, differing in the hydrogen bonding motif (i.e., the lactam hydrogen atom of HA forms a hydrogen bond with the hydroxyl oxygen atoms of Tyr121 in subsite 1, Tyr130 in subsite 2 and Ser122 in subsite 3; the pyridone oxygen atom of HA forms a hydrogen bond with the peptide hydrogen atoms of Gly119 in subsite 1, Ser124 in subsite 2 and Asp72 in subsite 3). These subsites share the cation - π interactions of the ammonium group of HA with the aromatic groups of Trp84 and Phe330 and the ionic interactions of the ammonium group with the carboxyl groups of Asp72 and Glu199. In the peripheral domain there is one site where the ammonium group of HA partially interacts with the indole ring of Trp279 and is exposed to the solvent, possibly forming hydrogen bonds with solvent molecules. At this site, the amide hydrogen atom of HA forms a hydrogen bond with the carbonyl oxygen atom of Arg289 and the pyridone oxygen atom of HA forms a hydrogen bond with the hydroxyl hydrogen atom of Ser286.

A novel new class of acetylcholinesterase inhibitors are the indanone - piperidine derivatives of which E-2020 (Figure 15) shows potent inhibitory action in both in vitro and ex vivo studies. The IC_{50} of E-2020 in vitro is 5.3 nM as compared to THA (52 nM) and physostigmine (0.43 nM). E-2020 inhibits acetylcholinesterase 570 - fold more

selectively than butyrylcholinesterase. A number of quantitative structure - activity relationship studies have been published before the availability of the crystal structure of acetylcholinesterase, focusing on the substituted indanone and benzylpiperidine rings of indanone-benzylpiperidine reversible inhibitors of acetylcholinesterase (Cardozo et al., 1992a and Cardozo et al., 1992b). Pang et al. employed their SYSDOC strategy to perform a docking analysis of E-2020 (Pang et al., 1994b). In terms of size and flexibility, E-2020 resembles DECA which bonds into the acetylcholinesterase cavity spanning the whole gorge with its two ammonium groups interacting with Trp84 at the bottom and Trp279 at the opening of the gorge. E-2020 possesses one ammonium group though which may interact with either Trp84 or Trp279. It also contains two aromatic functional groups and exhibits no stereoselectivity (both the R- and S-isomers are equally active). In their docking simulations, Pang et al. utilized a pre-E-2020 lacking the two methoxy groups to overcome the computational burden of the large number of torsional angles present. Their systematic search produced 120 different conformers of (R)-pre-E-2020 and 104 different conformers of (S)-pre-E-2020 which were docked into the 69 different conformers of *Torpedo Californica* AChE obtained with the molecular dynamics simulations. The pre-E-2020 docking revealed that 36 different conformers of the (R)-isomer and 24 different conformers of the (S) - isomer possess suitable backbone conformation to fit into the gorge of AChE. Then the docking of E-2020 was performed by adding the two missing methoxy groups. The docking studies revealed that (R)-E-2020 possesses three overlapping binding sites and that at each site it spans the whole gorge. Sites I and II are more favorable than site III based on the calculated binding energies. At site I, the ammonium group interacts with the aromatic groups of Trp84,

Phe330 and Tyr334 as well as the carboxyl group of Asp72; the phenyl group interacts with the aromatic groups of Trp84 and Phe330; the indanone moiety interacts with the aromatic groups of Tyr70, Tyr121, Trp279 and Phe290; the carbonyl oxygen atom forms a hydrogen bond with the amide hydrogen atom of Phe288; and the proton at the piperidine nitrogen forms a hydrogen bond with the hydroxyl oxygen atom of Tyr121. At site II, the ammonium group interacts with the aromatic groups of Trp84, Phe330 and Tyr334 as well as the carboxyl group of Asp72; the phenyl group interacts with the aromatic groups of Trp84 and His440; the indanone moiety interacts with the aromatic groups of Tyr70, Tyr334 and Trp279; the carbonyl oxygen atom forms a hydrogen bond with the hydroxyl hydrogen atom of Tyr121; and the proton at the piperidine nitrogen forms a hydrogen bond with the hydroxyl oxygen atom of Tyr121. At site III, the ammonium group interacts with the aromatic groups of Tyr70, Tyr121 and Trp279; the phenyl group interacts with the aromatic group of Trp279; the indanone moiety interacts with the aromatic groups Trp84, Phe330 and Tyr334; the methoxyl oxygen atom at the 6-position of the indanone forms a hydrogen bond with the hydroxyl hydrogen atom of Tyr121 and the proton at the piperidine nitrogen forms a hydrogen bond with the hydroxyl oxygen atom of Tyr70. Site I is different from site II only in that the hydrogen bond donor for the carbonyl oxygen atom of E-2020 is the amide hydrogen atom of Phe288 at site I and the hydroxyl hydrogen atom of Tyr121 at site II. The two methoxy groups of (R)-E-2020 are exposed to the solvent at sites I and II.

Similar to the (R)-E-2020, (S)-E-2020 possesses three overlapping binding sites, two of which (I and II) are more favorable than site III and at each site it spans the whole gorge. At site I, the ammonium group interacts with the aromatic groups of Trp84 and

Phe330 as well as the carboxyl group of Asp72; the phenyl group interacts with the aromatic groups of Trp84, Phe330 and His440; the indanone moiety interacts with the aromatic groups of Tyr70, Tyr121, Tyr334 and Trp279; the carbonyl oxygen atom forms a hydrogen bond with the amide hydrogen atom of Phe288; and the proton at the piperidine nitrogen forms a hydrogen bond with the hydroxyl oxygen atom of Tyr121. At site II, the ammonium group interacts with the aromatic groups of Trp84, Phe330 and Tyr334 as well as the carboxyl group of Asp72; the phenyl group interacts with the aromatic groups of Trp84, Phe330, Tyr334 and His440; the indanone moiety interacts with the aromatic groups of Tyr70, Tyr334 and Trp279; the carbonyl oxygen atom forms a hydrogen bond with the hydroxyl hydrogen atom of Tyr121; and the proton at the piperidine nitrogen forms a hydrogen bond with the hydroxyl oxygen atom of Tyr121. At site III, the ammonium group interacts with the aromatic groups of Tyr70 and Trp279; the phenyl group interacts with the aromatic groups of Tyr70 and Trp279; the indanone moiety interacts with the aromatic groups of Trp84, Phe330, Tyr334 and His440; the methoxyl oxygen atom at the 6-position of the indanone forms a hydrogen bond with the amide hydrogen atom of Gly119; and the proton at the piperidine nitrogen forms a hydrogen bond with the hydroxyl oxygen atom of Tyr70. Similar to (R)-E-2020, site I is different from site II only in that the hydrogen bond donor for the carbonyl oxygen atom of E-2020 is the amide hydrogen atom of Phe288 at site I and the hydroxyl hydrogen atom of Tyr121 at site II. The two methoxyl groups of the (S)-isomer are also exposed to the solvent at sites I and II. The authors concluded that sites I and II are the binding sites for both isomers of E-2020 with site III considered as an 'unlikely' one. They could not

though specify which site, I or II, is preferred for E-2020. Available structure - activity data support the availability of both sites I and II to E-2020.

The results of the docking analysis of Pang et al. (Pang et al., 1994b) are supported by the findings of the study of Villalobos et al. (Villalobos et al., 1994). Villalobos et al. report on the synthesis, structure-activity relationships and possible mode of binding of a series of N-benzylpiperidine benzisoxazoles and related derivatives, compounds that incorporate bioisosteric replacements for the benzoyl moiety and are devoid of chiral centers that could undergo facile racemization. Their modeling strategy consisted of an initial manual docking of a benzisoxazole inhibitor within the gorge by locating possible salt bridge and hydrogen -bonding sites on the protein that could complement those found on the inhibitor. Asp72 was the only accessible negatively charged amino acid and the inhibitor was placed in the gorge with the piperidine N-H oriented in a roughly perpendicular fashion to the plane defined by the carboxylate group of Asp72 and was consistent with the results of the study of Pang et al. (Pang et al., 1994b) for E-2020. Then, extended molecular dynamics calculations were performed on this system with explicit solvent. Their results indicate the presence of hydrogen bond between the positively charged piperidine and the carboxylate side chain of Asp72, 90% of the time, between the benzisoxazole oxygen and the backbone N-H of Phe288, 93% of the time. The N-benzyl substituent forms an off-center π - stacking interaction with the indole side chain of Trp84 with a distance near the minimum reported for a planar π - stacked interaction between two benzene rings in the gas phase. The phenyl ring of

Phe330 interacts with the phenyl ring of the benzisoxazole inhibitor and the indole chain of Trp279 forms an edge - to - face contact pair with the benzisoxazole.

Two putative binding sites for THA and other reversible acetylcholinesterase inhibitors in the three dimensional structure of *Torpedo Californica* AChE, one being the catalytic site and the other near the residues Trp279, Tyr70 and Phe290 were previously identified. The latter constitutes the so called peripheral site, located at the opening of the enzymatic binding pocket, far from the catalytic site at the bottom of the gorge. The catalytic site has been shown by x-ray crystallography to bind THA but no THA was found in the peripheral site. The peripheral site is absent from mammalian butyrylcholinesterase. Based on the presence of these two binding sites, a series of alkylene linked bis-THA and alkylene linked benzyl-THA analogs were developed (Pang et al., 1996). The alkylene linked bis-THA analogs were up to 10000-fold more selective and 1000-fold more potent than THA in inhibiting rat AChE and yet they required one simple reaction to synthesize. The best chain length for the bis-THA analogs was determined experimentally to be 7 methylene groups between the two THA's. A spacing of 7 methylene units was found to be optimal in the case of the alkylene linked benzyl-THA analogs which were though less potent than the bis-THA analogs. The results of that study demonstrate the powerful capabilities provided by the combination of docking analysis with structure - activity data in the rational drug design process.

Yamamoto et al. performed a docking analysis of a series of benzylamino acetylcholinesterase inhibitors with a phthalimide, benzoyl or indanone moiety (Yamamoto et al., 1994). Since there is no available three dimensional structure for the *human* AChE, based on its high amino acid sequence homology with the *Torpedo*

Californica AChE which was recently crystallized, and due to the fact that the residues constituting the surface of the ligand - binding pocket are identical in the two acetylcholinesterases except for Phe330 which is replaced with Tyr in the *Human* enzyme, they replaced Phe330 by Tyr with the identical conformation in the *Torpedo* AChE and used that as a model for the *Human* AChE in their docking studies. The program DOCK developed by one of the authors was employed in the their docking analysis. DOCK represents the negative image of the binding site as a cluster of spheres and docks the ligand molecule by a distance - matching algorithm. A modified version of DOCK, directed - DOCK combined with a systematic conformational search for docking flexible ligands was also used. Their results, concerning the behavior of more than 50 compounds, are consistent with the structure - activity data available for the compounds considered and seem to implicate the same amino acid residues recorded in the docking studies discussed above, in similar modes of interactions with the ligands. Specifically, Trp84 and Trp279, located at the bottom of the binding cavity and at the peripheral hydrophobic site, respectively, are observed to interact with the aromatic groups of the reversible inhibitors while the hydrogen bonding interactions of the hydroxyl group of the side chain of Tyr121 with the C = O group(s) of the ligand are proven to be significant for tight binding.

Recently, Inoue et al., performed a docking study of E-2020 and two of its analogs that differ in the length of the alkylene chain linking the indanone and the piperidine moieties (Inoue et al., 1996). The interactions of these compounds with both the free and the acylated *Torpedo Californica* AChE enzyme were studied using the available three-dimensional structure for *Torpedo* AChE and a Monte Carlo - based

stochastic docking algorithm developed in-house. Their docking strategy involved a series of operations consisted of mapping the receptor in a grid - point fashion according to van der Waals, electrostatic and hydrogen bonding potential characteristics of the atoms of the active site gorge, generating plausible initial binding-site coordinate sets on the basis of hydrogen bonding between donor - acceptor heteroatom pairs of the inhibitor and the active site gorge of the receptor, initial docking alignments based on steric and charge complementarity and Monte Carlo sampling to establish intermolecular low-energy alignments. Five types of key binding interactions were identified namely the interaction between the indanone ring and the indole chain of Trp279, the interaction between the methoxy group of the indanone ring and the main chain carbonyl of Arg289, the interaction between the carbonyl group in the indanone ring and the hydroxy group of Tyr121 or Tyr70, the interaction between the NH group in the protonated piperidine and the carboxyl group of Asp72, the phenyl ring of Phe330 or the hydroxy group of Tyr121 and the interaction between the phenyl ring of the benzyl piperidine and the indole ring of Trp84. The presence of these binding interactions was evaluated in all the models obtained through the docking strategy described. In general, all of the docking models have the benzyl group at the bottom of the active-site cavity and the indanone ring located at the entrance to the cavity, as realized in previously conducted docking studies.

Since the crystal structure for *Torpedo Californica* AChE became available recently, the number of docking studies concerning reversible acetylcholinesterase inhibition is limited, yet characterized by a wealth of information which along with structure - activity data has already led to the design of new more effective and selective potential treatments of Alzheimer's type senile dementia.

However, none of the currently existing studies in the literature considers an integrated picture of the human receptor in the form of some molecular - modeling methodology derived three-dimensional model in the absence of the more realistic image provided by crystallography.

The present study consists of an extensive series of docking simulations combined with structural analysis performed in an attempt to identify the modes of interactions of three potent reversible acetylcholinesterase inhibitors, for which biological activity data are available in the literature, with the amino acid residues located in the binding cavity confined by the active site gorge of the *Human* acetylcholinesterase considering for the first time a full three dimensional homology-based model for the human enzyme.

4.2 Methodology

Three analogs of the indanone-benzylpiperidine reversible acetylcholinesterase inhibitors were considered in the present study (Figure 15). These are compounds 2, 11 and 12 from the conformational analysis and molecular-shape comparison work of Cardozo et al. (Cardozo et al., 1992b).

The initial conformations for the three inhibitors were constructed using the available chemical fragments in SYBYL 6.2. The structures thus obtained were energy minimized with MAXIMIN2 in SYBYL 6.2 using the TRIPOS force field and their geometries were subsequently subjected to full optimization using MOPAC 6.0. The MNDO partial charges of the atoms of the optimized geometries were also calculated with MOPAC 6.0 within SYBYL 6.2.

Only the amino acid residues constituting the active site gorge of the human acetylcholinesterase with the added polar hydrogens were used as the receptor in this docking study. The corresponding residues were extracted from the three dimensional homology-based model of the human acetylcholinesterase derived as described in 2.3 and Kollman charges were assigned to the atoms of the receptor.

The docking searches were performed using AutoDock 2.4 (Morris et al., 1996). AutoDock uses a Monte Carlo simulated annealing technique for configurational exploration with a rapid energy evaluation using grid based molecular affinity potential combining the advantages of a large search space and a robust energy evaluation. The energy calculations allow the inclusion of van der Waals, electrostatics and hydrogen bonding interactions. The potential parameters provided with the program were used in this study with a sigmoidal distance-dependent dielectric function to model solvent screening. The grids of affinity potentials were calculated on a volume of $20 \times 20 \times 20$ Å and centered on the center of the receptor; the spacing between the grid points was 0.4 Å.

The extensive docking searches performed in this study involved 100 “jobs” for each one of the three considered reversible inhibitors. Each “job” consisted of 10 independent runs, each of which begins with the same initial conditions. A run was a sequence of 50 constant temperature annealing cycles each with a maximum of 30,000 steps rejected or 30,000 steps accepted. Each “job” was seeded with a time-dependent random number generator seed.

During each constant temperature cycle, random changes are made to the ligand's current position, orientation and conformation. The resulting new state is then compared to its predecessor; if the new energy is lower than the last, this new state is accepted. If

the new state's energy is higher than the last, this state is accepted probabilistically. The probability depends on the energy and cycle temperature.

An initial annealing temperature of 400 kcal/mol (RT in the Boltzmann factor) with a temperature reduction factor of 0.9 to avoid trapping the system in local energy minima.

Full flexibility of the ligands was allowed with a dihedral step of 1° while the maximum step sizes used for the ligands were 0.1 Å for translation and 1° for rotation.

AutoDock 2.4 consists of mainly three modules that accomplish the tasks of the preparation of the receptor in PDB-like file format, the preparation of the ligand identifying its rotatable bonds, the construction of the grids of the molecular affinity potentials and the actual docking searches.

During the course of this study, we developed an environment for the systematic performance and rapid and efficient evaluation, analysis and visualization of the docking calculations from AutoDock 2.4. This 'Automated Docking Environment' (ADE) was developed to minimize user interaction and consists of a series of FORTRAN and Sybyl Programming Language (SPL) codes and UNIX scripts assisting many of the tasks involved in initializing and analyzing automated docking calculations. ADE could therefore be easily applied in database screening for identifying potential leads.

Our docking approach consisted of selecting the lowest energy conformation from each one of the 100 docking 'jobs' for each of the inhibitors studied. The resulting 100 conformations for each ligand were subsequently visualized in SYBYL 6.2 as part of the ADE application. The selected 100 conformations of each inhibitor were categorized according to their geometric (torsional angles) and topologic (docking location within the

receptor) characteristics into ‘patterns’. The lowest energy representative of each ‘pattern’ was then used and the geometry of its complex with the full three dimensional model of the *Human* AChE was optimized with MAXIMIN2 using the Tripos force field to a gradient of $0.5 \text{ kcal mol}^{-1} \text{ \AA}^{-1}$. The energies of the resulting complexes were recorded and their structural features analyzed according to five key interactions of the ligand with the surrounding amino acid residues of the receptor.

4.3 Results

The five key interactions of the ligands with the amino acid residues of the active site gorge of *Human* AChE considered were: (KI1) the interactions of the carbonyl oxygen of the indanone ring, (KI2) the interactions of the piperidine nitrogen, (KI3) the interactions of the indanone ring with the aromatic groups of the surrounding amino acid residues, (KI4) the interaction of the piperidine ring with the surrounding aromatic groups and (KI5) the interactions of the methyl substituent of the piperidine nitrogen with the surrounding aromatic groups.

For Analog 1, twelve different patterns were initially identified. One of the identified patterns was though engaged in serious steric overlaps with the surrounding amino acid residues of the active site of *Human* AChE which were unable to be overcome and was therefore disregarded. The remaining patterns, indicated as Pattern A to Pattern K, the percentage of the conformations belonging to each pattern with the energy of the pattern’s lowest energy representative and the energy of its minimized complex with the human enzyme are given in Table 12. The optimized geometries of the complexes of the identified patterns with *Human* AChE are displayed in Figure 28.

For Analog 2, thirteen patterns were identified indicated as Pattern A to Pattern M, shown in Figure 29, and for Analog 3, twelve patterns were identified indicated as Pattern A to Pattern K, which are given in Figure 30. Tables 13 and 14 contain the percentage of conformations in each pattern, the lowest energy in each pattern and the energy of the minimized complexes for Analog 2 and Analog 3 respectively.

The analysis of the optimized geometries of the complexes of *Human AChE* with the large number of identified patterns for the three ligands studied, resulted in a wealth of structural information regarding the five key interactions of the three reversible inhibitors described above with the surrounding amino acid residues of *Human AChE*. This information has been summarized in Tables 15-19.

The first and most gratifying observation is the excellent prediction of the potencies of the three analogs considered by the automated docking calculations. Indeed, as can be seen in Tables 12 -14, the total binding energies calculated with AutoDock 2.4 for all the identified patterns of Analog 1, the least potent analog, are the highest of all the three analogs. The corresponding total binding energies for all the patterns of Analog 2 are the lowest, in agreement with the analog's highest inhibitory activity.

The most stable pattern for Analog 1, as predicted by AutoDock 2.4, is Pattern F, with -37.61 kcal/mol, for Analog 2, Pattern D was the most stable with a total binding energy of -48.72 kcal/mol and for Analog 3, Pattern E, the lowest energy one, has a total binding energy of -44.08 kcal/mol. Therefore, the rank in energy, $E1 > E3 > E2$ matches the rank in potency, $\text{Analog 1} < \text{Analog 3} < \text{Analog 2}$.

Automated docking calculations can therefore, in spite of their inherent simplicity in the consideration of the ligand-receptor interactions, successfully predict the binding

affinity of a series of ligands for a particular enzyme. This is particularly important when combined with the ease the developed Automated Docking Environment offers to perform database screening for potential new leads.

The calculated binding energies of the optimized geometries of the patterns of all the ligands with the human enzyme though, were not as exciting. In this case, Pattern H is the most stable one for Analog 1 with a total binding energy of -5,718.623 kcal/mol, Pattern K had the lowest energy among the patterns of Analog 2 with a total binding energy of -5,729.222 kcal/mol and for Analog 3, Pattern D was the most stable with a binding energy of -5,737.691 kcal/mol.

Therefore, in the case of the binding energies of the optimized structures of the complexes, the order is $E_3 < E_2 < E_1$ instead of the expected $E_2 < E_3 < E_1$.

For Analog 1, Patterns F and H, the former being the most stable according to AutoDock binding energy calculations and the latter according to the energy of the optimized complex geometry, appear to be located in a completely opposite way in the active site of *Human* AChE (Figure 31). In Pattern H, the indanone and piperidine rings are perpendicular to each other as has been confirmed and observed before (Cardozo et al., 1992b, Inoue et al., 1996). This is not the case for Pattern F. In Pattern H, the indanone ring is parallel to the indole side chain of Trp117 (Trp 84 in *Torpedo* AChE). This mode of interaction has been observed before as constituting a high energy conformer for E-2020 (Inoue et al., 1996). Pattern F, has the piperidine ring located in the bottom of the active site gorge of *Human* AChE. This mode of interaction has been identified previously (see for example Inoue et al., 1996) as being the most prevalent.

For Analog 2, Patterns D and K, the former the AutoDock minimum energy and the latter the minimum energy optimized complex, exhibit the same basic characteristics, both having the indanone ring and the piperidine ring perpendicular to each other (Figure 32). They also resemble Pattern H of Analog 1. In both patterns, the indanone ring points towards the bottom of the active site gorge. This has been identified as a high energy interaction for indanone-piperidine analogs (Inoue et al., 1996). In Pattern D, the indanone ring is found perpendicularly located with respect to Trp 117, similarly to Pattern H of Analog 1.

Finally, in Analog 3, Pattern D was the minimum energy one for the optimized complex and Pattern E the most stable as predicted by AutoDock 2.4. Both patterns have their indanone rings perpendicular to their indanone rings (Figure 33). Their piperidine rings are also located in the bottom of the active site gorge of the enzyme. This, as mentioned above, has been recognized as the most common and most likely binding mode for indanone-piperidine compounds (Inoue et al., 1996, among others). In both patterns, the indanone ring is also perpendicular to the indole side chain of Trp117, as was previously observed for similar compounds (Inoue et al., 1996).

A further thermodynamic analysis is necessary to be used along with the results of this study. These kind of calculations are very computationally intensive since they involve extensive molecular dynamics simulations for configurational sampling and estimation of free Gibbs energy values. Solvation energy calculations and in particular calculations of the electrostatic contribution in the binding energies are currently under way. These calculations generally require fewer computer resources and have been successfully employed in the prediction of the binding affinities of various ligands to

their receptors leading to very good agreement with experimental data (for *Torpedo Californica* AChE, see Wlodek et al., 1996).

CHAPTER 5

CONCLUSIONS AND RECOMMENDATIONS FOR FUTURE WORK

The controversial role of the electrostatic interactions in the process of steering of acetylcholine into the active site of acetylcholinesterases was investigated in the present study.

For the purpose of the simulation of the process of recognition of acetylcholine by wild type and charge neutralized mutated *Human* acetylcholinesterases, the three dimensional, homology-based models of the two enzymes were developed using the existing crystal structure of *Torpedo Californica* acetylcholinesterase as a template.

A novel methodology was designed and implemented to simulate the process of steering of the ligand into the active site of the studied enzymes. The obtained results suggest that the electrostatic field affects the steering of the ligand only when it is in close proximity to the entrance of the active site gorge of the enzymes. The steering process maybe diffusion-controlled when the ligand is further away from the surface of the enzymes. The electrostatic energy was the predominant form of energy of the complexes of acetylcholine with the studied acetylcholinesterases. The charge neutralized mutated *Human* acetylcholinesterase appeared to retain 35% of the electrostatic field of the negatively charged wild type *Human* acetylcholinesterase.

Three irreversible acetylcholinesterase inhibitors were also subjected to the methodology employed for the natural substrate acetylcholine. Their behavior in the steering process is in excellent agreement with the above mentioned findings pertaining to acetylcholine.

The global minimum of the studied complexes was consistently located in wild type *Torpedo Californica* and *Human* acetylcholinesterases. The organophosphate DFP was the only exception to that observation. A further investigation of this phenomenon and its link to the potency of inhibition of DFP is necessary. The correlation of the location of the global energy minimum and the diffusion-electrostatics border with inhibitory potency should also be further examined.

A number of transition states was also revealed by the simulation of the steering process. The role of the identified transition states should also be elucidated.

The covalent adducts of *Torpedo Californica* and *Human* AChE's with selected organophosphate inhibitors were modeled and subjected to structural analysis. A novel methodology was designed and implemented to perform the modeling of the covalent complexes. This methodology can be applied to other covalent docking problems.

The simulations predict the stereoselectivity of *Human* AChE but not of *Torpedo* AChE towards Sarin PS inhibitor. The aging predictions were though in conflict with previous observations.

The observed hydrophobic interactions of the organophosphate moieties with the surrounding aromatic amino acid residues of the active site of the enzymes were in very good agreement with the ones reported in the literature. A new mode of hydrophobic interaction of the organophosphate moiety with Trp233 (Trp267 in *Human* AChE) was identified in this study. The organophosphate moieties interact with the aromatic side chain of Trp84 in *Torpedo* but not with the homologous Trp117 residue of *Human* AChE.

The O γ atom of the active site serine in all the complexes modeled was hydrogen-bonded to Ala201 (Ala235 in *Human*) and the phosphonyl oxygen to Gly119 (Gly153 in *Human*). The close contacts of the phosphonyl oxygen with Gly118 (Gly152 in *Human*) and Ala201 (Ala235 in *Human*) were also successfully reproduced.

The proximity of Glu199 (Glu233 in *Human*), previously suggested as contributing to the charge stabilization of the leaving carbocation during the aging process, to the alkyl groups of the organophosphate moieties was not observed.

The organophosphate structural characteristics identified in the present study can be used for the design of more potent and selective irreversible acetylcholinesterase inhibitors.

The last part of this study involved a very extensive docking analysis for the prediction of the binding sites and bioactive conformations, in *Human* AChE, of three reversible acetylcholinesterase inhibitors, belonging to the family of indanone-piperidine compounds, clinically investigated for the treatment of Alzheimer's type senile dementia. An Automated Docking Environment and Methodology was developed based on AutoDock 2.4 to perform the docking simulations.

A wealth of structural information for the interactions of key chemical groups on the studied inhibitor analogs with the amino acid residues within the active site of *Human* AChE was obtained from the docking calculations. The simulations successfully reproduced the inhibitory activity of the studied analogs and the binding modes observed for structurally similar compounds in *Torpedo* AChE.

Molecular dynamics calculations coupled to automated docking and explicit solvent simulations are necessary to more accurately represent the binding environment of the studied analogs in *Human* AChE.

The Automated Environment and Methodology developed during the course of this study, can be directly applied to fastly screen drug databases for the identification of new lead compounds and predict their inhibitory potentials.

APPENDIX A

TABLES

Table 1. Variation of the total, electrostatic, 1-4 electrostatic and van der Waals energy values (in kcal/mol) of the *Torpedo* AChE-ACh complex relative to the global energy minimum with the distance (in Å) of the center of mass of ACh from the C α atom of the Ser200 residue of the active site of *Torpedo* AChE.

Distance	Total Energy	Electrostatic Energy	Electrostatic Energy 1-4	van der Waals Energy
5	158.357	165.551	-2.456	12.797
6	155.695	165.542	1.514	12.781
7	153.288	160.990	1.501	14.275
8	147.754	159.827	-0.233	12.153
9	145.669	161.135	-2.586	10.360
10	140.661	157.191	-3.749	7.475
11	152.341	170.996	-3.986	9.339
12	122.832	150.221	-4.744	-0.565
13	143.788	145.881	-4.413	6.403
14	62.441	61.872	-9.096	0.109
15	94.034	96.661	-10.954	2.270
16	0.000	0.000	0.000	0.000
17	118.473	112.020	0.233	10.989
18	128.155	122.891	-1.644	16.564
19	130.698	133.947	-2.533	16.137
20	147.897	148.758	-1.333	20.997
21	148.514	148.508	-1.667	22.335
22	165.768	177.839	-5.723	20.122
23	179.597	195.166	-4.307	21.217
24	189.717	202.743	-2.300	25.706
25	190.783	202.233	-2.266	27.312
26	192.373	201.659	-2.263	29.482
27	194.489	204.058	-2.283	29.259
28	195.631	204.367	-2.283	30.073
29	196.966	204.446	-2.291	31.336
30	195.517	202.593	-2.299	31.747
31	196.501	203.601	-2.294	31.716
32	198.201	205.113	-2.301	31.900
33	198.433	205.324	-2.300	31.924

Table 2. Variation of the total, electrostatic, 1-4 electrostatic and van der Waals energy values (in kcal/mol) of the *Human* AChE-ACh complex relative to the global energy minimum with the distance (in Å) of the center of mass of ACh from the C α atom of the Ser234 residue of the active site of *Human* AChE.

Distance	Total Energy	Electrostatic Energy	Electrostatic Energy 1-4	van der Waals Energy
5	42.878	35.457	8.899	5.102
6	38.939	38.585	6.317	0.717
7	1166.671	-42.932	17.237	422.641
8	23.586	12.860	8.281	-2.096
9	1070.608	45.744	4.018	373.961
10	999.984	-37.042	12.620	370.693
11	45.823	34.420	3.632	8.355
12	57.056	41.024	6.826	7.225
13	46.512	37.386	4.832	10.181
14	37.400	30.592	7.196	3.243
15	31.755	20.658	8.613	5.344
16	61.823	55.955	3.675	7.965
17	0.000	0.000	0.000	0.000
18	53.188	49.781	2.290	8.788
19	49.410	46.343	3.916	10.952
20	34.734	35.752	3.777	7.858
21	72.747	71.179	2.326	13.150
22	74.336	71.765	-0.551	16.432
23	82.564	83.077	-0.690	15.801
24	91.683	95.192	-2.919	15.112
25	92.019	93.248	-2.698	17.171
26	92.218	93.889	-2.669	16.705
27	94.070	92.876	-2.679	19.608
28	94.872	93.246	-2.673	20.035
29	95.746	93.865	-2.676	20.289
30	96.364	94.315	-2.674	20.452
31	97.079	94.930	-2.678	20.552
32	98.542	96.293	-2.678	20.646
33	99.234	97.020	-2.680	20.612
34	99.334	97.077	-2.680	20.654
35	99.505	97.223	-2.681	20.678

Table 3. Variation of the total, electrostatic, 1-4 electrostatic and van der Waals energy values (in kcal/mol) of the mutated *Human* AChE-ACh complex relative to the global energy minimum with the distance (in Å) of the center of mass of ACh from the C α atom of the Ser234 residue of the active site of mutated *Human* AChE.

Distance	Total Energy	Electrostatic Energy	Electrostatic Energy 1-4	van der Waals Energy
5	112.992	86.195	-1.921	11.717
6	57.899	51.105	-1.471	0.147
7	1311.024	105.187	-3.864	425.021
8	81.529	78.111	0.819	3.055
9	1845.454	85.951	-2.947	609.846
10	0.000	0.000	0.000	0.000
11	1167.597	45.310	-3.876	410.875
12	39.579	46.185	-4.611	-1.013
13	114.672	122.427	-11.077	4.223
14	44.987	58.273	-5.787	-2.706
15	42.965	52.871	-5.269	-2.400
16	8.490	18.212	-4.466	-2.585
17	12.977	20.602	-2.159	-4.005
18	111.209	125.116	-9.541	2.875
19	151.426	162.824	-14.526	9.740
20	170.820	173.604	-16.209	19.706
21	165.244	172.176	-16.321	17.210
22	174.604	183.856	-16.024	16.809
23	174.109	182.833	-16.015	17.441
24	174.323	182.431	-16.011	18.072
25	173.988	181.460	-16.028	18.746
26	174.738	180.549	-16.037	20.413
27	176.372	180.925	-16.045	21.671
28	177.166	181.331	-16.041	22.059
29	177.210	179.654	-16.056	23.774
30	176.972	179.815	-16.052	23.368
31	177.664	179.972	-16.054	23.905
32	178.354	180.326	-16.057	24.245
33	178.675	180.517	-16.059	24.373
34	178.787	180.552	-16.059	24.452
35	178.838	180.582	-16.059	24.472
36	178.875	180.606	-16.060	24.485

Table 4. Observed interactions of various organophosphate inhibitors with neighboring amino acid residues in the acetylcholinesterase-organophosphates adducts studied.

Adduct	Alkylated Oxygen	γ Oxygen	Phosphonyl Oxygen	Alkyl Groups
<i>Torpedo</i> -Sarin R	H440/c 2.70 Å	A201/a b 1.69 Å	G118/a 2.75 Å G119/a b 1.58 Å A201/a 2.97 Å	W84,233 F288,290,331
<i>Torpedo</i> -Sarin S	H440/c 2.93 Å	A201/a b 1.70 Å H440/c 3.18 Å	G118/a 3.52 Å G119/a b 1.61 Å A201/a 2.92 Å	W84,233 F288,290,331
<i>Torpedo</i> -DFP	H440/c 3.01 Å	A201/a b 1.66 Å H440/c 3.54 Å	G118/a 2.64 Å G119/a b 1.60 Å A201/a 3.16 Å	E199/d 3.53 Å W233,H440 F288,290,331
<i>Human</i> -Sarin R	H478/c 2.69 Å	A235/a b 1.66 Å H478/c 3.35 Å	G152/a 3.08 Å G153/a b 1.64 Å A235/a 3.15 Å	W267 F326,328,369
<i>Human</i> -Sarin S	H478/c 3.41 Å	A235/a b 1.72 Å	G152/a 3.88 Å G153/a b 1.59 Å A235/a 3.13 Å	W267 H478 F326,328,369
<i>Human</i> -DFP	H478/c 2.88 Å	A235/a b 1.70 Å H478/c 3.28 Å	G152/a 3.02 Å G153/a b 1.59 Å A235/a 3.07 Å	E233/d 3.95 Å W267,H478 F326,328,369

Notations: a interaction with amide hydrogen, b hydrogen bond interaction, c interaction with N ϵ 2 of His, d interaction with oxygens of Glu sidechains.

Table 5. Variation of the total, electrostatic, 1-4 electrostatic and van der Waals energy values (in kcal /mol) of the *Torpedo Californica* AChE-Sarin PR complex relative to the global energy minimum with the distance (in Å) of the center of mass of Sarin PR from the C α atom of the Ser200 residue of the active site of *Torpedo* AChE.

Distance	Total Energy	Electrostatic Energy	Electrostatic Energy 1-4	van der Waals Energy
5	31.281	32.442	0.194	2.915
6	29.373	33.004	0.800	-0.635
7	24.257	32.531	-2.140	-1.326
8	23.919	27.645	-3.020	2.650
9	26.054	31.105	-2.636	1.000
10	19.861	29.310	-2.869	0.560
11	17.179	22.371	-2.520	0.809
12	21.184	16.603	-2.222	3.948
13	35.020	28.762	-2.291	4.950
14	18.525	17.808	-1.695	1.827
15	32.685	29.001	-0.798	3.962
16	1406.858	8.182	-8.937	567.667
17	10.062	-2.093	0.501	1.791
18	0.000	0.000	0.000	0.000
19	32.527	24.278	-1.745	5.095
20	30.554	26.325	-2.173	5.073
21	20.163	26.799	-1.632	1.480
22	53.443	58.527	-2.221	7.040
23	25.002	30.755	-2.909	6.629
24	56.099	61.744	-2.502	10.358
25	57.520	62.281	-2.520	11.257
26	58.815	62.412	-2.530	12.458
27	59.201	62.010	-2.542	13.259
28	58.653	60.983	-2.585	13.773
29	59.272	61.193	-2.574	14.142
30	59.006	60.921	-2.584	14.174
31	59.232	61.098	-2.578	14.220
32	59.999	61.813	-2.579	14.265
33	60.103	61.913	-2.575	14.268
34	60.103	61.913	-2.575	14.268
35	60.103	61.913	-2.575	14.268

Table 6. Variation of the total, electrostatic, 1-4 electrostatic and van der Waals energy values (in kcal/mol) of the *Torpedo Californica* AChE-Sarin PS complex relative to the global energy minimum with the distance (in Å) of the center of mass of Sarin PS from the C α atom of the Ser200 residue of the active site of *Torpedo* AChE.

Distance	Total Energy	Electrostatic Energy	Electrostatic Energy 1-4	van der Waals Energy
5	74.899	80.532	1.298	7.183
6	83.171	89.627	2.770	7.682
7	80.210	88.036	4.263	5.826
8	85.832	87.812	2.284	11.368
9	85.956	83.812	3.286	12.994
10	69.456	81.735	2.691	4.824
11	75.283	85.006	2.527	6.041
12	71.703	81.129	2.657	5.701
13	67.361	68.218	3.631	4.685
14	68.017	68.569	3.289	7.268
15	75.667	74.522	2.332	9.452
16	93.752	78.421	1.761	10.334
17	0.000	0.000	0.000	0.000
18	86.675	73.851	5.266	15.884
19	86.821	83.717	5.257	13.050
20	88.272	80.773	2.742	18.032
21	88.251	90.293	3.427	12.832
22	108.917	118.714	2.946	14.013
23	104.355	113.527	2.645	15.842
24	106.016	113.574	2.539	17.722
25	108.081	114.081	2.502	19.363
26	109.125	114.285	2.488	20.233
27	110.087	114.372	2.455	21.156
28	109.852	113.991	2.444	21.339
29	111.389	115.172	2.403	21.714
30	110.816	114.328	2.385	21.999
31	110.815	114.290	2.398	22.031
32	111.512	114.935	2.383	22.083
33	111.637	115.063	2.388	22.086
34	111.637	115.063	2.388	22.086
35	111.637	115.063	2.388	22.086

Table 7. Variation of the total, electrostatic, 1-4 electrostatic and van der Waals energy values (in kcal/mol) of the *Torpedo Californica* AChE-DFP complex relative to the global energy minimum with the distance (in Å) of the center of mass of DFP from the C α atom of the Ser200 residue of the active site of *Torpedo* AChE.

Distance	Total Energy	Electrostatic Energy	Electrostatic Energy 1-4	van der Waals Energy
5	7.150	-17.999	6.661	7.548
6	26.145	14.186	3.432	7.056
7	27.859	16.224	0.336	4.846
8	18.591	12.087	-1.237	7.705
9	21.760	11.306	-2.153	7.996
10	24.671	15.454	-0.655	6.824
11	0.000	0.000	0.000	0.000
12	8.407	-1.887	-1.821	-0.053
13	32.523	-51.584	5.277	-6.591
14	20.631	5.070	-2.470	2.074
15	1003.948	-6.855	2.681	361.987
16	28.182	-0.077	-4.748	6.120
17	12.672	-8.492	4.894	8.759
18	37.376	8.255	2.122	14.183
19	17.727	1.663	0.377	9.612
20	24.854	11.624	1.629	10.277
21	18.345	8.228	0.046	9.132
22	17.667	11.678	-0.356	9.793
23	51.885	46.354	-0.517	17.130
24	50.018	44.715	-1.283	16.939
25	54.783	47.322	0.722	20.636
26	55.530	46.479	0.731	22.227
27	55.906	46.316	0.732	22.771
28	55.602	45.665	0.732	23.110
29	55.559	45.423	0.735	23.306
30	54.482	44.291	0.734	23.374
31	56.433	46.133	0.733	23.473
32	56.455	46.149	0.733	23.479
33	56.581	46.266	0.736	23.486
34	56.581	46.266	0.736	23.486

Table 8. Variation of the total, electrostatic, 1-4 electrostatic and van der Waals energy values (in kcal/mol) of the *Human* AChE-Sarin PR complex relative to the global energy minimum with the distance (in Å) of the center of mass of Sarin PR from the C α atom of the Ser234 residue of the active site of *Human* AChE.

Distance	Total Energy	Electrostatic Energy	Electrostatic Energy 1-4	van der Waals Energy
5	18.807	1.796	8.466	4.022
6	27.475	26.219	4.054	-2.182
7	25.094	23.945	-0.428	0.690
8	18.340	6.160	3.924	1.638
9	19.549	14.852	1.719	-0.109
10	11.447	14.715	-0.794	-3.695
11	32.466	22.252	2.638	-0.559
12	6.958	12.354	-4.297	-1.519
13	19.705	3.877	-1.087	5.526
14	1.227	-1.643	-1.668	5.904
15	0.000	0.000	0.000	0.000
16	10.759	15.854	2.000	-0.066
17	37.447	38.844	-2.682	3.764
18	5.563	10.299	0.789	-1.293
19	25.136	26.795	-0.228	2.481
20	36.442	39.142	-2.233	5.344
21	37.609	41.346	-2.190	4.933
22	45.338	51.084	-3.349	6.211
23	45.727	50.425	-3.279	7.178
24	46.189	50.121	-3.213	8.248
25	47.687	49.785	-3.281	10.090
26	47.451	49.160	-3.249	10.473
27	47.912	49.287	-3.232	10.801
28	48.332	49.476	-3.236	11.039
29	48.623	49.630	-3.223	11.173
30	49.383	50.327	-3.226	11.230
31	49.381	50.321	-3.224	11.237
32	50.040	50.929	-3.224	11.285
33	50.040	50.929	-3.224	11.285

Table 9. Variation of the total, electrostatic, 1-4 electrostatic and van der Waals energy values (in kcal/mol) of the *Human* AChE-Sarin PS complex relative to the global energy minimum with the distance (in Å) of the center of mass of Sarin PS from the C α atom of the Ser234 residue of the active site of *Human* AChE.

Distance	Total Energy	Electrostatic Energy	Electrostatic Energy 1-4	van der Waals Energy
5	36.113	33.052	0.593	3.819
6	10.019	6.971	2.011	3.216
7	35.643	21.934	1.371	5.405
8	4.315	-1.502	1.500	2.177
9	14.694	12.805	-0.032	3.152
10	19.870	22.800	-1.138	1.362
11	0.000	0.000	0.000	0.000
12	7.496	4.201	0.719	-0.721
13	23.149	16.390	-3.097	7.698
14	8.286	10.857	-3.375	2.951
15	11.921	15.412	-3.157	4.835
16	16.386	5.298	3.501	9.720
17	14.244	10.507	-0.641	9.085
18	33.267	31.447	-3.989	7.372
19	11.476	10.656	0.339	8.003
20	13.362	9.430	0.063	11.159
21	32.926	28.586	-1.796	13.519
22	44.617	42.866	-3.128	14.002
23	34.294	34.844	-2.074	12.569
24	41.666	41.266	-2.875	13.781
25	43.082	41.599	-2.845	14.896
26	43.766	41.552	-2.844	15.613
27	44.477	41.795	-2.849	16.093
28	43.949	41.040	-2.849	16.323
29	44.632	41.697	-2.831	16.341
30	44.843	41.821	-2.842	16.435
31	44.927	41.890	-2.842	16.449
32	45.558	42.461	-2.843	16.508
33	45.558	42.461	-2.843	16.508

Table 10. Variation of the total, electrostatic, 1-4 electrostatic and van der Waals energy values (in kcal/mol) of the *Human* AChE-DFP complex relative to the global energy minimum with the distance (in Å) of the center of mass of DFP from the C α atom of the Ser234 residue of the active site of *Human* AChE.

Distance	Total Energy	Electrostatic Energy	Electrostatic Energy 1-4	van der Waals Energy
5	0.000	0.000	0.000	0.000
6	62.395	54.845	-5.713	8.262
7	63.938	56.173	-7.608	11.639
8	15.924	7.964	-3.800	2.107
9	43.811	46.199	-8.233	1.814
10	1173.214	44.855	-12.885	442.904
11	176.092	58.870	-7.095	85.801
12	52.295	36.035	-3.106	12.318
13	48.450	41.308	-7.117	4.548
14	46.886	53.830	-11.080	6.112
15	64.420	62.932	-12.358	8.763
16	56.716	62.205	-7.948	8.015
17	62.827	58.319	-8.859	14.548
18	50.695	48.895	-7.419	7.957
19	68.347	73.091	-9.134	9.541
20	52.727	60.955	-8.160	9.470
21	91.345	94.092	-12.557	18.446
22	82.507	90.900	-13.167	16.385
23	87.640	97.008	-13.044	15.625
24	91.873	104.944	-15.320	14.009
25	92.776	103.820	-15.313	16.073
26	92.992	102.437	-15.309	17.676
27	92.108	101.308	-15.301	17.928
28	92.239	101.227	-15.299	18.140
29	92.697	101.494	-15.299	18.332
30	92.685	101.356	-15.302	18.457
31	93.086	101.696	-15.302	18.517
32	94.119	102.700	-15.299	18.543
33	94.119	102.700	-15.299	18.543

Table 11. Summary of the results of the simulation of the steering process of selected ligands and inhibitors into the active site gorge of acetylcholinesterases from different species.

Complex	Global Energy Minimum Location (Å)	Diffusion - Electrostatics Border (Å)	Transition States Locations (Å)
<i>Torpedo</i> - ACh	16	24	5 11 13 15
<i>Torpedo</i> - Sarin PR	18	24	5 9 13 16 19 22
<i>Torpedo</i> - Sarin PS	17	22	6 9 11 16
<i>Torpedo</i> - DFP	11	23	7 10 13 15 18 20
<i>Human</i> - ACh	17	24	5 7 9 12 16 18
mut <i>Human</i> - ACh	10	19	5 7 9 11 13
<i>Human</i> - Sarin PR	15	22	6 9 11 13 17
<i>Human</i> - Sarin PS	11	24	5 7 10 13 16 18 22
<i>Human</i> - DFP	5	21	7 10 15 17 19

Table 12. The percentage of conformations belonging to each pattern, the energy (in kcal/mol) of each pattern's lowest energy representative and the energy (in kcal/mol) of the complex of the lowest energy conformation of each pattern with *Human* AChE for Analog 1 ($IC_{50} = 8.4$ nM). The lowest energy pattern is highlighted in bold and italic

Pattern	Percentage	Lowest Energy	Energy of Complex
A	25	-37.24	-5,653.521
B	17	-37.17	-5,643.561
C	1	-33.20	-5,654.309
D	1	-36.82	-5,655.658
E	1	-33.65	-5,676.238
F	29	-37.61	-5,665.721
G	5	-33.77	-5,649.411
H	10	-35.48	-5,718.623
I	2	-37.19	-5,666.181
J	2	-35.57	-5,648.632
<i>K</i>	1	-32.95	-5,661.296

Table 13. The percentage of conformations belonging to each pattern, the energy (in kcal/mol) of each pattern's lowest energy representative and the energy (in kcal/mol) of the complex of the lowest energy conformation of each pattern with *Human* AChE for Analog 2 ($IC_{50} = 0.82$ nM). The lowest energy pattern is highlighted in bold and italic.

Pattern	Percentage	Lowest Energy	Energy of Complex
A	43	-47.22	-5,663.377
B	9	-45.39	-5,654.094
C	3	-44.74	-5,681.411
<i>D</i>	9	-48.72	-5,654.852
E	13	-47.85	-5,675.134
F	6	-46.78	-5,652.158
G	3	-44.87	-5,698.812
H	7	-43.54	-5,658.358
I	1	-44.14	-5,658.850
J	3	-45.03	-5,686.708
<i>K</i>	<i>1</i>	<i>-45.12</i>	<i>-5,729.222</i>
L	1	-42.57	-5,649.637
M	1	-43.90	-5,639.814

Table 14. The percentage of conformations belonging to each pattern, the energy (in kcal/mol) of each pattern's lowest energy representative and the energy (in kcal/mol) of the complex of the lowest energy conformation of each pattern with *Human* AChE for Analog 3 (IC₅₀ = 3.0 nM). The lowest energy pattern is highlighted in bold and italic.

Pattern	Percentage	Lowest Energy	Energy of Complex
A	14	-40.71	-5,676.727
B	18	-42.74	-5,671.110
C	2	-41.37	-5,664.049
<i>D</i>	<i>1</i>	<i>-40.34</i>	<i>-5,737.691</i>
<i>E</i>	<i>18</i>	<i>-44.08</i>	<i>-5,671.496</i>
F	13	-42.22	-5,662.448
G	14	-41.21	-5,691.094
H	7	-41.89	-5,721.157
I	11	-41.05	-5,679.341
J	1	-41.62	-5,690.431
K	1	-36.74	-5,661.910

Table 15. Observed interactions (distances in Å) of the carbonyl oxygen atom (K11) of the indanone ring of the three analogs studied with atoms of the surrounding amino acid residues of *Human* AChE. The lowest energy pattern of each analog is highlighted.

Pattern	Analog 1 (<i>IC</i> ₅₀ = 8.4 nM)	Analog 2 (<i>IC</i> ₅₀ = 0.82 nM)	Analog 3 (<i>IC</i> ₅₀ = 3.0 nM)
A	G152/a 3.50	D105/a 3.98 S156/c 2.96	S156/c 3.50
B	G152/a 3.95	Y164/c 3.78	Y480/c 3.70
C	-	Y368/c 3.95	G152/a 3.32 S234/c 3.45
D	-	G152/a 3.68 Y164/c 3.73	G152/a 3.85
E	S156/c 3.92	S156/b c 2.27	S156/b c 2.56
F	-	Y155/c 3.95 S156/c 3.33	G157/a 4.00
G	-	G152/a 3.41 S234/c 3.44	Y164/c 3.27
H	Y368/c 2.50 Y372/c 3.53	S156/b c 2.29	G152/a 3.30 S234/c 3.21
I	S156/c 3.02	G151/a 3.63 G152/a 2.96 Y164/c 2.81	-
J	G152/a 3.34	W117/a 3.41	Y368/c 3.90
K	-	S156/c 3.22	-
L	N/A	-	N/A
M	N/A	N118/a 3.74	N/A

Notations: a interaction with amide hydrogen, b hydrogen bond interaction, c interaction with hydroxyl hydrogen.

Table 16. Observed interactions (distances in Å) of the nitrogen atom (KI2) of the piperidine ring of the three analogs studied with atoms of the surrounding amino acid residues of *Human* AChE. The lowest energy pattern of each analog is highlighted.

Pattern	Analog 1 ($IC_{50} = 8.4 \text{ nM}$)	Analog 2 ($IC_{50} = 0.82 \text{ nM}$)	Analog 3 ($IC_{50} = 3.0 \text{ nM}$)
A	A158/a b 1.81	G153/a 3.44	-
B	A158/a 3.13	G153/a 3.40	A158/a 3.83
C	A158/a 3.94	G157/a 3.97 A158/a 3.78	G157/a 3.605
D	A158/a 3.31	<i>G153/a 3.40</i>	<i>G152/a 3.71</i>
E	G157/a 3.97 A158/a 3.43	-	-
F	<i>G157/a 3.75</i> <i>A158/a 3.22</i>	G151/a 3.95 A158/a 3.95 Y164/c 3.36	G153/a 3.40
G	G152/a 3.37 G153/a 3.34 S234/c 3.64	G151/a 3.94 Y164/c 3.35	G153/a 3.48
H	<i>G153/a 3.42</i>	Y480/a 3.97	G157/a 3.61
I	-	G153/a 3.41	-
J	A158/a 3.54	G153/a 3.52	-
K	G152/a 3.81	<i>G153/a 3.45</i>	G157/a 3.24
L	N/A	G153/a 3.86	N/A
M	N/A	-	N/A

Notations: a interaction with amide hydrogen, b hydrogen bond interaction, c interaction with hydroxyl hydrogen.

Table 17. Observed interactions (symbols in parentheses, i.e. \perp perpendicular) of the indanone ring (KI3) of the three analogs studied with aromatic sidechains of the surrounding amino acid residues of *Human* AChE. The lowest energy pattern of each analog is highlighted.

Pattern	Analog 1 ($IC_{50} = 8.4 \text{ nM}$)	Analog 2 ($IC_{50} = 0.82 \text{ nM}$)	Analog 3 ($IC_{50} = 3.0 \text{ nM}$)
A	W117, H478 (\perp)	-	Y164 (\perp)
B	W117 (\parallel)	Y164	Y155, F369, Y368, H478
C	H478 (\perp), Y368 (\perp) F369 (\perp)	F369, Y155, H478	Y155, F369, Y368, H478
D	W117 (\parallel)	<i>W117 (\parallel), Y164</i>	<i>Y155 (\perp), F369 (\perp) H478 (\perp)</i>
E	W117 (\parallel), H478 (\perp) Y368	H478, Y155	<i>Y155 (\perp), F369 (\perp) H478 (\perp)</i>
F	<i>Y368, H478</i>	Y155 (\perp), F328(\perp) F369 (\perp), H478 (\perp)	Y164 (\parallel), W117 (\parallel)
G	Y164 (\perp)	Y155 (\perp), F328(\perp) F369 (\perp), H478 (\perp)	P119
H	<i>W117 (\parallel)</i>	Y164 (\perp)	Y155 (\perp), F328(\perp) F369 (\perp), H478 (\perp)
I	H478 (\perp), F369 (\perp) F328 (\perp), Y155 (\perp)	Y164	Y164 (\perp)
J	Y368 (\perp)	Y164 (\perp)	Y155 (\perp), F328(\perp) F369 (\perp), H478 (\perp)
K	Y164, W117	<i>Y164 (\perp)</i>	Y480 (\parallel), W117 (\parallel)
L	N/A	Y164 (\perp)	N/A
M	N/A	Y164 (\perp)	N/A

Table 18. Observed hydrophobic interactions (symbols in parentheses, i.e. \perp perpendicular) of the piperidine ring (KI4) of the three analogs studied with aromatic sidechains of the surrounding amino acid residues of *Human* AChE. The lowest energy pattern of each analog is highlighted.

Pattern	Analog 1 ($IC_{50} = 8.4 \text{ nM}$)	Analog 2 ($IC_{50} = 0.82 \text{ nM}$)	Analog 3 ($IC_{50} = 3.0 \text{ nM}$)
A	Y164 (\perp)	Y155 (\perp), F369 (\perp), H478 (\perp)	Y480, H478 W117 (\parallel)
B	Y164 (\perp), Y150 (\perp)	Y155 (\perp), F369 (\perp), H478 (\perp)	W117 (\perp), Y164 (\parallel)
C	Y164 (\perp)	Y164 (\parallel), W117 (\perp)	Y164
D	Y150 (\perp), Y164 (\perp)	<i>Y155, F369, H478</i>	<i>W117 (<)</i>
E	Y150 (\perp), Y164 (\perp)	W117 (\parallel)	<i>W117 (\parallel)</i>
F	-	Y164	Y155 (\perp), F369 (\perp), H478 (\perp)
G	H478 (\perp)	Y164	Y155 (\perp), F369 (\perp), H478 (\perp)
H	<i>Y155 (\perp), F369 (\perp), H478 (\perp)</i>	W117 (\parallel), H478	Y164 (\perp)
I	W117 (\parallel)	Y155, F369, H478	Y368, F369, H478
J	Y164 (\perp)	Y155, F369, H478	Y164 (\parallel), W117 (\perp)
K	F369 (\perp), H478 (\perp)	<i>Y155, F369, H478</i>	-
L	N/A	F369, H478	N/A
M	N/A	W117 (\parallel)	N/A

Table 19. Observed hydrophobic interactions (symbols in parentheses, i.e. \perp perpendicular) of the methyl substituent of the piperidine ring (KI5) of the three analogs studied with aromatic sidechains of the surrounding amino acid residues of *Human* AChE. The lowest energy pattern of each analog is highlighted.

Pattern	Analog 1 ($IC_{50} = 8.4 \text{ nM}$)	Analog 2 ($IC_{50} = 0.82 \text{ nM}$)	Analog 3 ($IC_{50} = 3.0 \text{ nM}$)
A	-	F326 (\parallel), W267 (\parallel)	Y480
B	-	F328 (\parallel), F326	P119 (\parallel)
C	-	P119	Y150 (\leftarrow)
D	-	W267 (\parallel), F326 (\parallel) F328	Y150 (\parallel), Y164
E	Y150, Y164	Y480 (\perp)	Y480 (\parallel)
F	-	Y150	F326 (\parallel), W267 (\parallel) F328
G	F326, F328	Y150	F326 (\parallel), W267 (\parallel) F328
H	W267 (\parallel), F326 (\parallel)	Y480	Y150 (\parallel)
I	-	F326 (\parallel), W267 (\parallel) F328	F369 (\parallel) Y155, F328
J	-	F326 (\parallel), W267 (\parallel) F328	P119 (\parallel)
K	F326, F369, Y155 F328 (\parallel)	F326 (\parallel), W267 (\parallel) F328	Y164
L	N/A	Y155, F369 F328 (\parallel)	N/A
M	N/A	Y480 (\parallel), H478	N/A

Table 20. List of amino acid residues of the *Human* AChE involved in interactions with the identified patterns of the three reversible inhibitors studied and their homologous residues in *Torpedo Californica* AChE.

<i>Torpedo Californica</i> AChE	<i>Human</i> AChE
TYR 70	TYR 103
ASP 72	ASP 105
TRP 84	TRP 117
GLY 119	GLY 153
TYR 121	TYR 155
SER 122	SER 156
SER 124	ALA 158
TYR 130	TYR 164
GLU 199	GLU 233
TRP 279	TRP 317
SER 286	SER 324
PHE 288	PHE 326
ARG 289	ARG 327
PHE 290	PHE 328
PHE 330	TYR 368
PHE 331	PHE 369
TYR 334	TYR 372
GLY 335	GLY 373

APPENDIX B

FIGURES

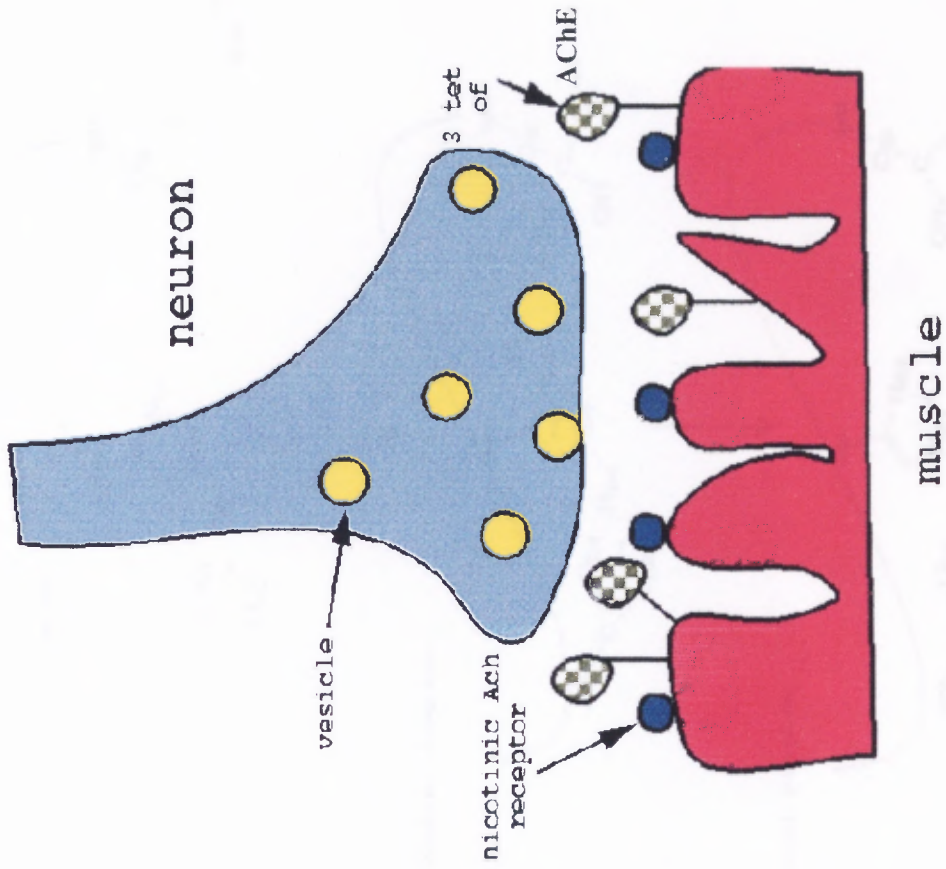


Figure 1. Schematic of the neuromuscular junction. Acetylcholinesterase is located in the synaptic cleft (after <http://chemcca10.ucsd.edu/~chem215/lectures/lecture5/lecture5/node28.html>).

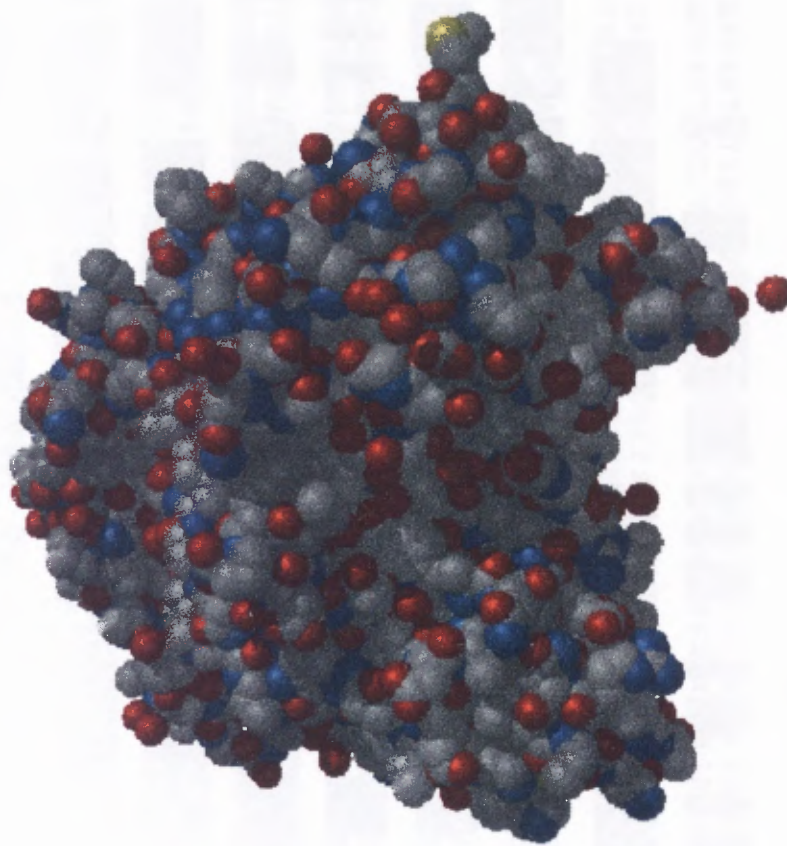


Figure 3. Space-fill model of the crystal structure of *Torpedo Californica* Acetylcholinesterase (after gopher://pdb.pdb.bnl.gov:7019/PDB/Entries/1acj/1acj.gif).

```

aces_torca      ~~~~~~NLL~TSS~GVL~LHLV~LCCQ~D~HSEL~LVNT~SC~MCT~F~PVLSSH
aces_human      MRPPQCLLHTPS~ASP~LLL~LML~LCCV~CAE~R~D~AELL~VTV~CC~RCI~R~KTPCGPV

aces_torca      SAFLGIPFPPEPP~ENMFRFRPEPKKPMSCVMNA~T~PNN~CQ~YVLEQ~PCFSCSEMMNPN
aces_human      SAFLGIPFPPEPP~CPRRFLPEPKQPMSCVVD~A~T~FQSV~CYQYVETL~PCFECSEMMNPN

aces_torca      REMSEDCLYLN~M~VPSRPKS~T~TV~VM~IYGGPYSCSE~LDVYNG~L~AYT~EVV~LVSL
aces_human      REMSEDCLYLN~M~TPEPRPTS~PT~PV~VM~IYGGPYSCSE~LDVYDCA~L~VQA~ERTV~LVSM

aces_torca      SYRVERFGFLRLH~GSEQERPNVGLLDQR~ALQWVH~EN~Q~FFCGDPK~VT~FGESAC~RSV
aces_human      NYRVERFGFLRLP~GSRERPNVGLLDQR~ALQWVQ~EN~AA~FFCGDPT~VT~FGESAC~RSV

aces_torca      QNH~LSP~CSRDLF~RR~A~LQSC~SPN~CPMR~SVS~E~RRRA~VEL~GRN~NC~*~*~*~NLNS~DBEL
aces_human      QNH~LSP~PSRCLF~HRA~LQSC~APN~CPMR~VCA~E~RRRA~TQL~L~HL~C~PFCCT~COND~TEL

aces_torca      HCLREK~K~PQ~EL~DVE~M~VLP~P~S~FRFS~FYPV~DE~FF~PPT~L~ES~M~NS~GNF~KKTQ~L~L~G
aces_human      A~CL~RT~P~A~Q~V~L~NHE~M~VLP~Q~ES~FRFS~FYPV~DE~FL~SD~P~EAL~NA~GDF~HCLQ~L~L~G

aces_torca      VNKDECS~FL~YCA~P~C~F~S~K~D~S~E~S~K~I~S~R~E~E~F~S~G~V~S~Y~P~H~A~N~D~L~L~L~A~V~T~L~Q~Y~T~D~M~D~D~N
aces_human      VYKDECS~FL~YCA~P~C~F~S~K~D~N~E~S~L~I~S~R~A~E~F~A~Q~V~P~C~V~P~Q~V~S~D~L~A~A~V~V~L~H~Y~T~D~M~H~P~E

aces_torca      NCI~NR~Q~E~D~D~V~G~D~H~N~V~C~P~M~H~F~V~N~Y~T~K~F~N~G~T~Y~L~Y~F~F~N~H~R~A~S~N~I~V~M~P~E~M~G~V~I~H~G~Y
aces_human      DPA~R~L~R~L~L~S~D~V~G~D~H~N~V~C~P~A~Q~L~A~C~P~L~A~A~Q~C~A~R~V~Y~A~Y~V~F~E~H~R~A~S~T~L~S~M~P~L~M~G~V~P~H~C~Y

aces_torca      EIEF~F~G~P~L~V~K~E~L~N~Y~T~B~E~E~A~L~S~R~E~M~H~Y~M~T~F~A~T~G~N~P~N~E~P~H~S~Q~E~S~*~K~M~P~L~T~T~K~E~Q~K
aces_human      EIEF~F~G~P~L~D~P~S~R~N~Y~T~B~E~E~K~I~F~A~Q~R~M~R~Y~M~N~P~A~T~G~D~E~N~E~P~R~D~P~K~A~E~Q~M~E~P~T~A~C~A~Q~Q

aces_torca      F~I~D~L~N~T~E~F~K~V~H~Q~R~L~R~V~Q~M~G~V~F~M~M~Q~F~L~P~K~L~L~N~R~T~A~C~D~G~E~L~S~S~S~G~T~S~S~S~K~G~I~F~Y~T~P~S~I~L
aces_human      F~I~S~L~D~L~R~E~E~V~Y~R~R~C~L~R~A~Q~A~C~A~F~M~M~R~F~L~P~K~L~L~S~A~T~D~T~L~D~E~A~E~R~Q~W~K~A~E~F~H~R~W~S~S~Y~M~H~K~N

aces_torca      YLIF~~~~~
aces_human      QFDHYSKQDRCSDL

```

Figure 4. Alignment of the amino acid sequences of *Torpedo Californica* (aces_torca) and *Human* (aces_human) AChE's. Identical and similar amino acids are highlighted black and gray respectively. The calculated percent similarity is 62.63 and the percent identity is 54.10.

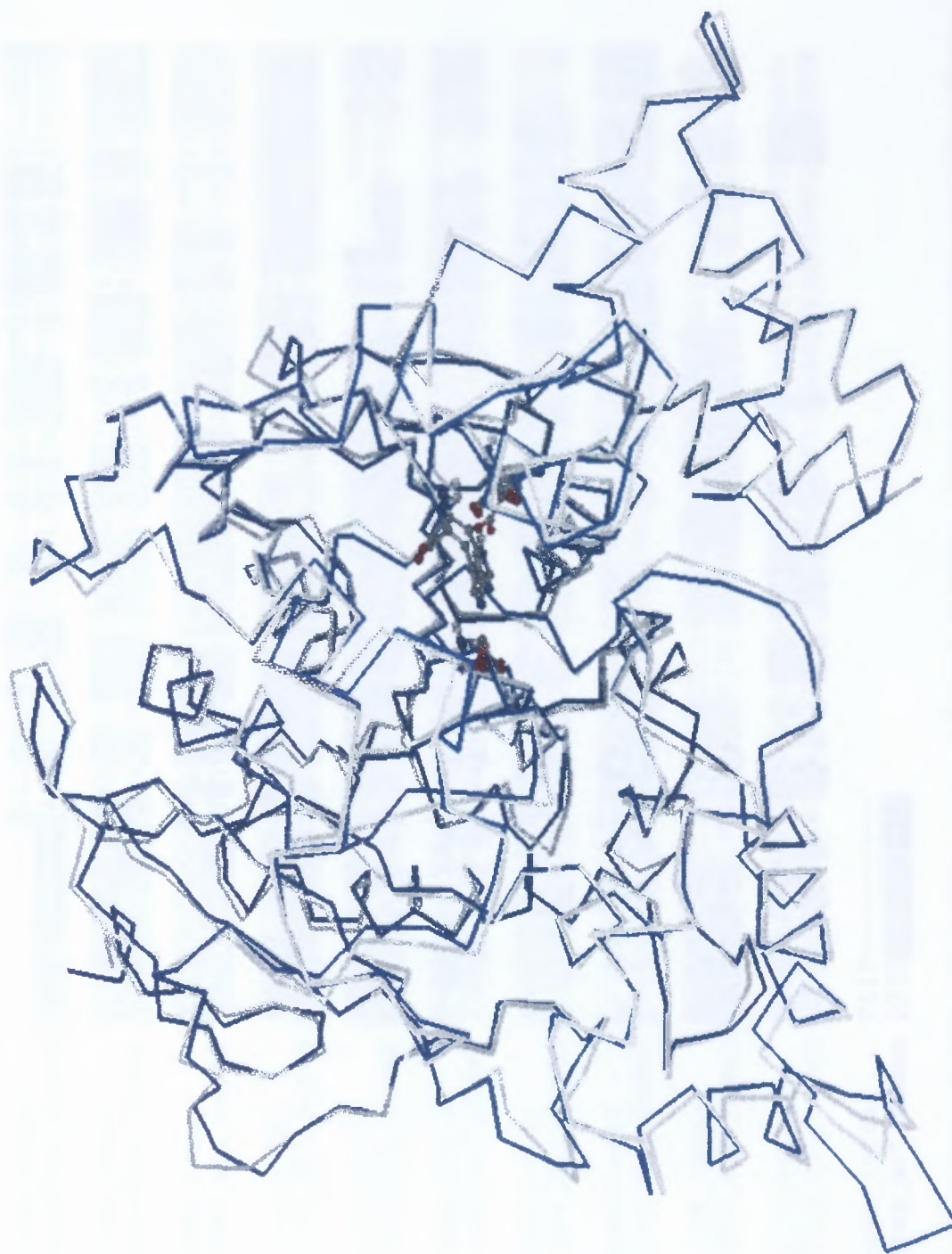


Figure 5. Superposition of the structures of *Torpedo Californica* (grey) and *Human* (blue) AChE's with respect to the C α atoms of their backbones (rms deviation 0.827 Angs.). The catalytic triads of the enzymes are displayed in ball-and-stick mode.

```

aces_torca      ~~~~~MNLSTSSLCVLLHLLVLCQDDHSELLVNTKSCKIMCTRMTPVYLSSH
aces_mut_human MRPPQCLLHTPSGASPLLLLMLLCCGCAEGRDDELLLYTVRGCGRRCIRIKTPGCPV

aces_torca     SAFLGIFFAEPPGCMNRRFRPEPKKPMSCGMNPNSTYPNNGQQYVDEQEFPGFSGSEMMNPN
aces_mut_human SAFLGIFFAEPPGCMRRRFLPEPKQPMSCGVDAITQSVCYQYVDTLTPGFECTQMMNPN

aces_torca     REMSEDCLYLNQVPSRPKSLTVMVMYICGCPVSCSSTLDVYNGKQLAYTEVVLVSL
aces_mut_human REMSEDCLYLNQVTEYPRHTSETPYVMYIYCCGPTSCASSLDYIDCFRVDYQAEKTYLVSQ

aces_torca     SYRVCAFGPLALHGSQBAEAPENVGLLDQRFALQWHEMVFQFGGDEKVTTFCESSACGASY
aces_mut_human NYRVCAFGPLALPGRBAEAPENVGLLDQRFALQWQENYRAFGGDETSVTFCESSACGASY

aces_torca     GMHLLSPGSRDLFRRAALQSESPNCPWZSVSVEEERRRRVEIDGRNINC...NLNSDEEL
aces_mut_human GMHLLSPGPSGLFHRQVLOSCAPNCPWZNVYCGEARRRRDTQLAHLVCCPPGCTCGNDTEL

aces_torca     IHCLEEKKPELDYEMNVLFPDSPPRSTPYVDCFFPPTSLESMMNSGNFKKTQDLGC
aces_mut_human MACLEKTPAQVLINHAMHVLQASVPRPSVYVDCFFLSDMPELAINAGDFHGLQVLCG

aces_torca     VNKDEGSFLYCAPOPSKDSSEKISHEDFMSVTSVPHANDLCLDAVTLQYTDMDDDN
aces_mut_human VVKDEGSFLYCAPOPSKNNESLISHAQFLAQRVYQVQVSDLADEAVVHHTDMTHP

aces_torca     NCIKNRDELDDVEDHNVCFEMH FVNKYTKFNGTYLYFENHRSNLYMPEMNGVIHGY
aces_mut_human NPARRLRDELSDVEDHNVCFEVAQLACKLAAQGRRVYAYVFEHRASTLSQELMNGYPPHGY

aces_torca     EIEHVFQPIVYKELNYTAEERALSREEMHVMATPATCENPNEPHSQESXMPLETTXEQK
aces_mut_human EIEHVFQPIVDDPSRNYTAEKIFAQRUMRYMANPATCENPNEPRDPKAPQMPPTAGAQQ

aces_torca     QLDLNTFPMKXHQRLRVQMGVFMNQLFLKLLNATACDGEELSSSGTSSSKGIFFVTFPSIL
aces_mut_human QSLDLRPLEVRRGLRAQACAFMNRFLFKLLSATDLDERERQWKAEFHRWSSYGVHWNK

aces_torca     YLIF~~~~~
aces_mut_human QFDHYSKODRCSDL

```

Figure 6. Alignment of the amino acid sequences of *Torpedo Californica* (aces_torca) and charge neutralized *Human* (aces_mut_human) AChE's. Identical and similar amino acids are highlighted black and grey respectively. The calculated percent similarity is 62.12 and the percent identity is 53.75.



Figure 7. Superposition of the structures of *Torpedo Californica* (grey) and charge neutralized mutated *Human* (blue) AChE's with respect to the C α atoms of their backbones (rms deviation 0.865 Angs.). The catalytic triads of the enzymes are displayed in ball-and-stick mode.

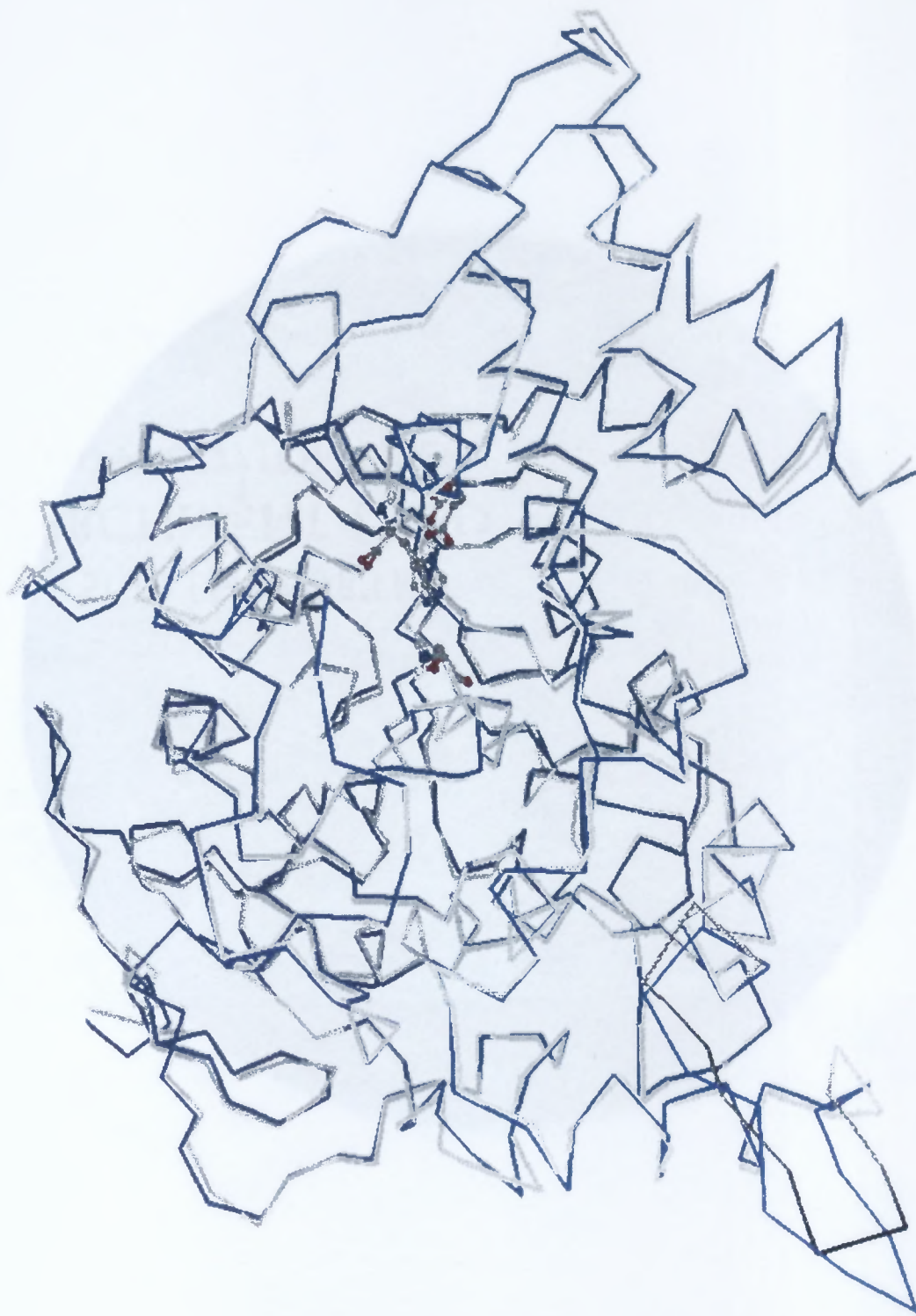


Figure 8. Superposition of the structures of *Human* (grey) and charge neutralized mutated *Human* (blue) AChE's with respect to the C α atoms of their backbones (rms deviation 0.672 Angs.). The catalytic triads of the enzymes are displayed in ball-and-stick mode.

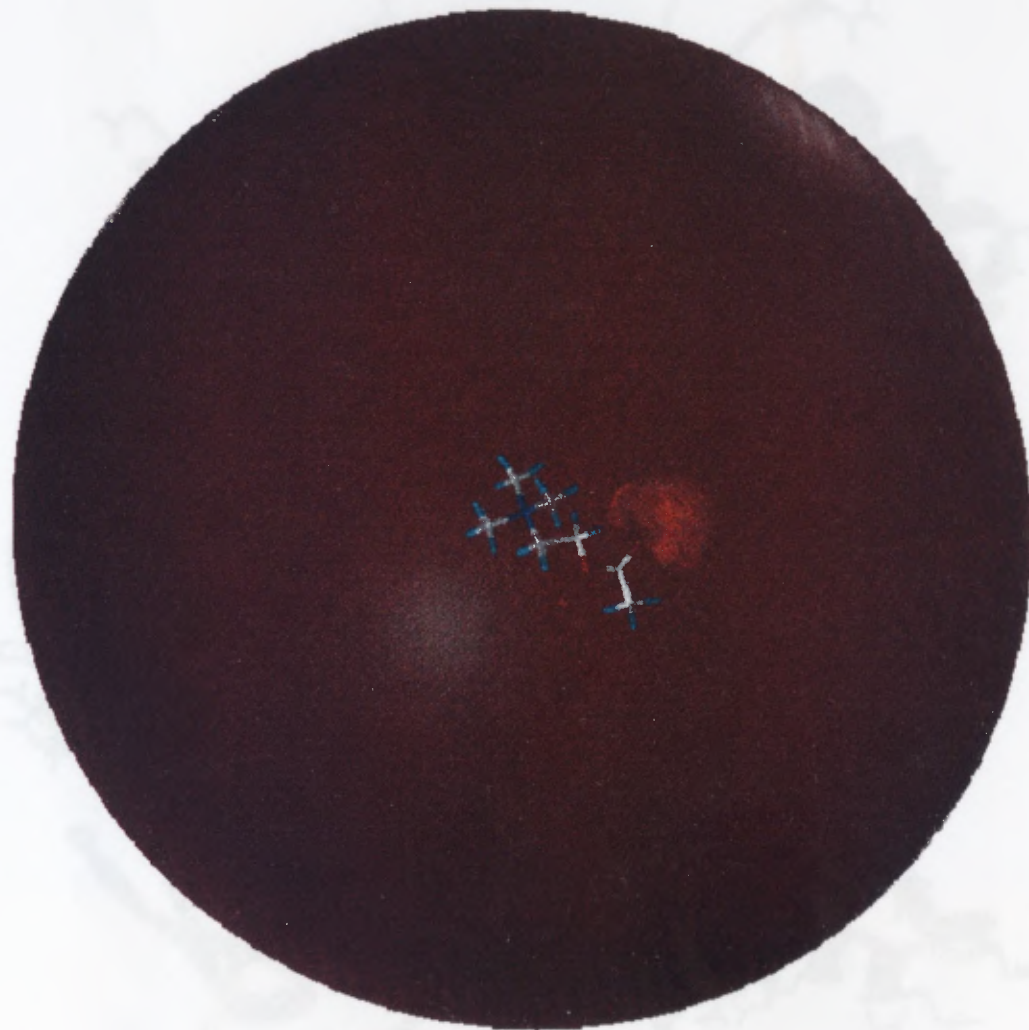


Figure 9. Calculated electrostatic potential map around acetylcholine. The +1 contour is displayed in red.

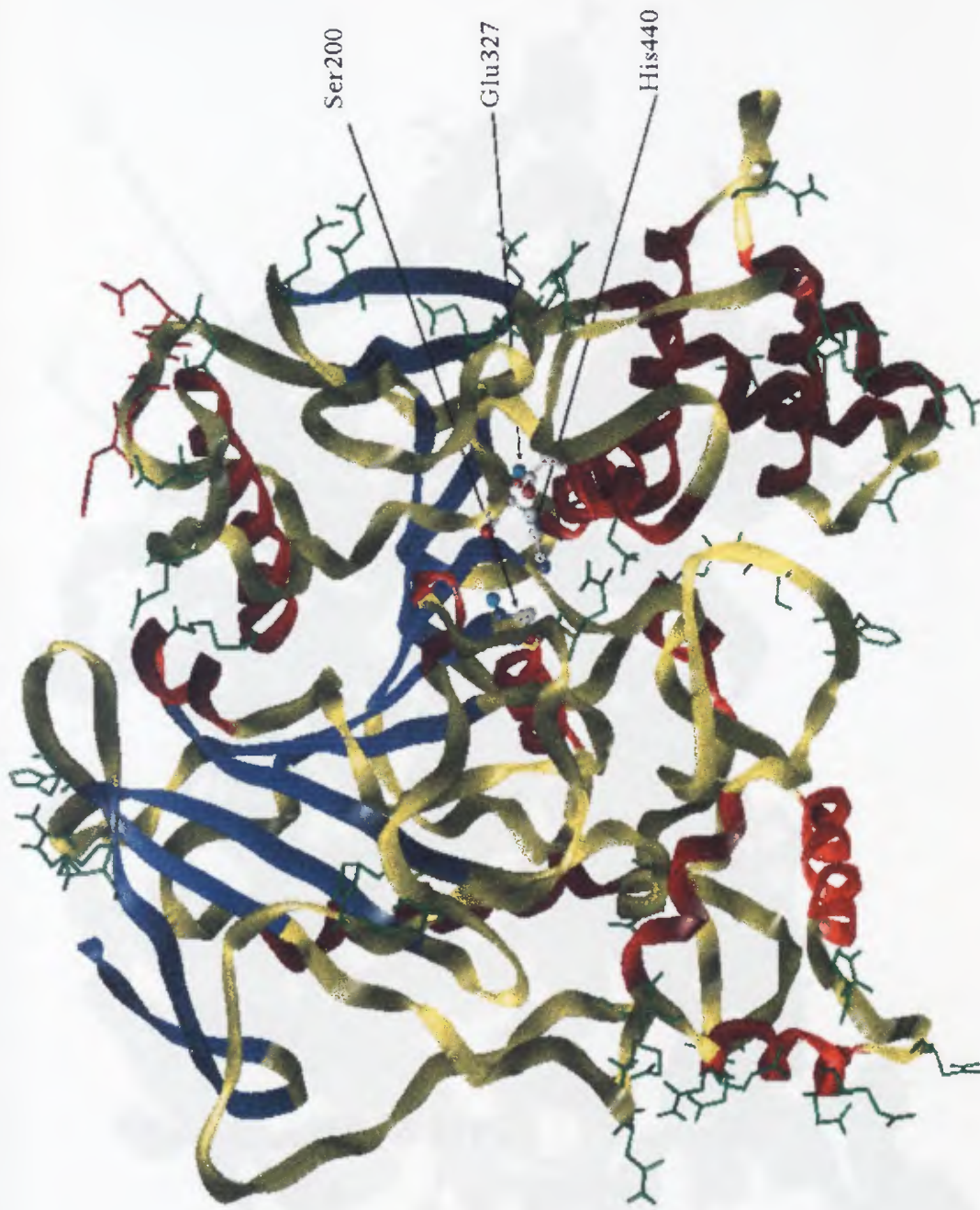


Figure 10. Three dimensional model of *Torpedo Californica* AChE. The blue, red and yellow ribbons denote β -sheets, α -helices and loop regions respectively in the secondary structure of the enzyme. The active site residues are shown in ball-and-stick. The added sidechains and loop are colored green and red respectively.



Fig. 11. Homology-based model of a charge-neutralized mutant *Human* Acetylcholinesterase with secondary structure features. The mutated amino acid residues are colored purple. The amino acid residues of the enzyme's catalytic triad are also shown.

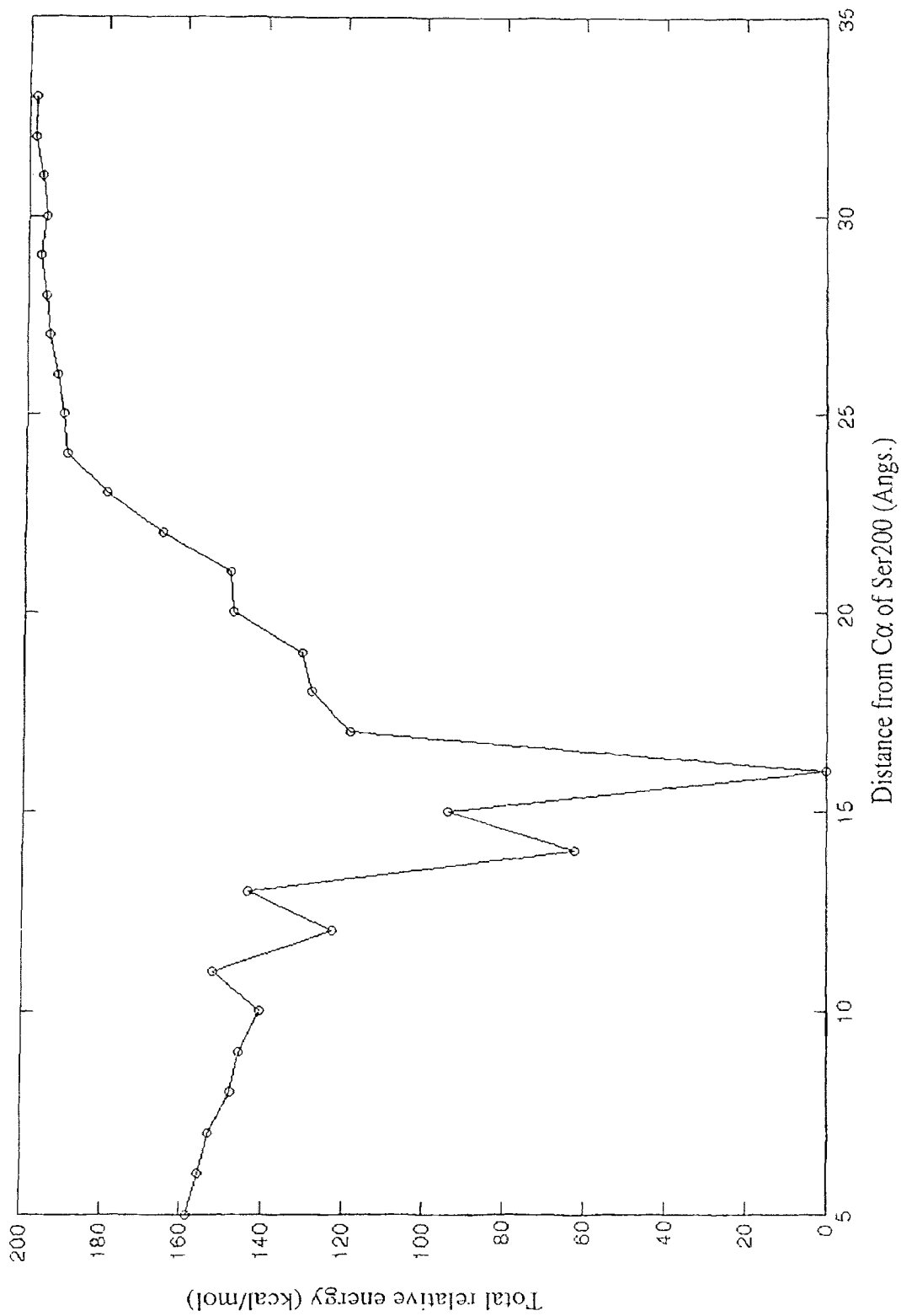


Figure 12. Relative total energy of the *Torpedo* AChE-ACh complex as a function of the distance of the center of mass of ACh from the C α atom of Ser200 residue of the active site of *Torpedo* AChE.

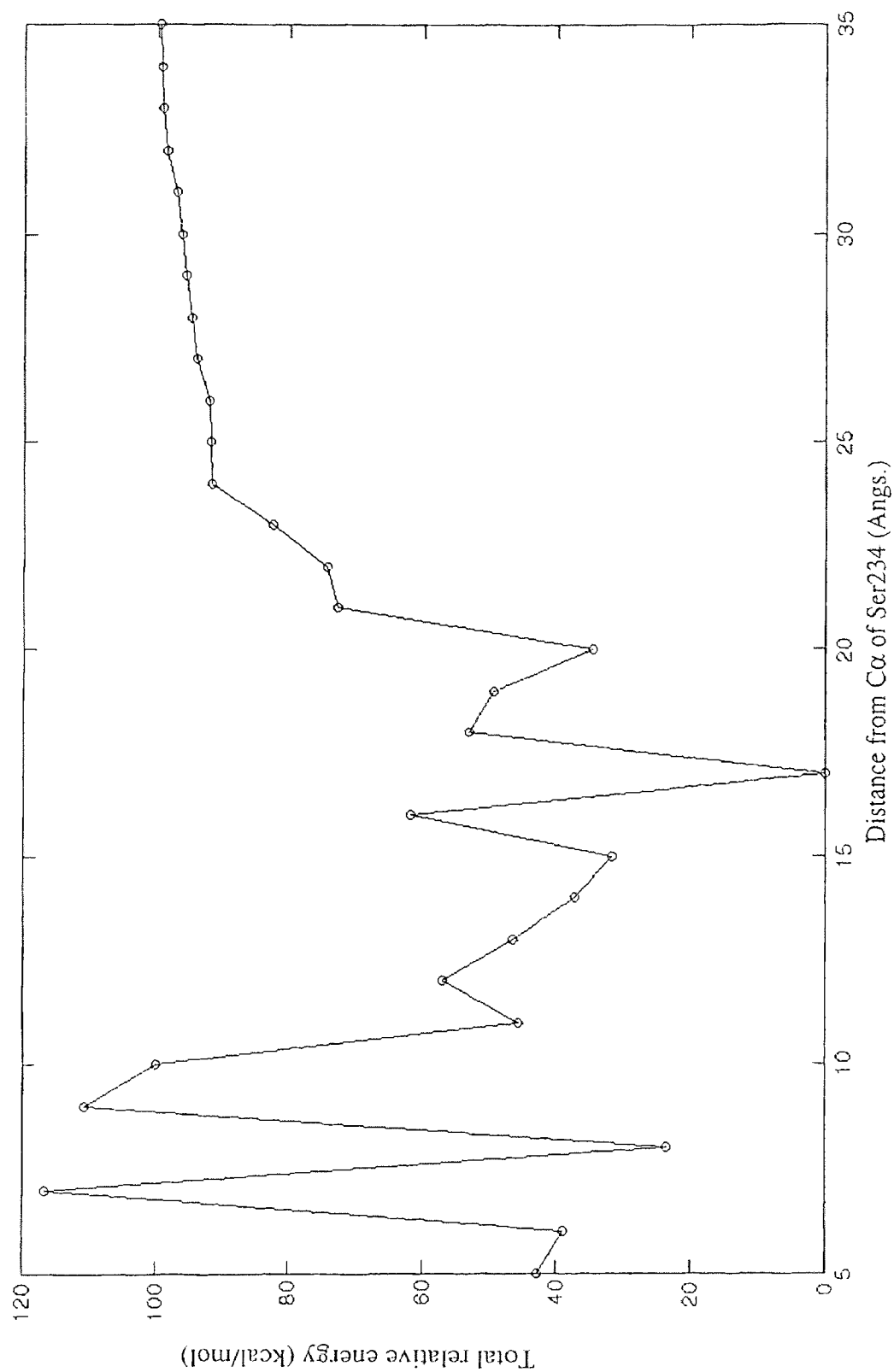


Figure 13. Total relative energy of the *Human AChE-ACh* complex as a function of the distance of the center of mass of ACh from the C α atom of Ser234 residue of the active site of *Human AChE*.

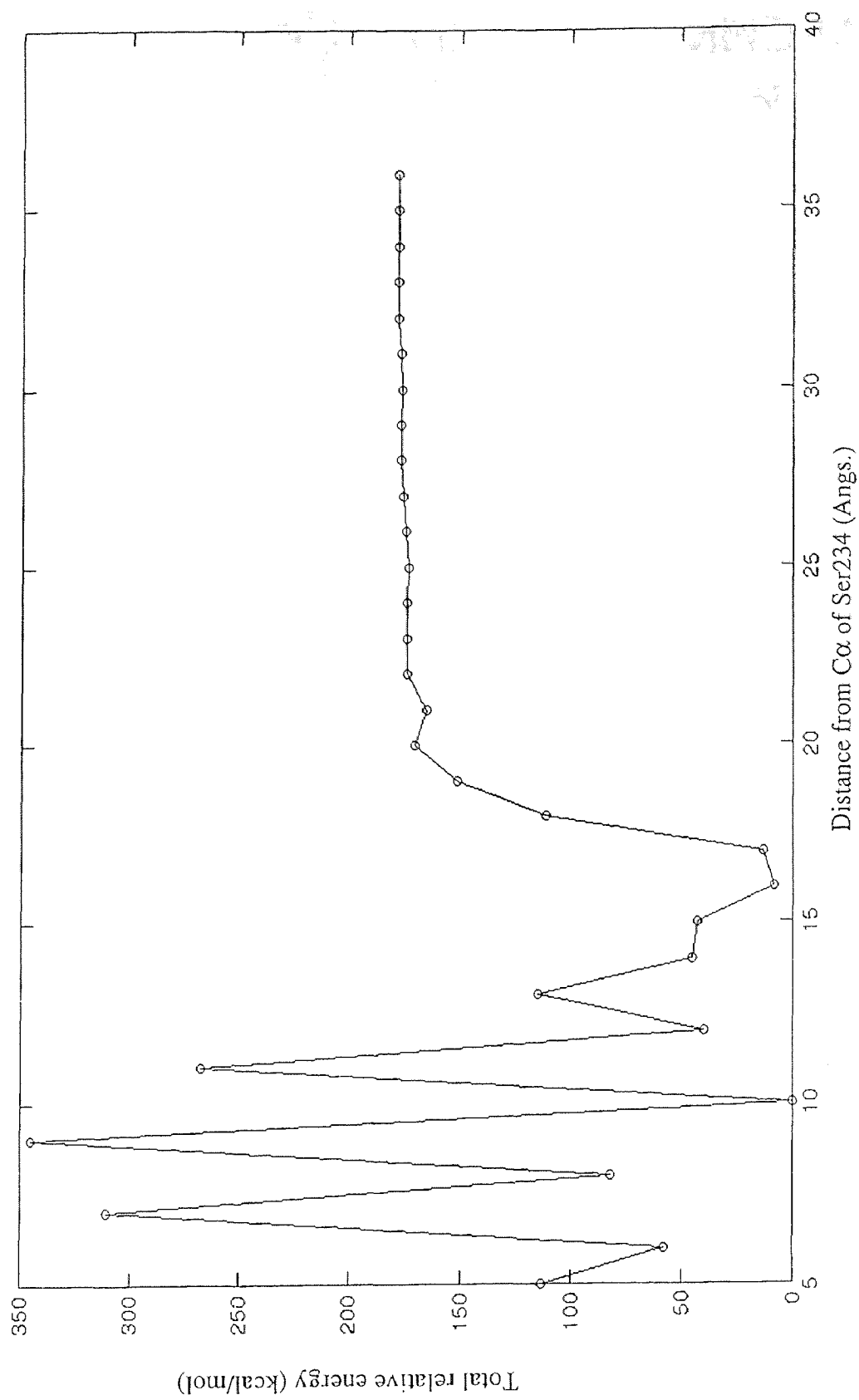


Figure 14. Relative total energy of the mutated *Human AChE-ACh* complex as a function of the distance of the center of mass of ACh from the C α atom of the Ser234 residue of the active site of the mutated *Human AChE*.

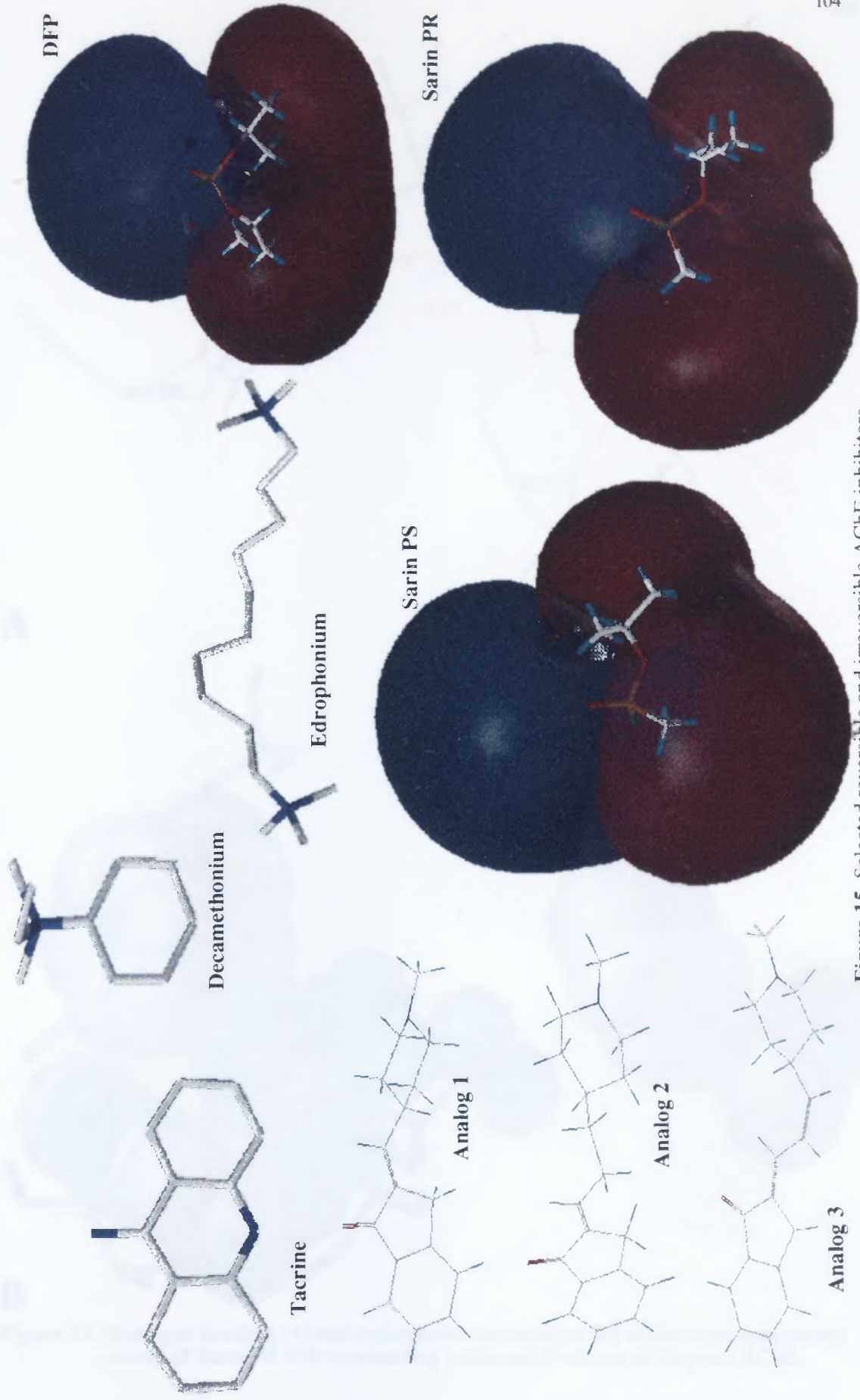


Figure 15. Selected reversible and irreversible AChE inhibitors

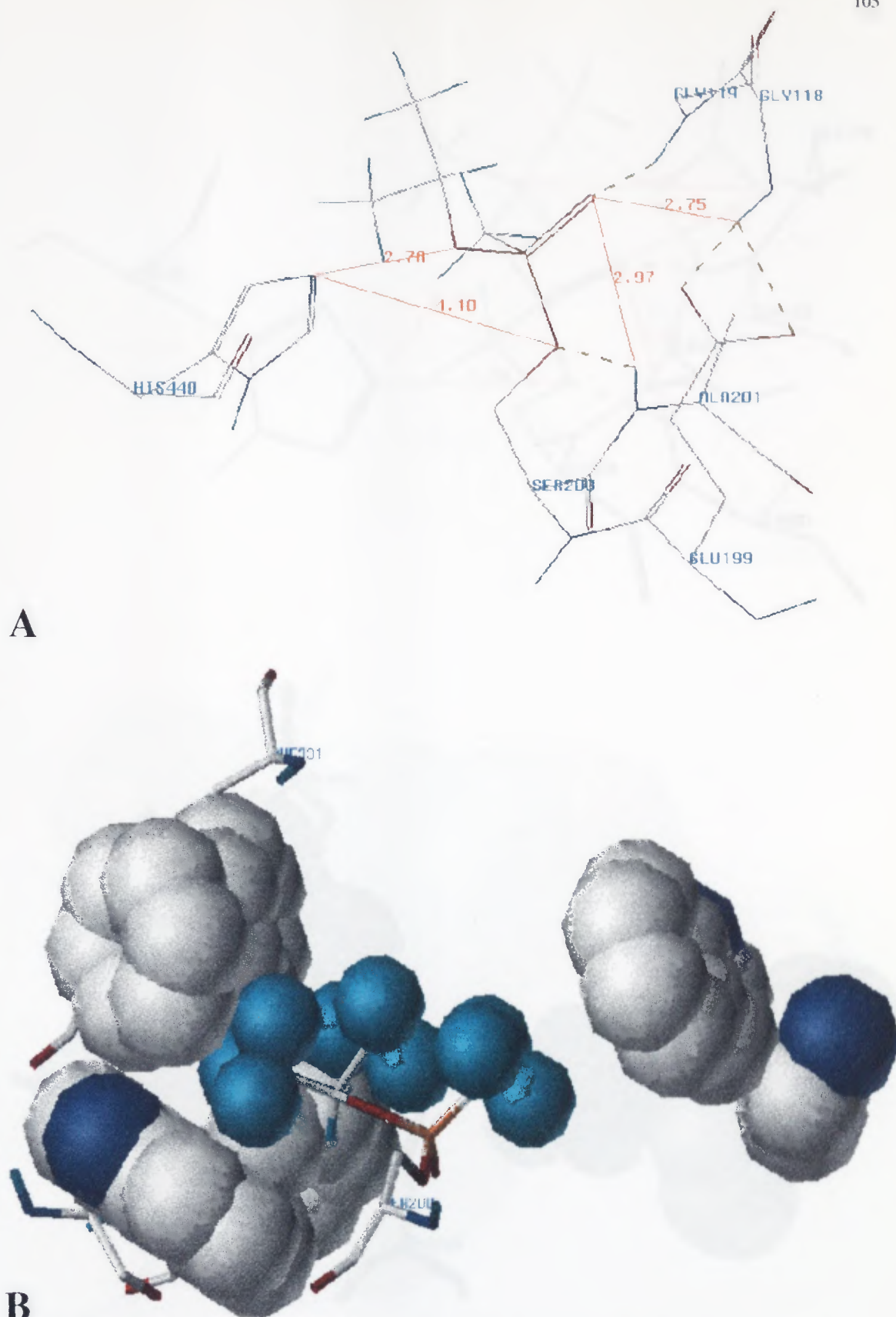
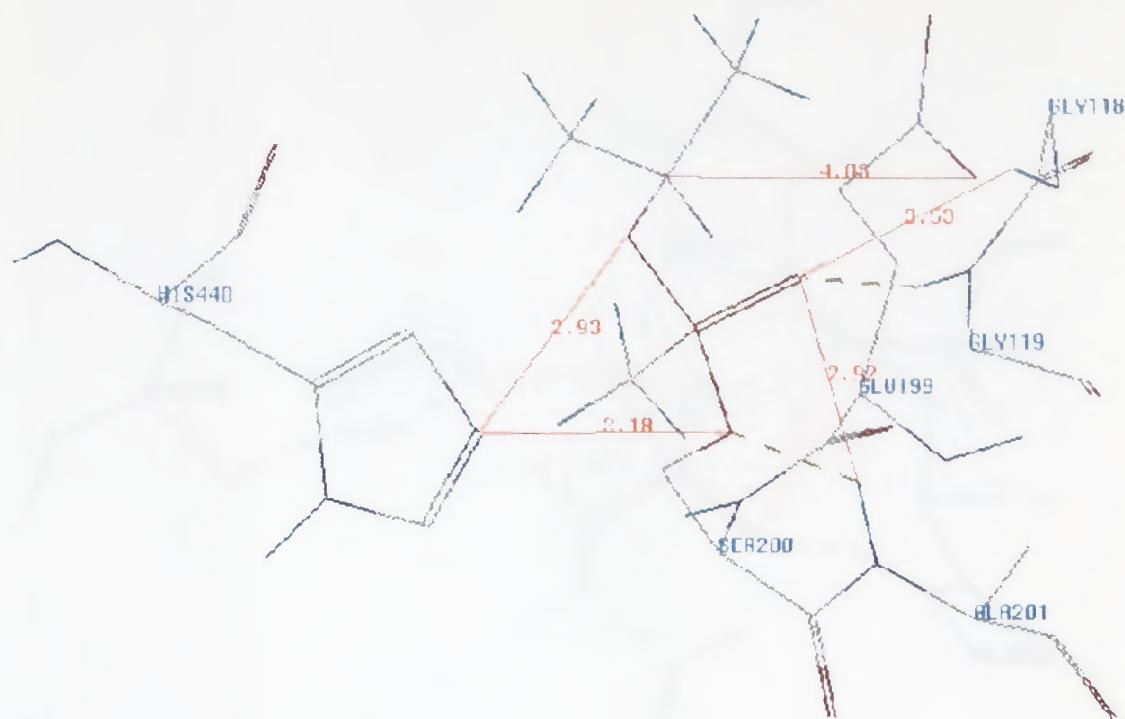
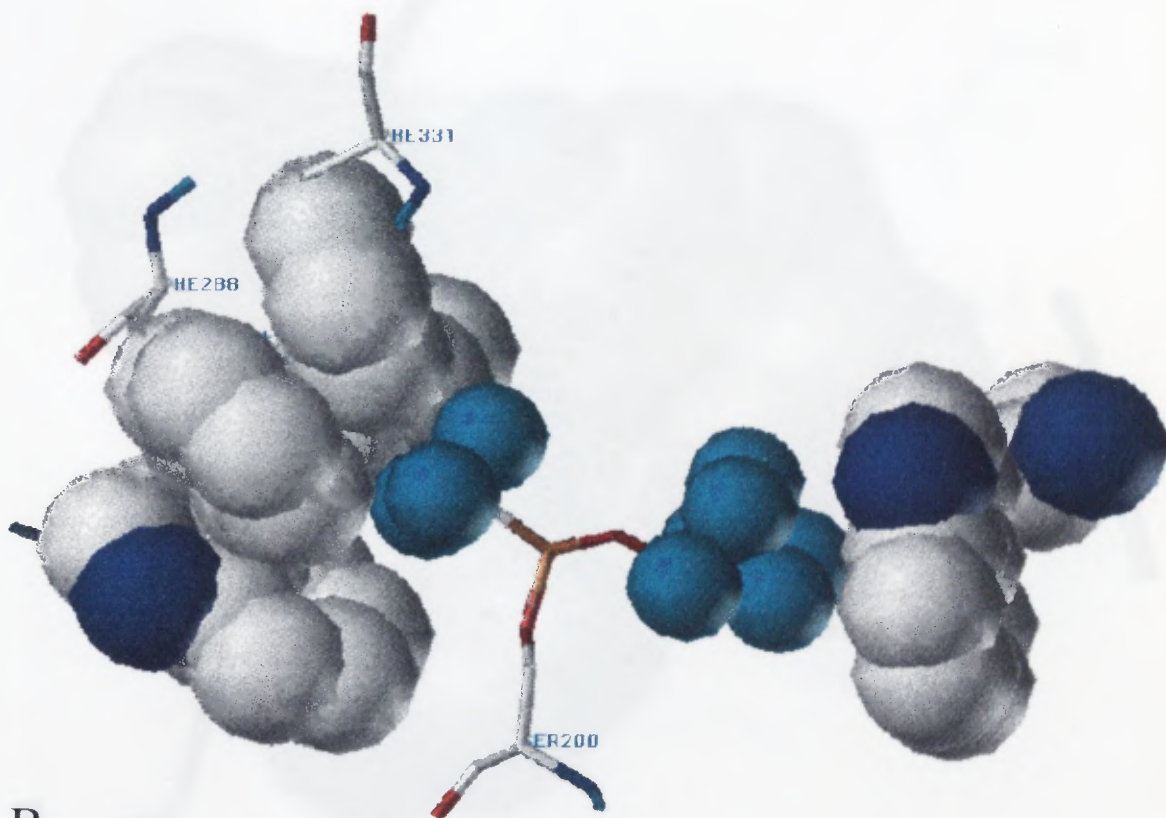


Figure 16. Hydrogen bonding (A) and hydrophobic interactions (B) of the organophosphate moiety of Sarin PR with surrounding amino acid residues of *Torpedo* AChE.



A



B

Figure 17. Hydrogen bonding (A) and hydrophobic interactions (B) of the organophosphate moiety of Sarin PS with surrounding amino acid residues of *Torpedo* AChE.

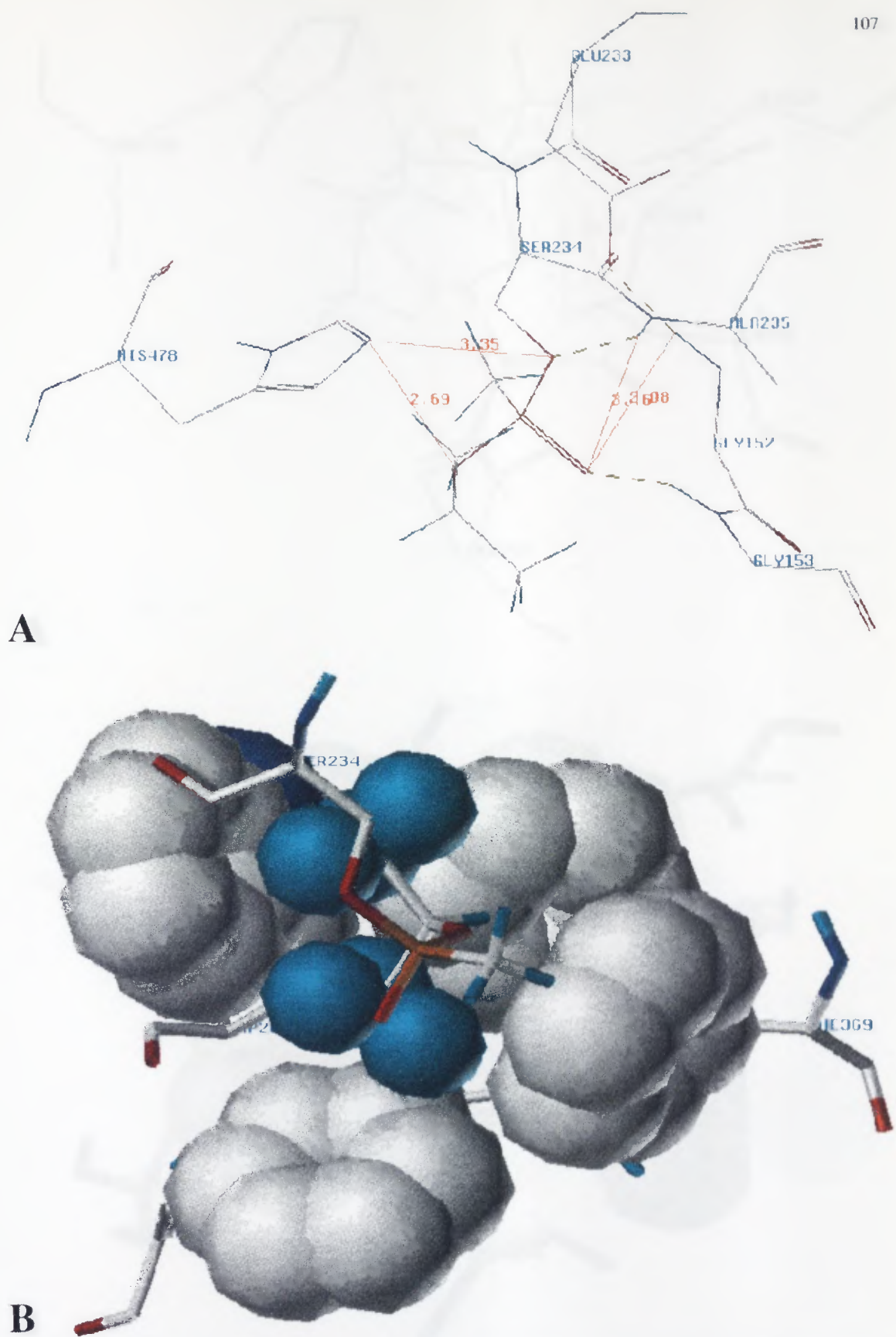
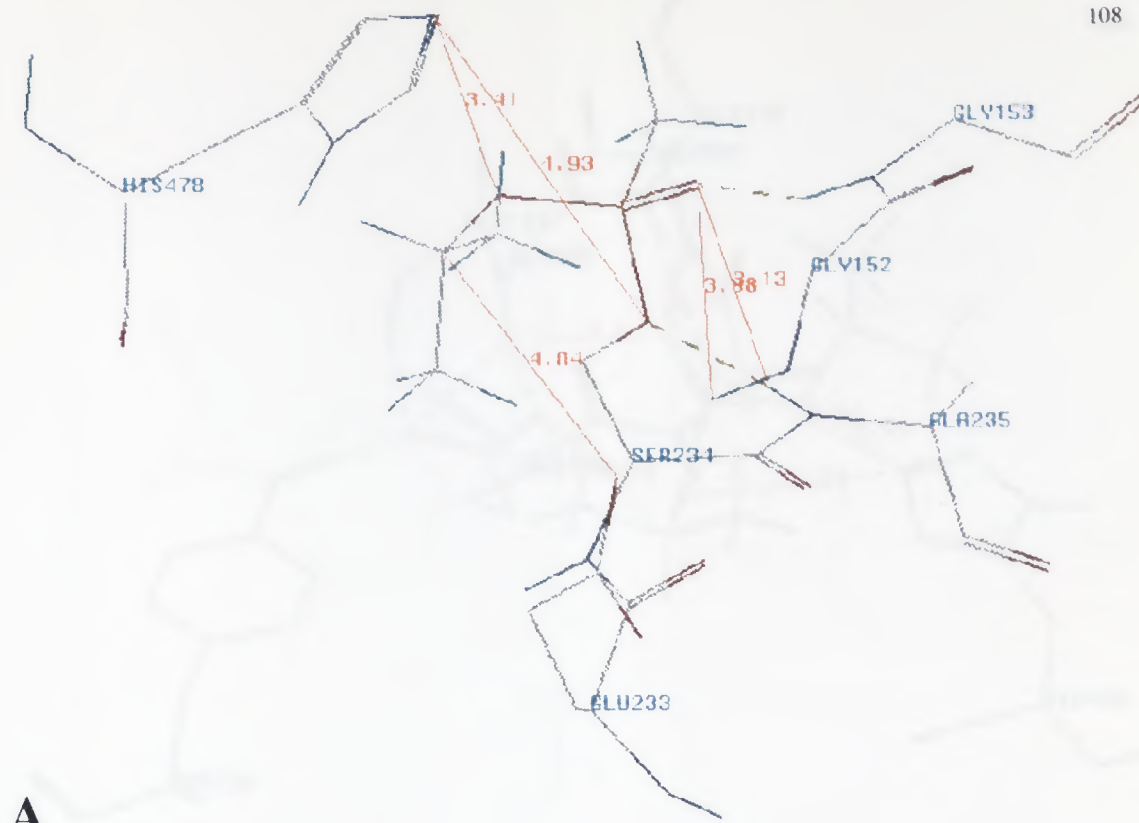
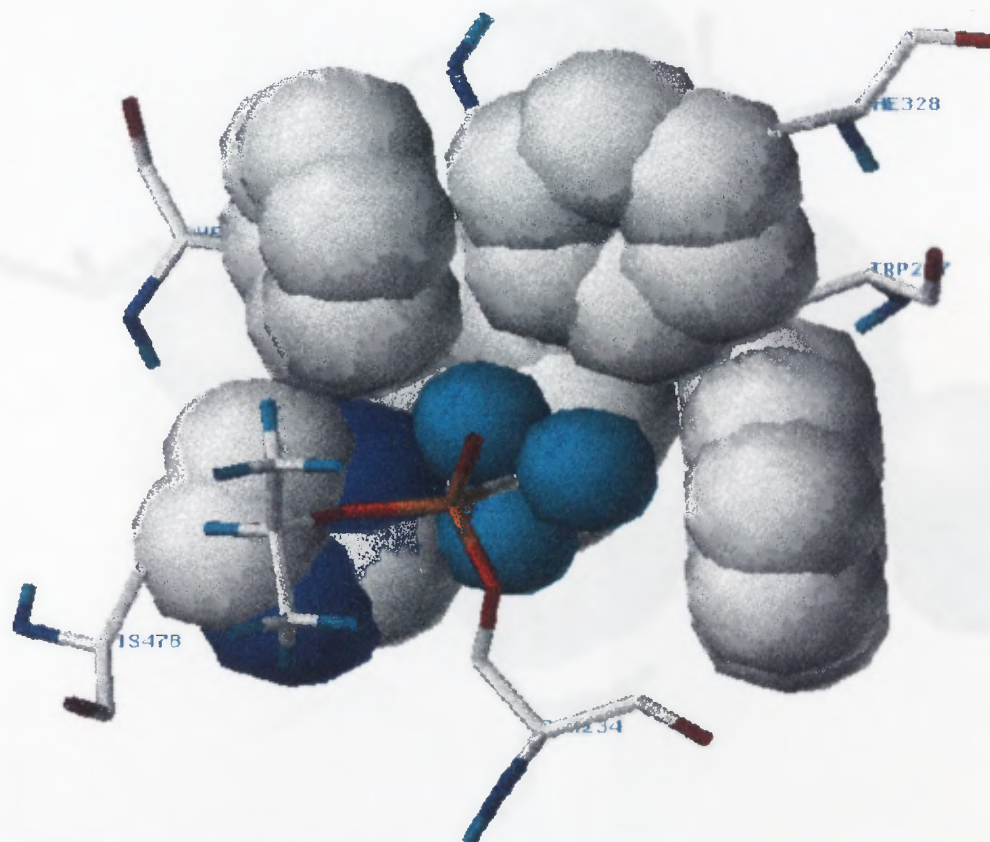
**B**

Figure 18. Hydrogen bonding (A) and hydrophobic interactions (B) of the organophosphate moiety of Sarin PR with surrounding amino acid residues of *Human AChE*.



A



B

Figure 19. Hydrogen bonding (A) and hydrophobic interactions (B) of the organophosphate moiety of Sarin PS with surrounding amino acid residues of *Human AChE*.

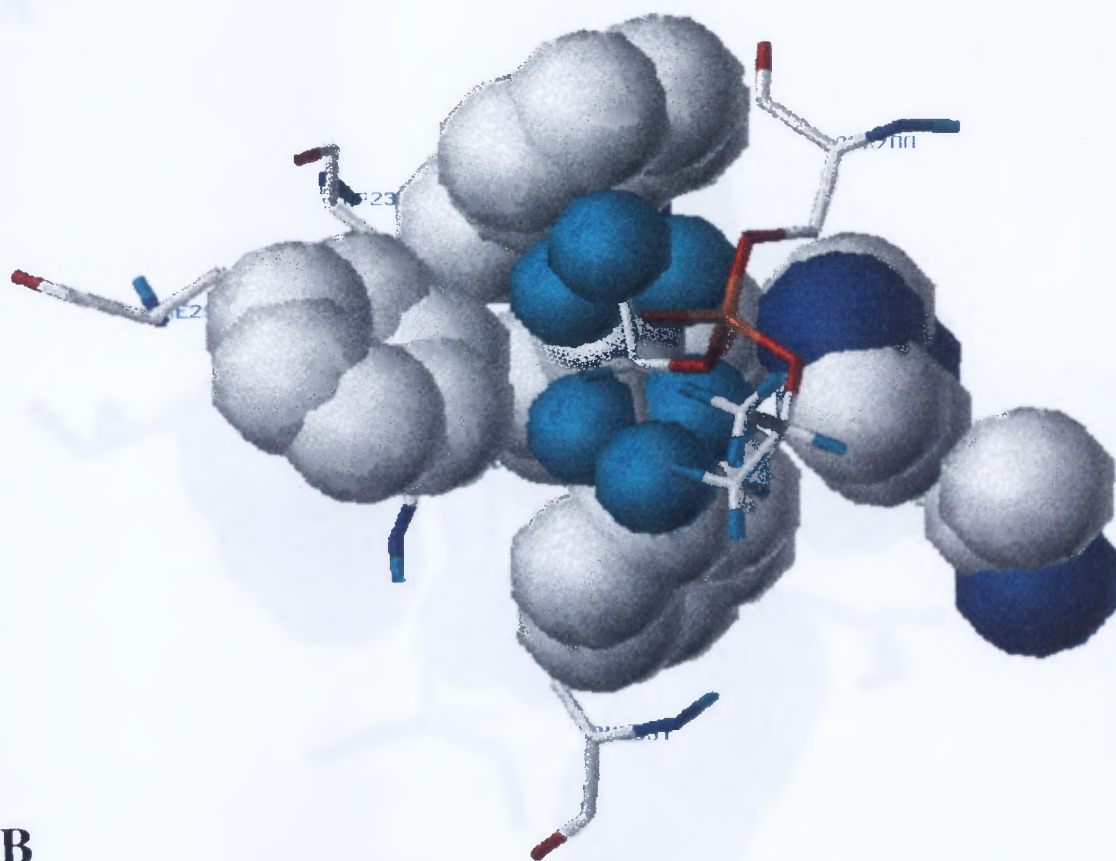
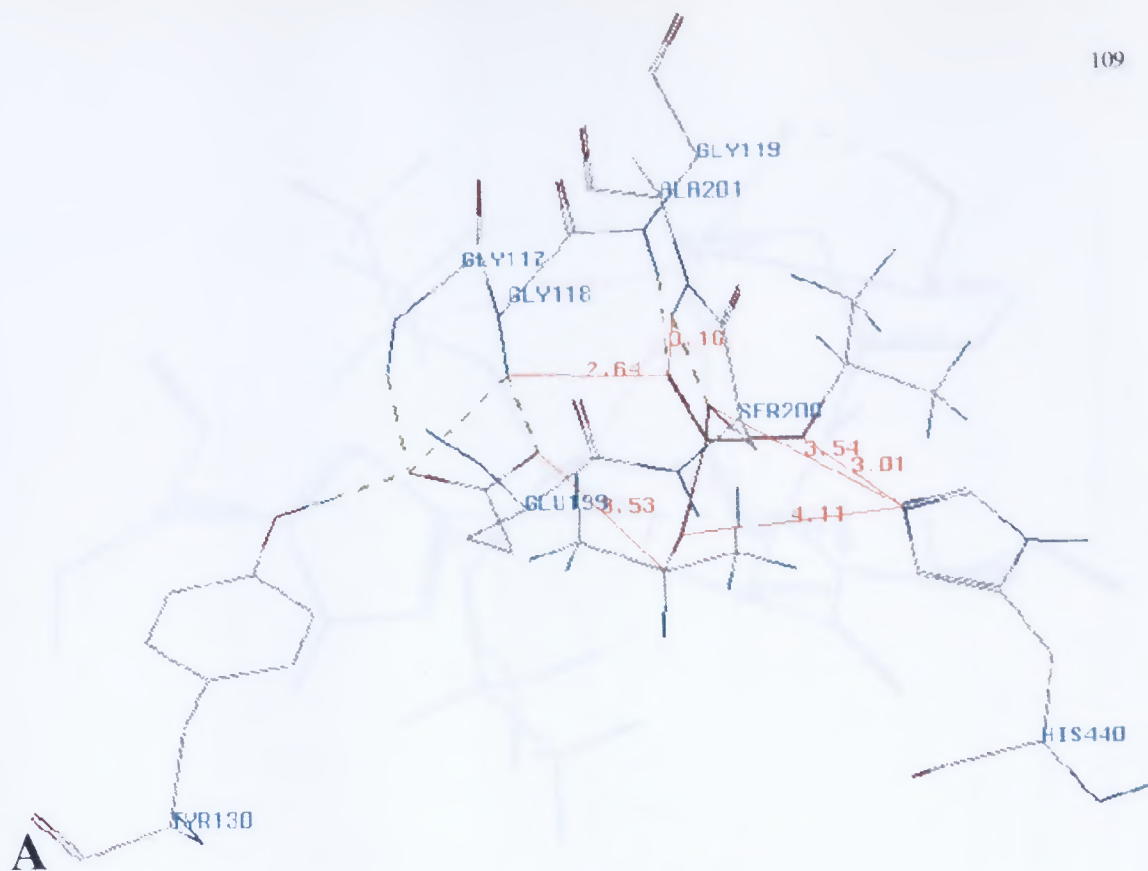


Figure 20. Hydrogen bonding (A) and hydrophobic interactions (B) of the organophosphate moiety of DFP with surrounding amino acid residues of *Torpedo Californica* AChE.

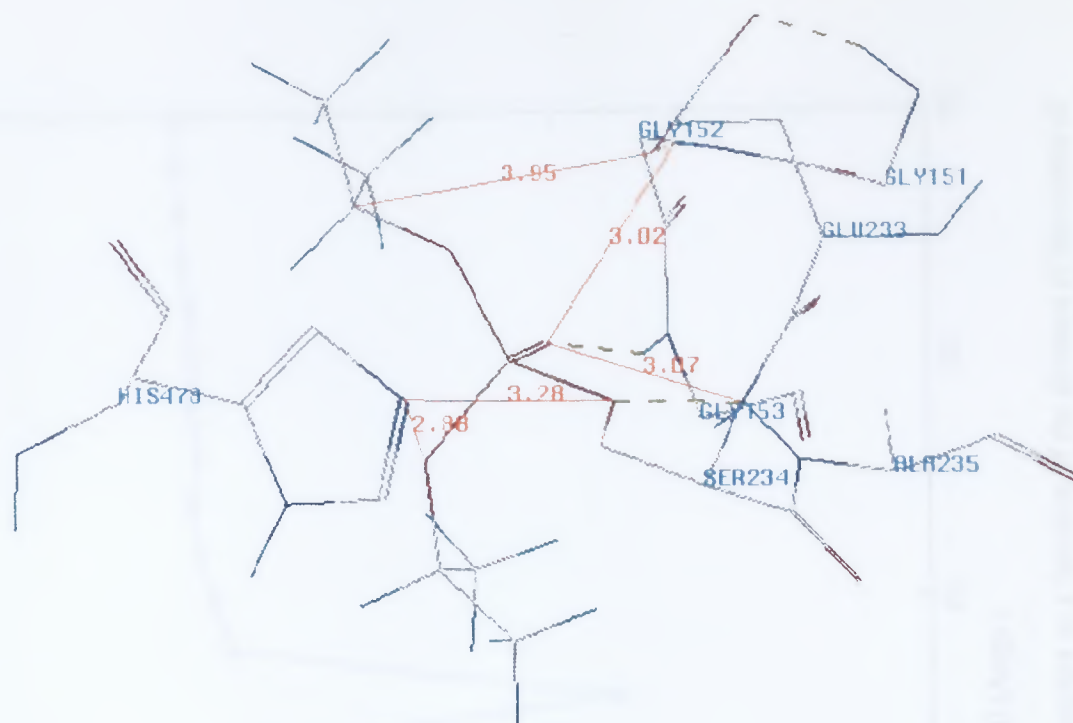
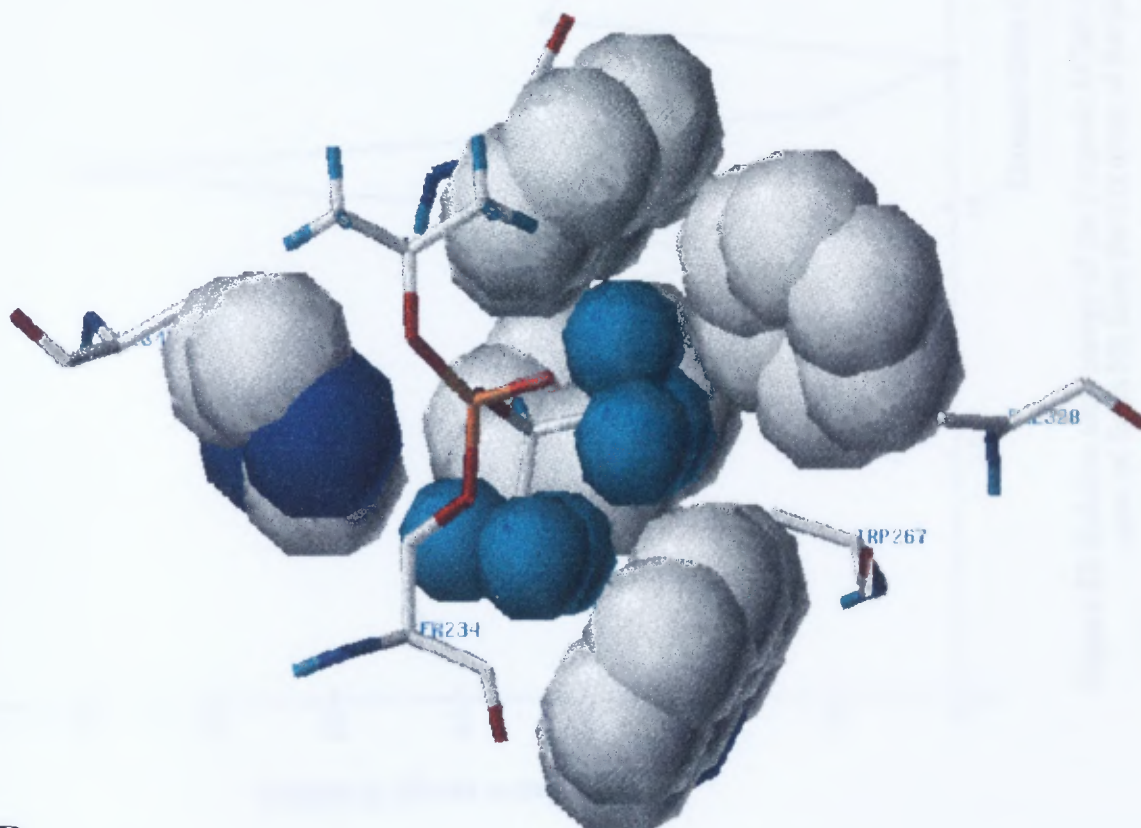
**A****B**

Figure 21. Hydrogen bonding (A) and hydrophobic interactions (B) of the organophosphate moiety of DFP with surrounding amino acid residues of *Human AChE*.

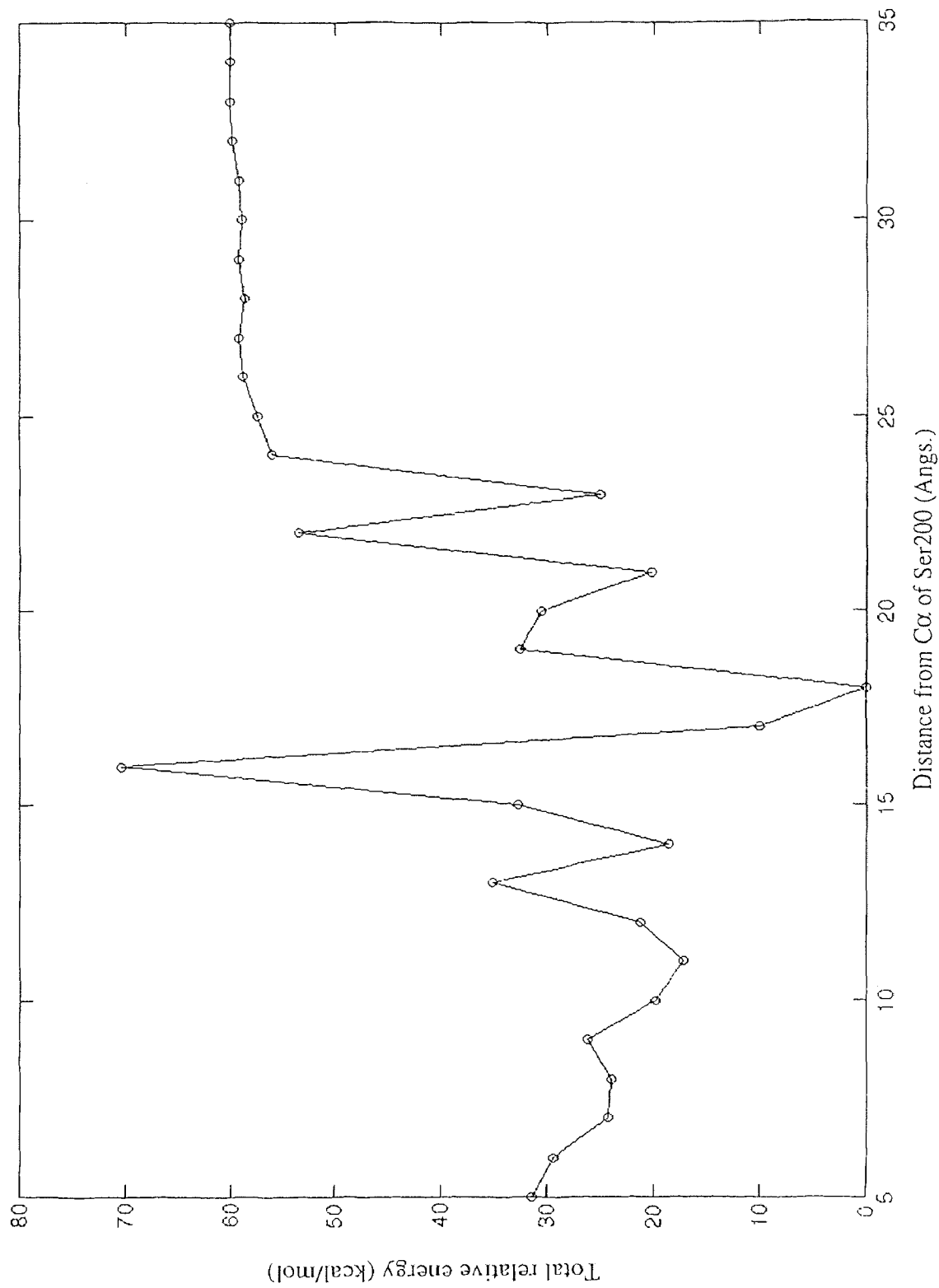


Figure 22. Relative total energy of the *Torpedo* AChE-Sarin PR complex as a function of the distance of the center of mass of Sarin PR from the C α atom of the Ser200 residue of the active site of *Torpedo* AChE.

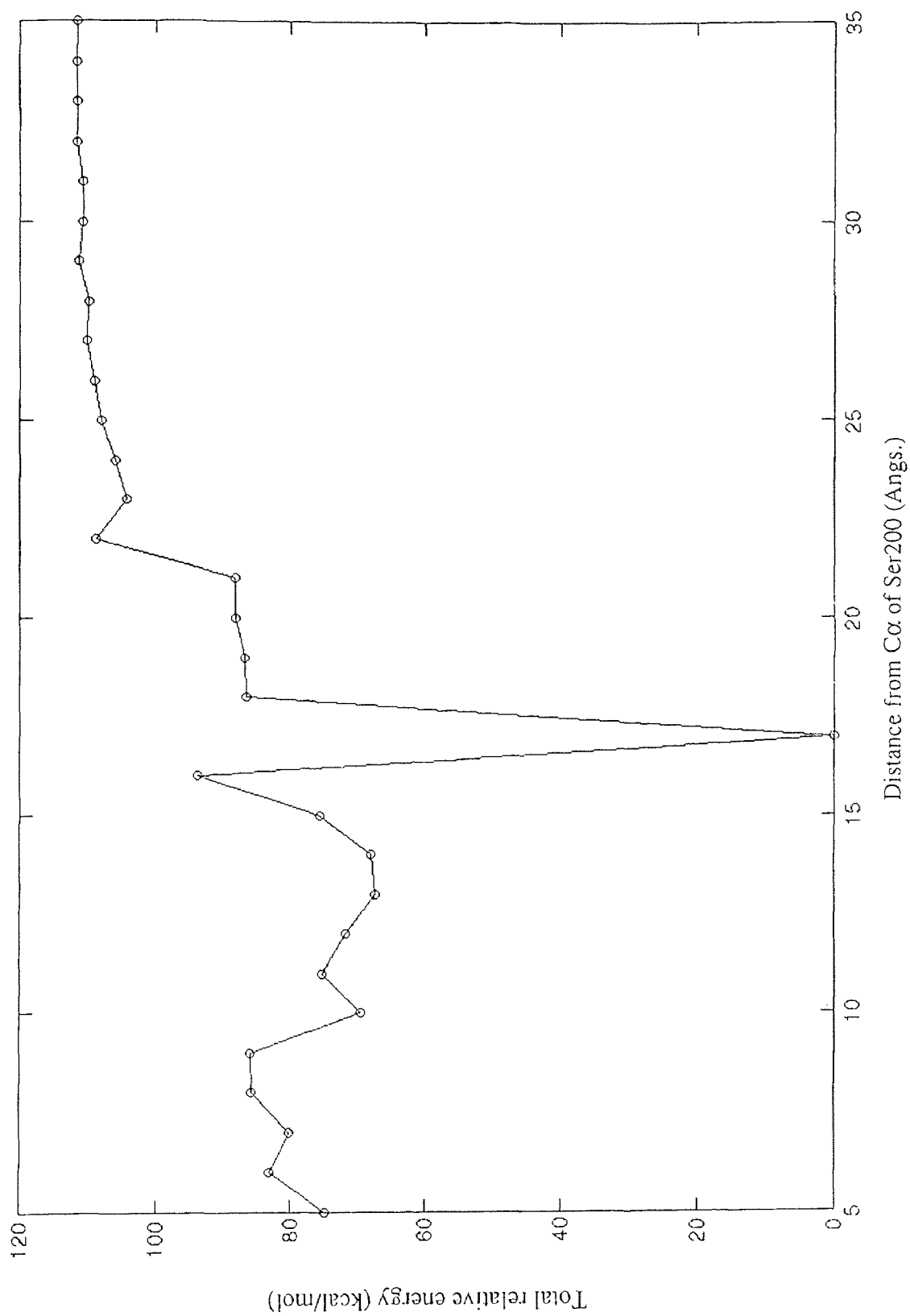


Figure 23. Relative total energy of the *Torpedo* AChE-Sarin PS complex as a function of the distance of the center of mass of Sarin PS from the C α atom of the Ser200 residue of the active site of *Torpedo* AChE.

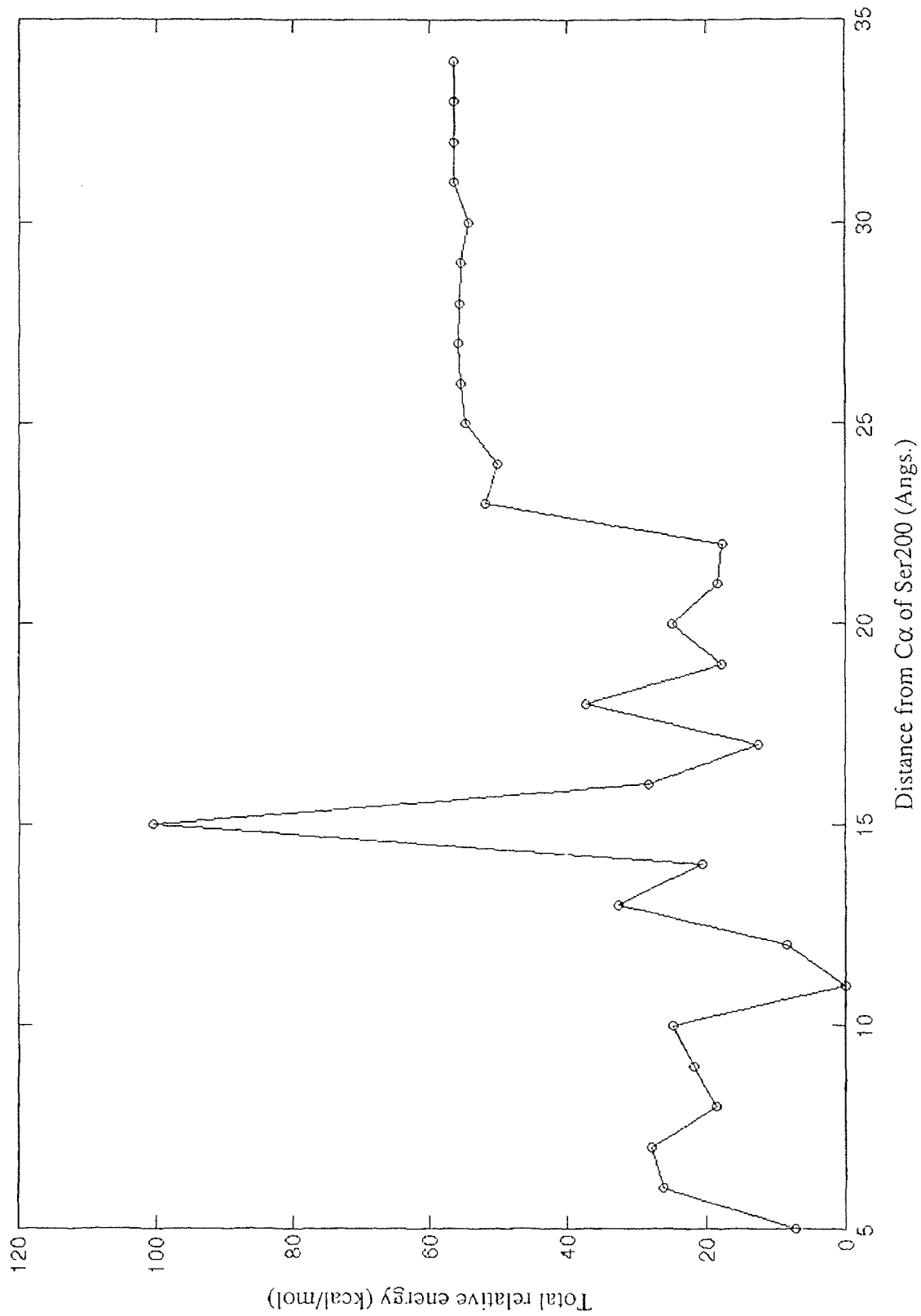


Figure 24. Relative total energy of the *Torpedo* AChE-DFP complex as a function of the distance of the center of mass of DFP from the C α atom of the Ser200 residue of the active site of *Torpedo* AChE.

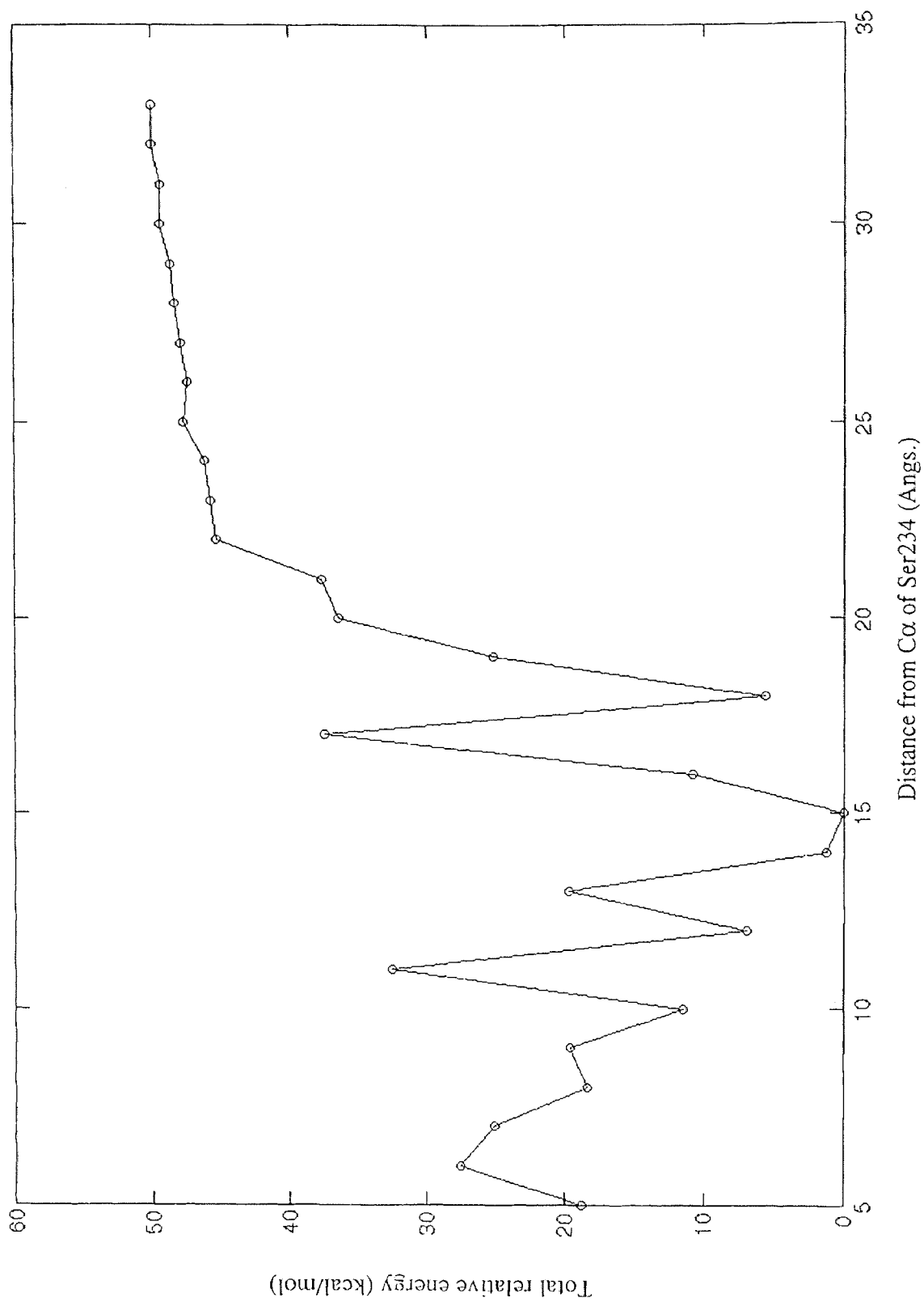


Figure 25. Relative total energy of the *Human AChE-Sarin PR* complex as a function of the distance of the center of mass of Sarin PR from the C α atom of the Ser234 residue of the active site of *Human AChE*.

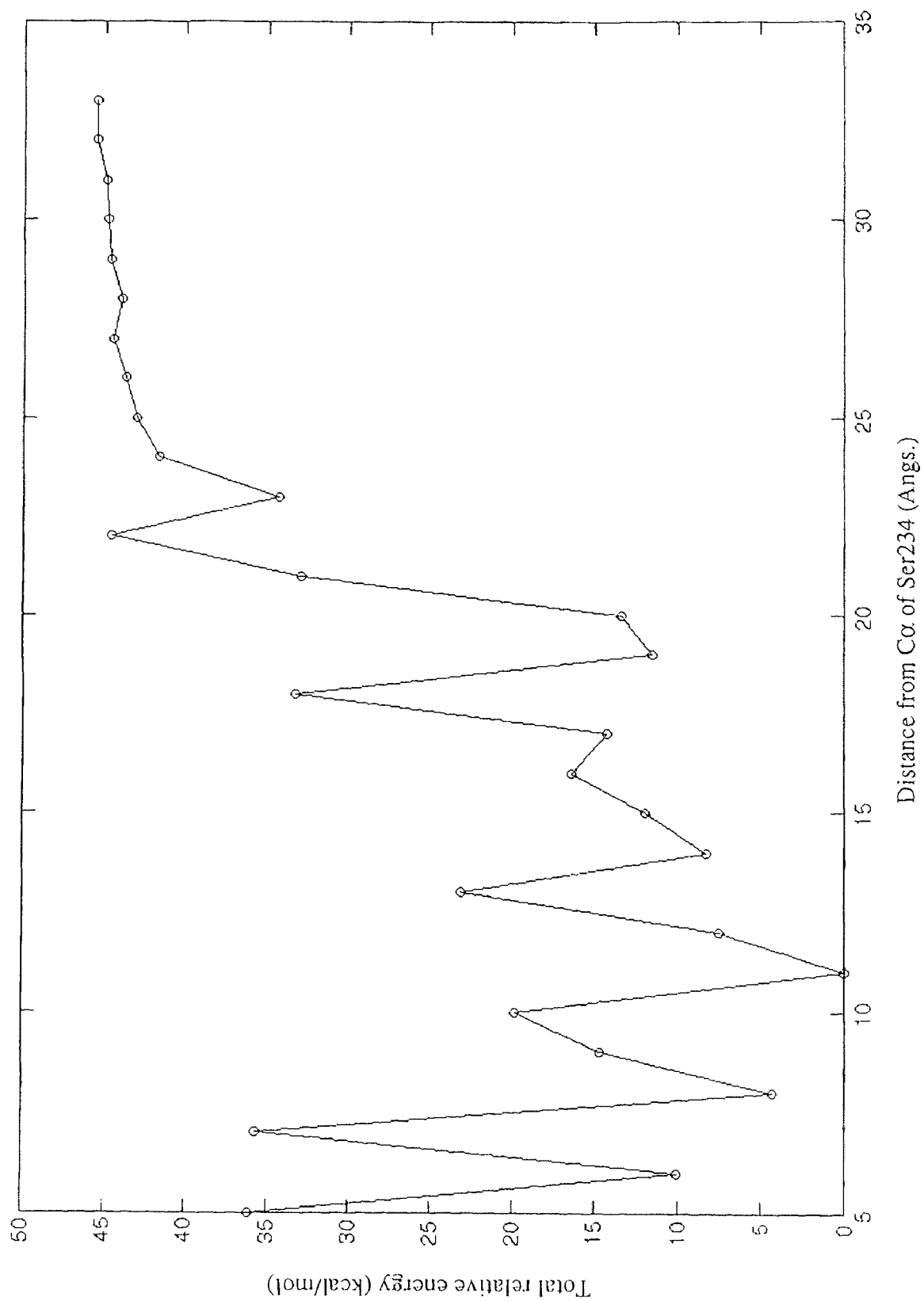


Figure 26. Relative total energy of the *Human AChE-Sarin PS* complex as a function of the distance of the center of mass of Sarin PS from the C α atom of the Ser234 residue of the active site of *Human AChE*.

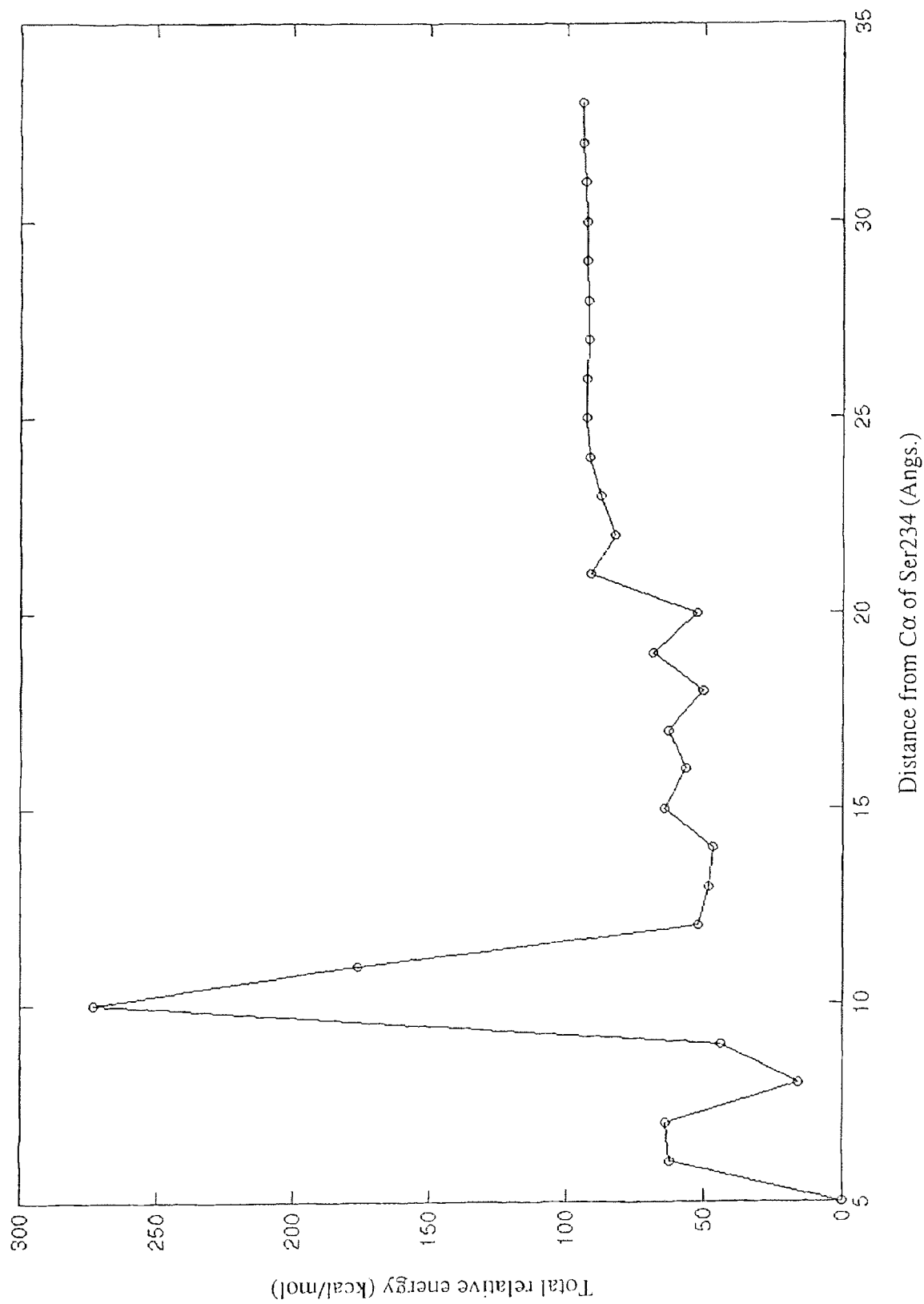


Figure 27. Relative total energy of the *Human AChE-DFP* complex as a function of the distance of the center of mass of DFP from the C α atom of Ser234 residue of the active site of *Human AChE*.

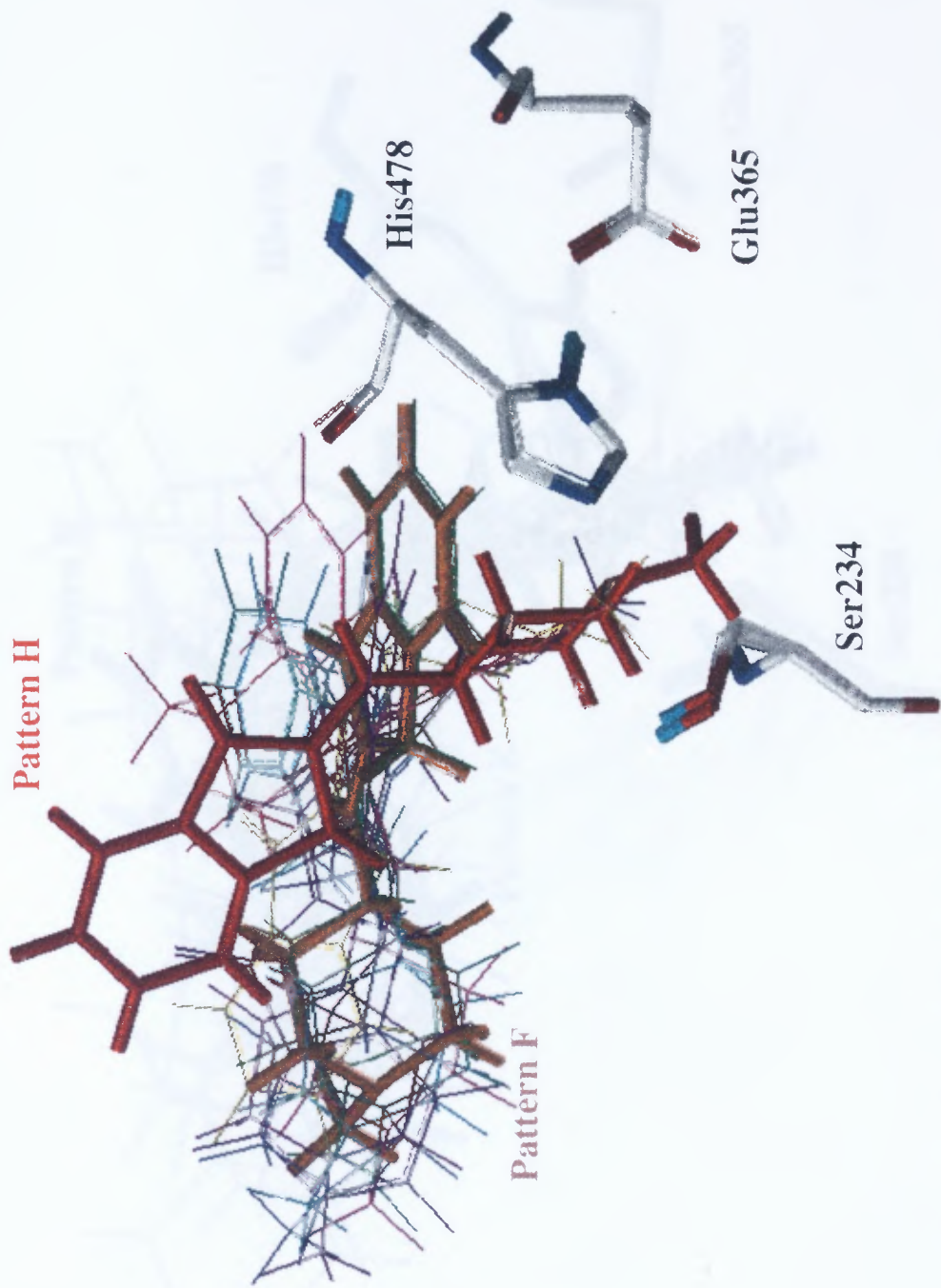


Figure 28. Superposition of the eleven identified docking conformations of Analogue 1 within the active site gorge of *Human AChE*.

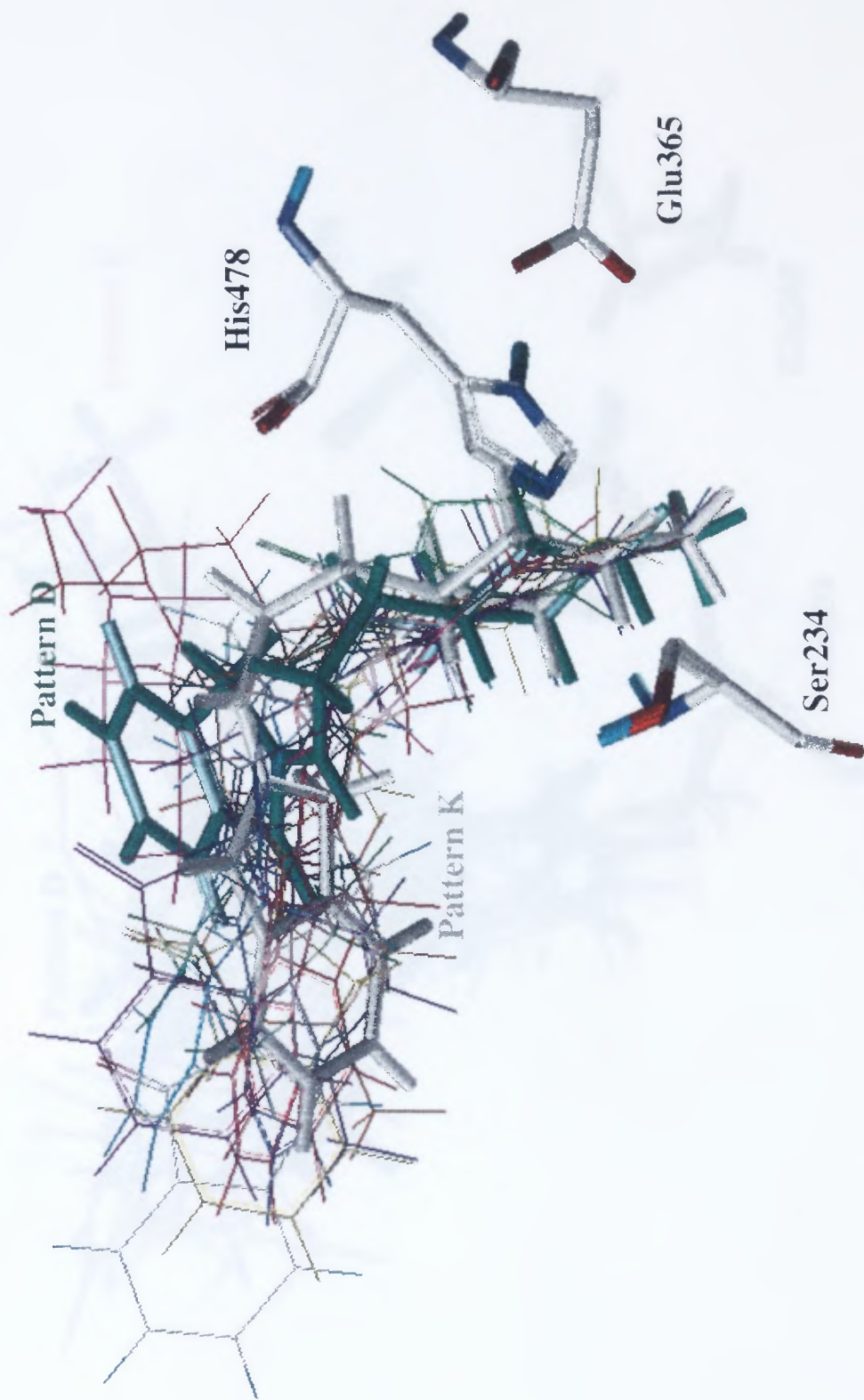


Figure 29. Superposition of the thirteen identified docking conformations of Analog 2 within the active site gorge of *Human AChE*.

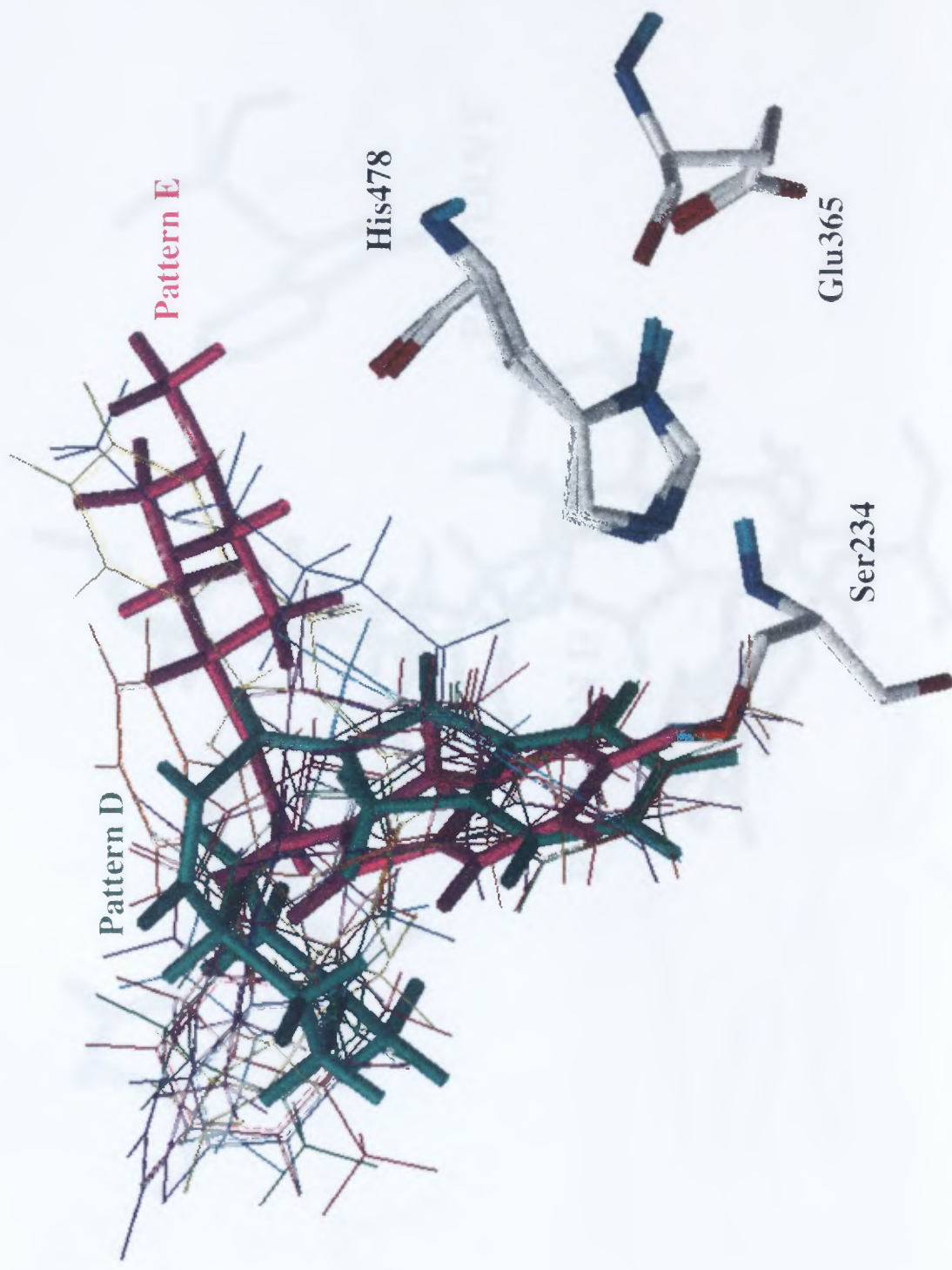


Figure 30. Superposition of the eleven identified docking conformations of Analog 3 within the active site gorge of *Human AChE*

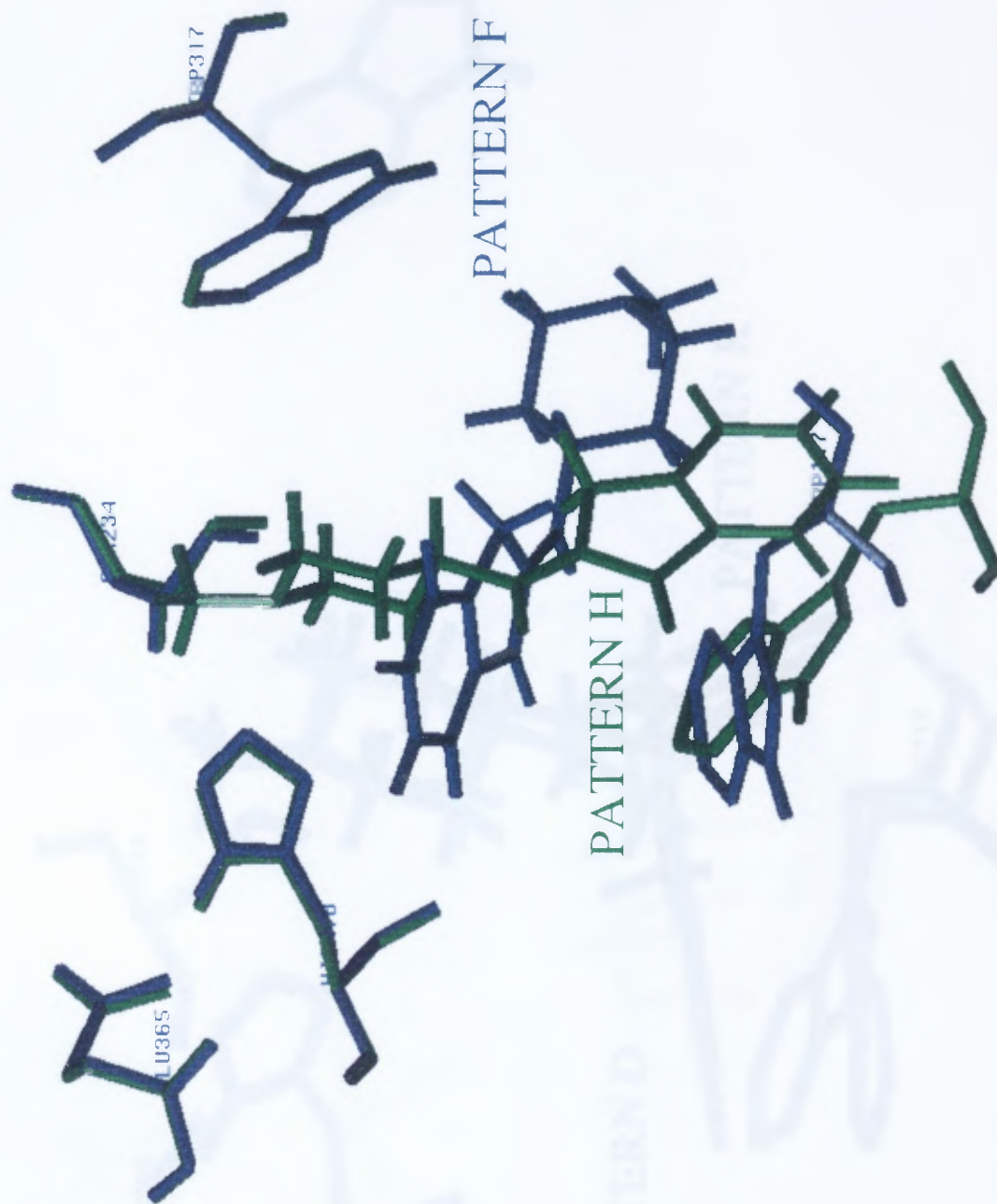


Figure 31. Predicted lowest energy binding conformations of Analog 1 in *Human Acetylcholinesterase*.

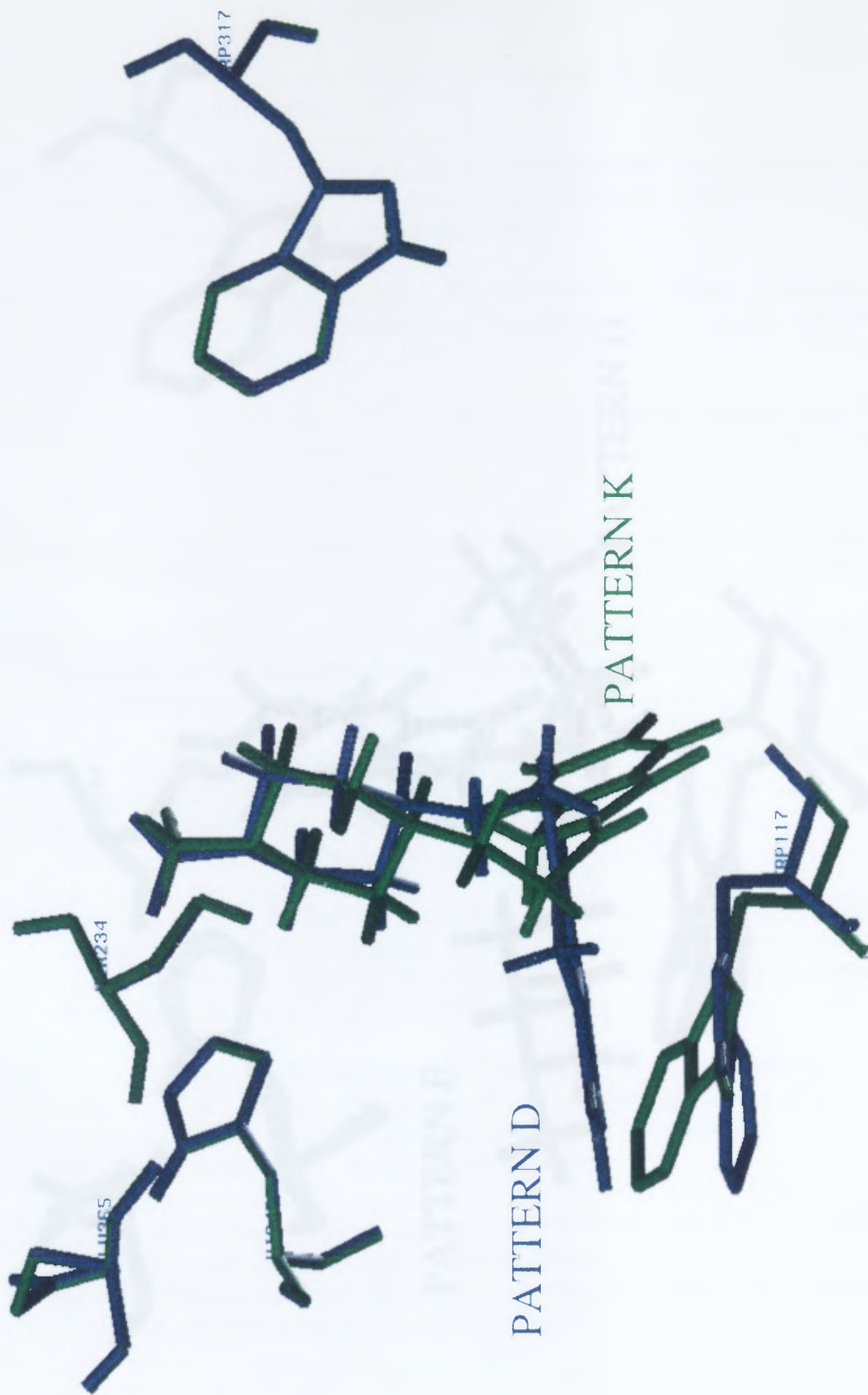


Figure 32. Predicted lowest energy binding conformations of Analogue 2 in Human Acetylcholinesterase.

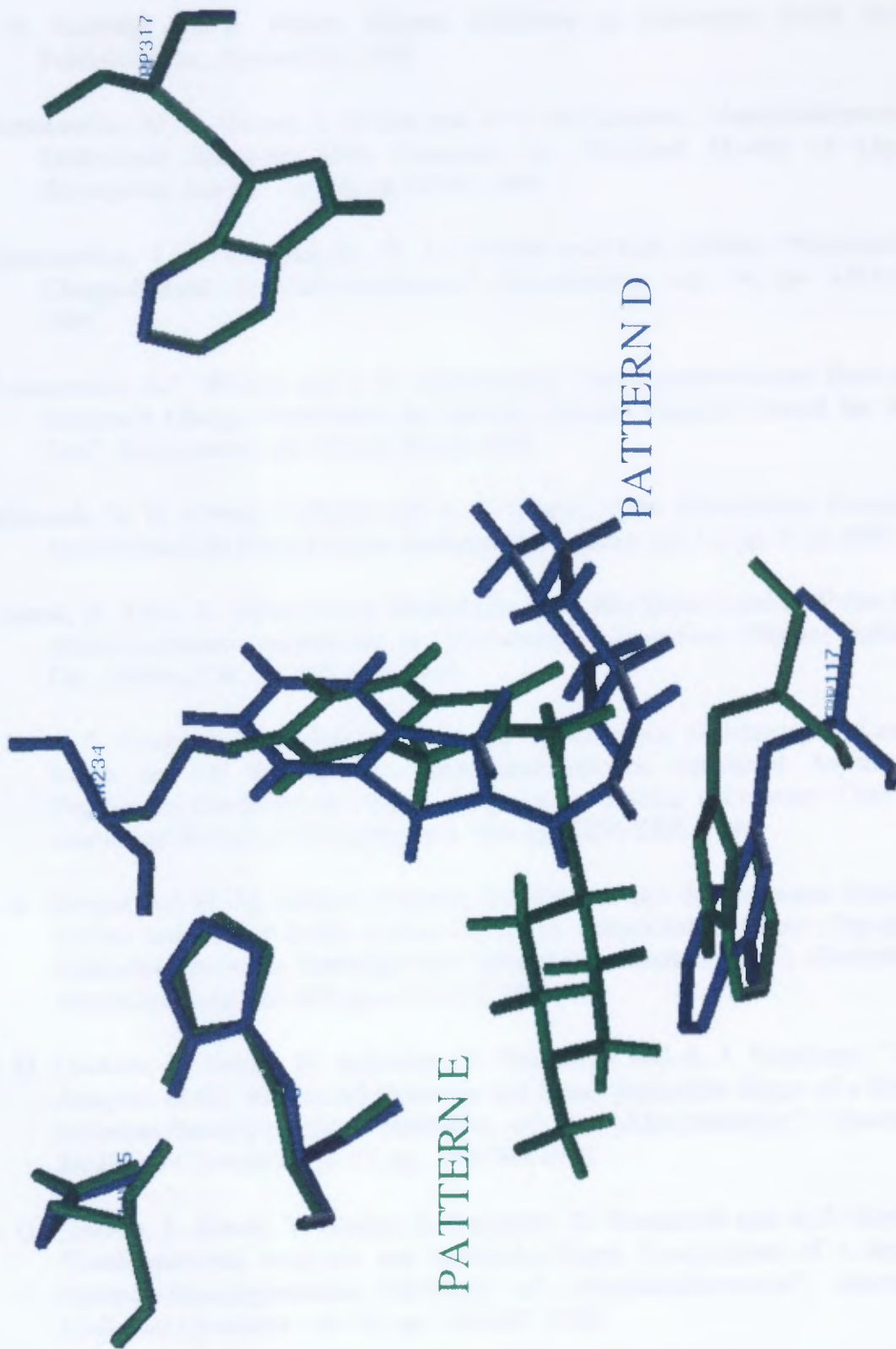


Figure 33. Predicted lowest energy binding conformations of Analog 3 in *Human Acetylcholinesterase*.

REFERENCES

- W. N. Aldridge and E. Reiner, *Enzyme Inhibitors as Substrates*, North Holland Publishing Co., Amsterdam, 1972.
- J. Antosiewicz, M. K. Gilson, I. H. Lee and J. A. McCammon, "Acetylcholinesterase: Diffusional Encounter Rate Constants for Dumbbell Models of Ligand", *Biophysical Journal*, vol. 68, pp. 62-68, 1995.
- J. Antosiewicz, J. A. McCammon, S. T. Wlodek and M.K. Gilson, "Simulation of Charge-Mutant Acetylcholinesterases", *Biochemistry*, vol. 34, pp. 4211-4219, 1995.
- J. Antosiewicz, S.T. Wlodek and J. A. McCammon, "Acetylcholinesterase: Role of the Enzyme's Charge Distribution in Steering Charged Ligands Toward the Active Site", *Biopolymers*, vol. 39, pp. 85-94, 1996.
- J. Bajorath, D. H. Kitson, J. Kraut and A. T. Hagler, "The Electrostatic Potential of Escherichia Coli Dihydrofolate Reductase", *Proteins*, vol. 11, pp. 1-12, 1991.
- D. Barak, N. Ariel, B. Velan and A. Shafferman in A. Shafferman and B. Velan (eds.), *Multidisciplinary Approaches to Cholinesterase Functions*, Plenum Publishing Co., London, UK, pp. 195-199, 1992.
- D. Barak, C. Kronman, A. Ordentlich, N. Ariel, A. Bromberg, D. Marcus, A. Lazar, B. Velan and A. Shafferman, "Acetylcholinesterase Peripheral Anionic Site Degeneracy Conferred by Amino Acid Arrays Sharing a Common Core", *The Journal of Biological Chemistry*, vol. 264, pp. 6296-6305, 1994.
- H. A. Berman and M. M. Decker, "Kinetic, Equilibrium and Spectroscopic Studies on Cation Association at the Active Center of Acetylcholinesterase: Topographic Distinction between Trimethyl and Trimethylammonium Sites", *Biochimica et Biophysica Acta*, vol. 872, pp. 125-133, 1986.
- M. G. Cardozo, Y. Iimura, H. Sugimoto, Y. Yamanishi and A. J. Hopfinger, "QSAR Analyses of the Substituted Indanone and Benzylpiperidine Rings of a Series of Indanone-Benzylpiperidine Inhibitors of Acetylcholinesterase", *Journal of Medicinal Chemistry*, vol. 35, pp. 584-589, 1992.
- M. G. Cardozo, T. Kawai, Y. Iimura, H. Sugimoto, Y. Yamanishi and A. J. Hopfinger, "Conformational Analyses and Molecular-Shape Comparisons of a Series of Indanone-Benzylpiperidine Inhibitors of Acetylcholinesterase", *Journal of Medicinal Chemistry*, vol. 35, pp. 590-601, 1992.

- M. Clark, R. D. Cramer and N. Van Opdenbosch, "Validation of the General Purpose Tripos 5.2 Force Field", *Journal of Computational Chemistry*, vol. 10, pp. 982-1012, 1989.
- M. E. Davis, J. D. Madura, J. Sines, B. A. Luty, S. A. Allison and J. A. McCammon, "Diffusion-Controlled Enzymatic Reactions", *Methods in Enzymology*, vol. 202, pp. 473-497, 1991.
- B. P. Doctor, T. C. Chapman, C. E. Christner, C. D. Deal, D. M. De La Hoz, M. K. Gentry, R. A. Ogert, R. S. Rush, K. K. Smyth and A. D. Wolfe, "Complete Amino Acid Sequence of Fetal Bovine Serum Acetylcholinesterase and its Comparison in Various Regions with other Cholinesterases", *FEBS Letters*, vol. 266, pp. 123-127, 1990.
- GCG 8.0, Genetics Computer Group, Madison, WI, 1994.
- M. Harel, C. T. Su, F. Frolow, Y. Ashani, I. Silman and J. L. Sussman, "Refined Crystal Structures of "Aged" and "Non-aged" Organophosphoryl Conjugates of γ -Chymotrypsin", *Journal of Molecular Biology*, vol. 221, pp. 909-918, 1991.
- M. Harel, I. Schalk, L. Ehret-Sabatier, F. Bouet, M. Goeldner, C. Hirth, P. H. Axelsen, I. Silman and J. L. Sussman, "Quaternary Ligand Binding to Aromatic Residues in the Active-Site Gorge of Acetylcholinesterase", *Proceedings of the National Academy of Sciences of the United States of America*, vol. 90, pp. 9031-9035, 1993.
- Insight II 95.0, Biosym/MSI, San Diego, CA, 1995.
- A. Inoue, T. Kawai, M. Wakita, Y. Iimura, H. Sugimoto and Y. Kawakami, "The Simulated Binding of (\pm)-2,3-Dihydro-5,6-dimethoxy-2-[[1-(phenylmethyl)-4-piperidinyl]methyl]-1*H*-inden-1-one Hydrochloride (E2020) and Related Inhibitors to Free and Acylated Acetylcholinesterases and Corresponding Structure-Activity Analyses", *Journal of Medicinal Chemistry*, vol. 39, pp. 4460-4470, 1996.
- M. Levitt, "Protein Folding by Restrained Energy Minimization and Molecular Dynamics", *Journal of Molecular Biology*, vol. 170, pp. 723-764, 1983.
- M. Levitt, "Accurate Modeling of Protein Conformation by Automatic Segment Matching", *Journal of Molecular Biology*, vol. 226, pp. 507-533, 1992.
- LOOK 2.0, Molecular Applications Group, Palo Alto, CA, 1995.
- B. A. Luty, R. C. Wade, J. D. Madura, M. E. Davis, J. M. Briggs and J. A. McCammon, "Brownian Dynamics Simulations of Diffusional Encounters between Triose

Phosphate Isomerase and Glyceraldehyde Phosphate: Electrostatic Steering of Glyceraldehyde Phosphate”, *Journal of Physical Chemistry*, vol. 97, pp. 233-237, 1993.

- A. R. Main in A. M. Goldberg and I. Hanin (eds.), *Biology of Cholinergic Function*, Random Press, New York, pp. 269-353, 1976.
- G. M. Morris, D. S. Goodsell and R. Huey, *AutoDock 2.4, Automated Docking of Flexible Ligands to Receptors*, 1996.
- S. B. Needleman and C. D. Wunsch, “A General Method Applicable to the Search for Similarities in the Amino Acid Sequence of Two Proteins”, *Journal of Molecular Biology*, vol. 48, pp. 443-453, 1970.
- A. Ordentlich, C. Kronman, D. Barak, D. Stein, N. Ariel, D. Marcus, B. Velan and A. Shafferman, “Engineering Resistance to “Aging” of Phosphylated Human Acetylcholinesterase”, *FEBS Letters*, vol. 334, pp. 215-220, 1993.
- Y. Pang and A. P. Kozikowski, “Prediction of the Binding Sites of Huperzine A in Acetylcholinesterase by Docking Studies”, *Journal of Computer-Aided Molecular Design*, vol. 8, pp. 669-681, 1994.
- Y. Pang and A. P. Kozikowski, “Prediction of the Binding Site of 1-benzyl-4-[(5,6-dimethoxy-1-indanon-2-yl)methyl]piperidine in Acetylcholinesterase by Docking Studies with the SYSDOC Program”, *Journal of Computer-Aided Molecular Design*, vol. 8, pp. 683-693, 1994.
- Y. Pang, P. Quiram, T. Jelacic, F. Hong and S. Brimijoin, “Highly Potent, Selective, and Low Cost Bis-tetrahydroaminacrine Inhibitors of Acetylcholinesterase”, *The Journal of Biological Chemistry*, vol. 271, pp. 23646-23649, 1996.
- N. Quian and I. Kovach, “Key Active Site Residues in the Inhibition of Acetylcholinesterase by Soman”, *FEBS Letters*, vol. 336, pp. 263-266, 1993.
- D. M. Quinn, “Acetylcholinesterase: Enzyme Structure, Reaction Dynamics and Virtual Transition States”, *Chemical Reviews*, vol. 87, pp. 955-979, 1987.
- D. R. Ripoll, C. H. Faerman, P. H. Axelsen, I. Silman and J. L. Sussman, “An Electrostatic Mechanism for Substrate Guidance Down the Aromatic Gorge of Acetylcholinesterase”, *Proceedings of the National Academy of Sciences of the United States of America*, vol. 90, pp. 5128-5132, 1993.
- A. Shafferman, A. Ordentlich, D. Barak, C. Kronman, R. Ber, T. Bino, N. Ariel, R. Osman and B. Velan, “Electrostatic Attraction by Surface Charge does not

- Contribute to the Catalytic Efficiency of Acetylcholinesterase”, *The EMBO Journal*, vol. 13, pp. 3448-3455, 1994.
- I. Silman, M. Harel, P. Axelsen, M. Raves and J. L. Sussman, “Three-dimensional Structures of acetylcholinesterases and of its Complexes with Anticholinesterase Agents”, *Biochemical Society Transactions*, vol. 22, pp. 745-749, 1994.
- J. J. P. Stewart and F. J. Seiler, *MOPAC: A General Molecular Orbital Package (Version 6.0)*, U.S. Air Force Academy, CO.
- L. Stryer, *Biochemistry*, W. H. Freeman and Co., New York, 1988.
- J. L. Sussman, M. Harel, F. Frolow, C. Oefner, A. Goldman, L. Toker and I. Silman, “Atomic Structure of Acetylcholinesterase from *Torpedo californica*: A Prototypic Acetylcholine-Binding Protein”, *Science*, vol. 253, pp. 872-879, 1991.
- SYBYL 6.2, Tripos Inc., St. Louis, MI, 1995.
- R. C. Tan, T. N. Truong, J. A. McCammon and J. L. Sillman, “Acetylcholinesterase: Electrostatic Steering Increases the Rate of Ligand Binding”, *Biochemistry*, vol. 32, pp. 401-403, 1993.
- A. Villalobos, J. F. Blake, C. K. Biggers, T. W. Butler, D. S. Chapin, Y. L. Chen, J. L. Ives, S. B. Jones, D. R. Liston, A. A. Nagel, D. M. Nason, J. A. Nielsen, I. A. Shalaby and W. F. White, “Novel Benzisoxazole Derivatives as Potent and Selective Inhibitors of Acetylcholinesterase”, *Journal of Medicinal Chemistry*, vol. 37, pp. 2721-2734, 1994.
- S. T. Wlodek, J. Antosiewicz, J. A. McCammon, T. P. Straatsma, M.K. Gilson and J. M. Briggs, “Binding of Tacrine and 6-Chlorotacrine by Acetylcholinesterase”, *Biopolymers*, vol. 38, pp. 109-117, 1996.
- Y. Yamamoto, Y. Ishihara and I. D. Kuntz, “Docking Analysis of a Series of Benzylamino Acetylcholinesterase Inhibitors with a Phthalimide, Benzoyl, or Indanone Moiety”, *Journal of Medicinal Chemistry*, vol. 37, pp. 3141-3153, 1994.